Universidade do Minho
Escola de Engenharia

Catarina Isabel da Silva Oliveira

Tailored deposition of coloured coatings: on the widening of the available colour range

outubro de 2015

Tailored deposition of coloured coatings:
on the widening of the available colour range
Catarina Isabel da Silva Oliveira
UMinho | 2015

Universidade do Minho
Escola de Engenharia

Catarina Isabel da Silva Oliveira

Tailored deposition of coloured coatings: on the widening of the available colour range

Dissertação de Mestrado
Ciclo de Estudos Integrados Conducentes ao
Grau de Mestre em Engenharia de Materiais

Trabalho efectuado sob a orientação de
Professor Doutor Luís António Carvalho Gachineiro da Cunha

e coorientação do
Doutor Diego Martínez Martínez

outubro de 2015

DECLARAÇÃO

Catarina Isabel da Silva Oliveira

Endereço eletrónico: a61940@alunos.uminho.pt Telefone:919607461

Número do Bilhete de Identidade: 14506040

Título da Tese: Tailored deposition of coatings: on the widening of the available colour range

Orientador:

Doutor Luís António Carvalho Gachineiro da Cunha

Coorientador:

Doutor Diego Martínez Martínez

Ano de conclusão: 2015

Tese submetida na Universidade do Minho para a obtenção do grau de:

Mestre em Engenharia de Materiais

Universidade do Minho, ___/___/_____

Assinatura: _____

To my parents and boyfriend

Acknowledgements

Though out this project I had the fortune of having the support of several people which contributed in a very positive way to the realization of this thesis. Without this persons this task would be much more difficult to accomplish, so here I leave my sincere acknowledgement to them.

First I want to to thank to Professor Luis Cunha, my supervisor, for allowing the realization of this work, and for his incentive and guidance thought out the work.

I want to acknowledge Dr. Diego Martinez for his presence each set of the way, for his extremely helpful advices and for always taking the time to elucidate all my draughts always contributing to my learning. The name 'Co-supervisor' does not make justice to his role in this work. .

I would also like to thank to the researchers of the Laboratory of functional coatings III, Joel Borges, Marco Rodrigues and Claudia Lopes, for their sympathy and for always helping me around the lab.

To Mihai Apreutesei, from MATEIS Laboratory-INSA de Lyon, for performing the XRD measurements in my samples.

To Professor Carlos Tavares for providing the software required to analyses the XRD measurements.

To the technicians from the science school of Universidade do Minho for their technical support.

To my family, my mother and brothers, for always being present and for giving me the strength and support to achieve all my goals.

To my boyfriend, for being my safe spot, for his kind words, and for always standing by my side in the good and bad times.

At last, but definitely, not least, to my friends. Either the ones that I met during my academic journey and with whom I shared so many good memories, or the ones prior to that who occupy a special place in my life. All of them are incredible and I am lucky enough to call them ‘friends’.

Abstract

Decorative coatings are important for several consumer products such as jewellery, eyeglass frames, and wristwatch casing among others. They are supposed to provide properties such as scratch-resistance and protection against corrosion. But from a consumer's point of view, it is important that those objects process an appealing appearance, and colour is fundamental to achieve that goal.

Decorative coatings have been largely based binary nitrides, witch possess outstanding optical and mechanical properties but lack in terms of the available colour range which is restricted to colours as golden yellows, greys, and black.

Additionally, over the time the requirements of decorative coatings are more and more demanding leading to the application of physical vapour deposition (PVD) processes. However, in order to obtain different coloured coatings, it is necessary to use different target materials and/or the reactive gas. This is time consuming, and not economically viable, and even so, there are still some colour limitations.

Recently a new class of materials became important regarding decorative applications, the metal oxynitrides. This materials allow tailor the properties of the film between a metal nitride and a metal oxide. This could allow to obtain a range of colours, within the same system, by simply varying the ratio between oxygen and nitrogen.

So in order to obtain new coloured coatings, zirconium oxynitride thin films were deposited using reactive magnetron sputtering, in several batches and varying different deposition parameters. Some of the samples were also doped with titanium.

The samples were then characterized in terms of: microstructure using Scanning Electron Microscopy, chemical composition by mean of Rutherford Backscattering Spectroscopy, structure by X-ray diffraction and colour through spectrophotometry.

The results indicate a tight relation between the chemical composition and the structure and colour of the films, and it was possible to verify that a certain compositional range leads to a certain structure.

In terms of the colours obtained the films are restricted to silver, golden-yellow and dark-greys, besides the interference colours.

Keywords: Colour, Decorative coatings, Reactive magnetron sputtering, Titanium, Zirconium oxynitrides.

Resumo

Os revestimentos decorativos são importantes em diversos produtos de consumo tais como joias, armações de óculos, caixas de relógio de pulso, entre outros. Estes revestimentos devem possuir propriedades tais como resistência ao risco e proteção contra a corrosão. Mas, do ponto de vista do consumidor, é extremamente importante que os objetos tenham uma aparência apelativa e, para isso, a cor é fundamental.

Os revestimentos decorativos têm sido maioritariamente baseados em nitretos binários, sendo que estes possuem excelentes propriedades óticas e mecânicas, mas, por outro lado, têm um número muito reduzidos de cores que se limitam a amarelos- dourados, cinzentos e pretos.

Adicionalmente, ao longo do tempo, os requisitos dos revestimentos decorativos são cada vez mais exigentes levando a que a produção se direcione para o uso de processos por deposição física de vapores (PVD). Contudo, de forma a obter filmes com cores variadas normalmente é necessário recorrer a diferentes materiais para o alvo e/ou para os gases reativos. Esta constante mudança de materiais leva tempo, e não é viável do ponto de vista económico, e mesmo assim, há, ainda, limitações em termos das cores obtidas.

Recentemente uma nova classe de materiais tem-se tornado importante em termos de aplicações decorativas, os oxinitretos de metais. Estes materiais permitem ajustar as propriedades dos filmes entre as propriedades de nitretos e óxidos metálicos. Isto pode permitir a obtenção de uma gama de cores usando o mesmo sistema, simplesmente variando o rácio entre oxigénio e azoto.

Assim, de forma a obter revestimentos com novas cores, oxinitretos de zircónio foram depositados através de deposição física de vapores, em várias series e com parâmetros de deposição diferentes. Algumas das amostras foram dopadas com titânio.

As amostras foram depois caracterizadas em termos de microestrutura usando microscopia ótica de varrimento, composição química através de espectroscopia de retrodispersão de Rutherford, estrutura através de difração de raio-x e cor por espetrofotometria.

Os resultados indicam uma íntima relação entre a composição química a estrutura e a cor dos filmes, e foi possível verificar que uma certa gama de composições leva a uma certa estrutura.

Em relação a gama de cores obtida, os filmes estão restritos a cores como prateado, amarelo-dourado e cinzentos-escuros, além das cores de interferência.

Palavras-chave: Cor, Revestimentos decorativos, pulverização catódica reativa em magnetrão, Titânio, Oxinitretos de zircónio

Table of Contents

List of Figures

List of Tables

Abbreviations

AFM	Atomic Force Microscopy
BB	Bragg Brentano
BCC	Body Centred Cubic
DC	Direct Current
EDS	Energy-dispersive X-ray Spectroscopy
FCC	Face Centered Cubic
MIRR	Modulated Infrared Radiometry
OSA	Optical Society
PVD	Physical Vapour Deposition
RBS	Rutherford Backscattering Spectroscopy
RGPP	Reactive Gas Pulsing Process
SCCM	Standard Cubic Centimeters per Minute
SD	Standard Deviation
SEM	Scanning Electron Microscopy
SZM	Structure Zone Model
XPS	X-ray Photoelectron Spectroscopy
XRD	X-ray Diffraction

CHAPTER 1

Introduction

1.1. Decorative thin films

Modern societies have high standards and demands and the pursuit for quality products is constant[1]. Nevertheless bulk materials often fail to provide all the desirable properties (mechanical, optical, electrical...) for a certain application[2]. In that manner coatings may provide a competitive path to modify the surface of materials in order to achieve those properties[2]. Among all the properties achieved by coatings, colour is of interest when it comes to consume products such as jewellery[1], eyeglass frames[1,3,4], wristwatch casings[1,3,4], and wristbands[1,3,4], among others. These coatings, whose aesthetic function is important, are called decorative coatings and, besides their decorative functions, they are expected to provide scratch-resistance and protection against corrosion among other properties[1,3,4].

Over the past years decorative coatings have been largely based on elementary materials and binary nitrides (TiN, ZrN, HfN)[3]. Transition metal nitrides have outstanding optical and mechanical properties such as high hardness[1], good wear and corrosion resistance[1] and adhesion[1]. But despite that, with this composition, the colour tones achievable are limited to golden yellows[3,5], greys[3,5] and black[3,5]. Furthermore, over the time the requirements of decorative coatings are more and more demanding leading to the application of physical vapour deposition (PVD) processes, which allow to fulfil these requirements[5]. However, in order to obtain different coloured coatings, there is the need to use different target materials and/or the reactive gas, which is time consuming, and not economically viable, and even so, there are still some colour limitations[5].

In order to avoid the issues above mentioned (colour tones limitations and practical and economic issues), other materials are being explored. Recently, a new class of materials became important regarding decorative applications, the metal oxynitrides MO_xN_y (M= early transition metal). The importance of the transition metal oxynitrides arises from the presence of oxygen which makes possible to tailor the properties of the film between a metal nitride and a metal

oxide[3–5]. This could allow to obtain a range of colours, within the same system, by simply varying the ratio between oxygen and nitrogen

1.2. Motivation

There are several examples of metal oxynitrides systems using titanium and/or zirconium as transition metal in the production of decorative coatings[1,5–8]. The colour range achieved with this system ranges from golden, several shades of grey, to bluish and reddish coatings. But despite that, white, green and light blue coatings are yet to be achieved using this systems. In fact a German company named Biointerface GmbH is actively interested in obtain light blue and white colorations for decoration of its products. Therefore, this thesis aims to successfully deposit zirconium oxynitride thin films with new colour tones such as the ones referred above by reactive dc magnetron sputtering technique.

1.3. Objectives

The main goal of this work is to produce new coloured coatings mainly white and light blue ones using zirconium oxynitrides, for decorative applications.

The coatings will be produced by reactive dc magnetron sputtering which is a type of physical vapour deposition (PVD) technique. The samples will be deposited in glass, silicon and high-speed steel substrates. Several depositions will be made with different parameters, and adding titanium, as a dopant, in some cases, in order to study the influence of these parameters on the properties of the coatings.

The depositions will be made in several sequential batches in order to characterize the samples between depositions and adjust properly the parameters for the following batch. The samples will be characterized in terms of chemical, morphological and structural characteristics as well as in terms optical properties.

1.4. Organization and structure of the thesis

CHAPTER 2 consists on a general introduction to the main topics discussed in this thesis. First, a brief description to colour and light phenomena is made. After that, the decorative coatings are briefly introduced as well as the concept of intrinsic colour. Further ahead, the

oxynitride films and its properties and applications are revised. In the next subchapter, the deposition of the oxynitride thin films by physical vapour deposition is addresses and some examples present on the literature are referred. The state of the art ends with a detailed analyses of the main results of a previous Ph D thesis carried out in this research group on a similar topic. These results will serve as a guide line to the work developed in this thesis.

CHAPTER 3 describes the experimental details of the samples deposited in this work, starting with the methodology used and followed by a description of the deposition technique. After that, the deposition conditions of the different sets of samples are reported. Finally, the characterization techniques are briefly introduced together with the operational parameters used in each one of them.

CHAPTER 4 is the first chapter of the results and discussion, and it is focused in the base series of samples where the influence of the flow of the N_2+O_2 gas mixture is studied. The aim of this chapter is to evaluate the reproducibility of the main results of the prior Ph.D. thesis on the same field in our deposition setup and conditions. Therefore, the differences and similarities with previous results are analysed in detail. This base series is used in the following chapter as the 'baseline' to evaluate the influence of the different deposition parameters.

In CHAPTER 5 the results and discursion of the exploration of the deposition parameters space are presented, namely the bias voltage, working gas flow, target current and deposition time, in comparison with the base series. The aim of this chapter is to understand the effect of the different deposition parameters in the system and its effect in the colour properties of the films, and evaluate if new characteristics are achievable.

CHAPTER 6 is similar to the previous one, since it involves a modification of the base series, in this case by the doping of the samples with titanium. Similarly to the Chapter 5, the objective of this chapter is to understand the effect of the Ti in the Zr-N-O system, with the final goal of finding new colours.

CHAPTER 7 englobes the main conclusions archived thought the realization of this work and the proposals for the next steps necessary to the concretization of the objectives of this thesis.

CHAPTER 2

State of the art

With the constant development of modern societies, the consumer is becoming increasingly demanding. Additionally, nowadays a great importance is placed in one's appearance and some objects such as jewellery, glasses and watches tend to be viewed as a symbol of social status. In that way, from a consumer's point of view, it is important that those objects process an appealing appearance, and colour is fundamental to achieve that goal

2.1. Colour and light

Colour has a great importance in the daily lives of humans. Large amounts of information about the surrounding world are gathered by the vision, and colour plays an important role in this flow of information [9].

Colour is usually experienced due to interaction of light, materials and the human visual system (eye and brain) as depicted in Figure 2.1 even though, it is possible to experience colour for example by direct stimulation of brain cells, or in dreams[9,10]. Contrarily to the common belief that colour is a property of objects, facts like variation of colour experience as a consequence of the modification of illumination refute that[9].

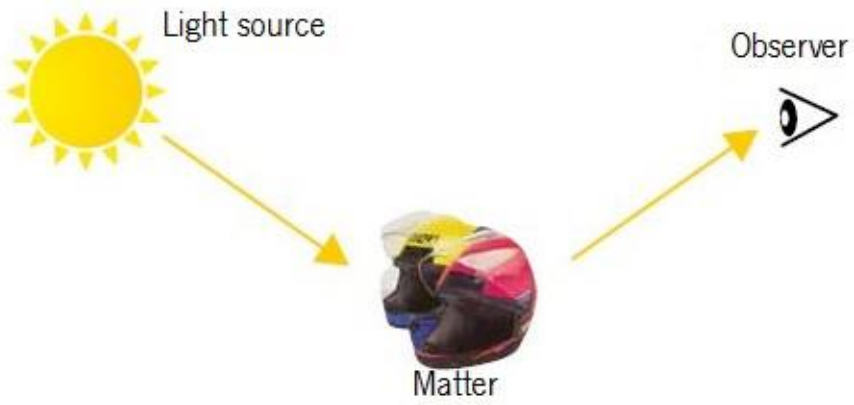

Figure 2.1 Colour experiencing (adapted from[11])

Over the years there has been difficulty to reach an agreement in colour description. The Calorimetry Committee of the Optical society (OSA) has been divided between the physicist and psychological views of colour. Initially, the colour definition was purely physical to be latter re-evaluated in order to include the perception-based psychological concept. Even though, the committee was, still, divided between definitions. They finally agreed to relate the concept of colour to psychological category and light to physical category[12].

Nowadays colour can be described through colour attributes. Colour technologists of the Society of Dyers and Colourists have defined the three colour attributes: Hue, Strength - depth, Dullness – brightness[13,14].

1. Hue: Attribute of colour whereby it is recognised as being predominantly red, green, blue, yellow, violet, brown, etc.
2. Strength (of a dye): the colour yield of a given quantity of dye in relation to an arbitrarily chosen standard (of a dyeing or print) synonymous with depth.
3. Dullness (of a colour): that colour quality an increase in which is comparable to the effect of the addition of a small quantity of a neutral grey, whereby a match cannot be made by adjusting the strength. The opposite of brightness.

Several processes are known to result in colour experiences, Nassau identified what he called the '*15 causes of colour*', In Table 2.1 are listed those causes and respective examples[9,15].

Independently of the cause, colour phenomenon has one common denominator: light.

Light or electromagnetic radiation, has different names depending on its energy content (X-rays, ultraviolet radiation, infrared radiation...) and the wavelength limits of the different regions are merely an approximation once the regions form a continuum with one another with limits that are, in a certain range, undefined[9,14].

Visible light consists in the range of electromagnetic radiation that can be perceived by the human eye, with wavelengths ranging roughly from 400 to 700 nm (Figure 2.2)[10,15].

Table 2.1 The 15 causes of colour and examples[15]

Simple excitations and vibrations
1. Incandescence:
Hot objects, the sun, flames, filament lamps, carbon arcs, limelight, lightning*, pyrotechnics*.
2. Gas excitations:
Vapour lamps, neon signs, corona discharges, auroras, lightning*, pyrotechnics*, lasers*.
3. Vibrations and rotations:
Water, ice, iodine, bromine, chlorine, blue gas flame.
Transitions involving ligand field effects
4. Transition metal compounds:
Turquoise, malachite, chrome green, rhodochrosite, smalt, copper patina, fluorescence*, phosphorescence*, lasers*, phosphors*.
5. Transition metal impurities:
Ruby, emerald, alexandrite, aquamarine, citrine, red iron ore, jade*, glasses*, dyes*, fluorescence*, phosphorescence*, lasers*.
Transitions between molecular orbitals
6. Organic compounds:
Dyes*, biological colorations*, fluorescence*, phosphorescence*, lasers*.
7. Charge transfer:
Blue sapphire, magnetite, lapis lazuli, ultramarine, chromates, Painted Desert, Prussian blue.
Transitions involving energy bands
8. Metals and alloys:
Copper, silver, gold, iron, brass, "ruby" glass.
9. Pure semiconductors:
Silicon, galena, cinnabar, vermillion, cadmium yellow and orange, colorless diamond.
10. Doped semiconductors:
Blue and yellow diamonds, light-emitting diodes, lasers*, phosphors*.
11. Colour centers:
Amethyst, smoky quartz, desert "amethyst" glass, fluorescence*, phosphorescence*, lasers*.
Geometrical and physical optics
12. Dispersion, polarization, etc.:
Rainbows, halos, sun dogs, photoelastic stress analysis, "fire" in gemstones, prism spectrum.
13. Scattering:
Blue sky, red sunset, blue moon, moonstone, blue eyes, blue skin, blue butterflies*, blue bird feathers*, other blue biological colours*, Raman scattering.
14. Interference:
Oil sHck on water, soap bubbles, coatings on camera lenses, biological colours*.
15. Diffraction:
Aureole, glory, diffraction gratings, opal, liquid crystals, biological colours*, diffraction spectrum.

* Only in part.

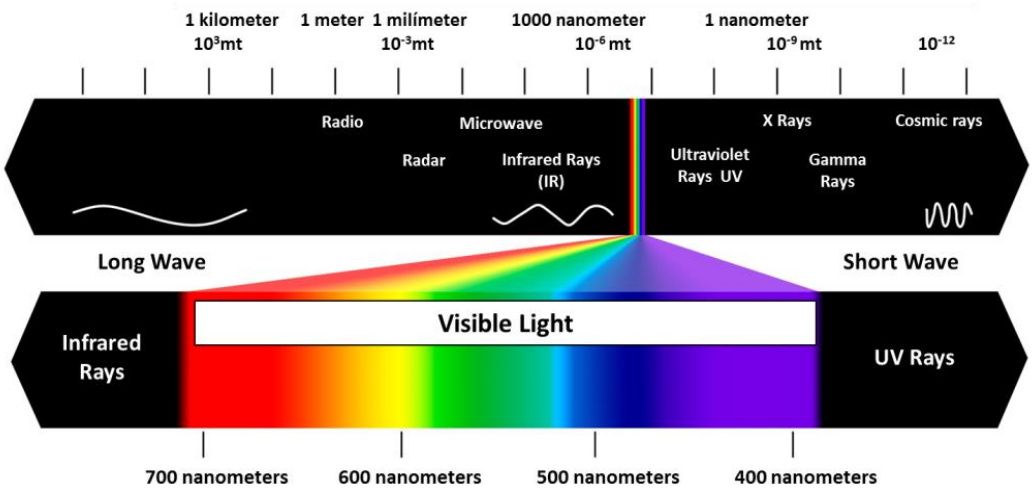

Figure 2.2 Schematic representation of the electromagnetic spectrum[16]

Since its origin, light passes through several stages, selective actions at certain energy levels can lead to changes in the spectral power distribution and lead to colour experiences.

There are several processes through whom light interacts with matter and could lead to colours experiences. Typically, the observed colours are a combination of several of this processes even though they may have different contributes (e.g. selective absorption of certain wavelengths coupled with transmission, reflection and scattering of the incident radiation)[14]. In the following, the light- matter interaction process will be briefly described.

Absorption:

When light arrives to the material, the part of the light with frequency comparable to the frequency of the lattice vibrations is selectively absorbed (Figure 2.3a), the atoms of the material became excited and during the vibration the electrons in the atoms interact with the neighbouring atoms, converting the vibrational energy in thermal energy. The remaining light is emitted with a lower energy or transmited[9].

Transmission:

Transmission (Figure 2.3b) is the unimpeded passage of light through a transparent object such as a layer of water. After passing through, some of the light is absorbed or reflected, but the transmitted light has the original wavelength [9].

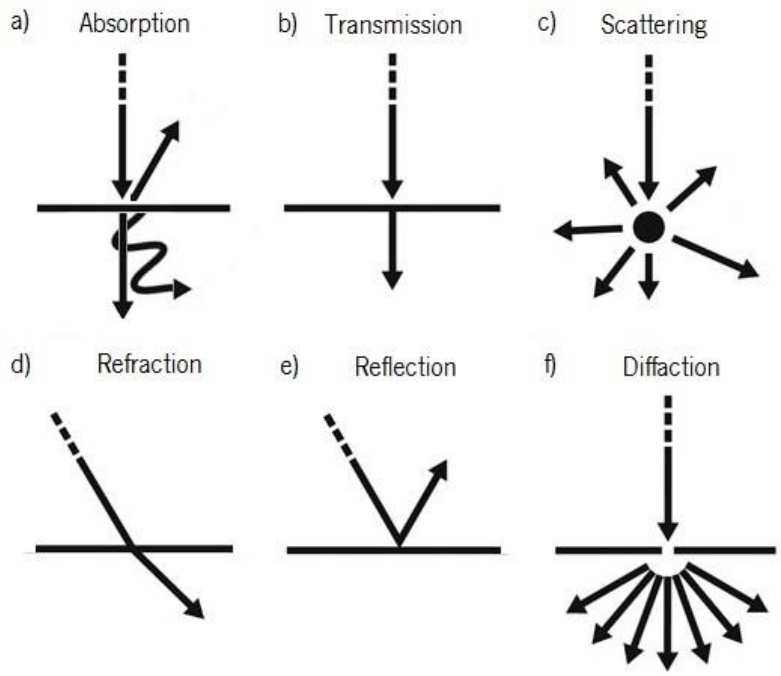

Figure 2.3 Schematic representation of the light-matter interaction processes: a) Absorption; b) Transmission; c) Scattering; d) Refraction; e) Reflection; f) Diffaction[16].

Scattering:

Is the change of direction in radiation that collides with, for instance, rough-surfaced materials, or with fine particles with ununiformed or varying shape (Figure 2.3c). In this case the reflection occurs in many directions. The materials can look smooth but the microscopic rough surface causes the scattering of incident light[9].

Refraction:

Refraction (Figure 2.3d) consists in the change of direction of light when passing form one medium to another. The magnitude of the change of direction is a function of the optical densities of the two mediums, and of the energy of the photons. Thus, the greater the photon's energy and the density of the medium, the greater the change in direction will be. Snell's law (2.1) expresses the relation of the angles of incidence and refraction and the density of the two medium[9].

$$n_1 \sin \theta_1 = n_2 \sin \theta_2 \quad (2.1)$$

Reflection:

Reflection (Figure 2.3e) is a type of scattering. It is the process in which photons

reaching a material with a smooth surface change their direction on impact and are returned. In this form of scattering, due to the smooth surface of the material, the reflection angle is the same as the angle of the incident light[9].

Interference:

Interference colours differ from the scatter-effect colours. In interference colour the hue and intensity of the colours varies with the angle at which the surface is viewed. Interference is the term used to refer to the physical effect in which light waves temporarily split into parts that are latter recombined. The light waves, after the splitting, can be in or out of phase when they recombine, depending on the path the beams components follow. If they are in phase, the intensity of the resulting beam is the sum of the components, if they are not, the components will cancel each other. A common example of interference is when thin layer of oil in water. Whether or not the reflected light is in phase depends on the thickness of the film. If the reflected light is in phase, light of several wavelengths will emerge at correspondent angles giving rise to colour stimuli, the colours will depend on the angle of viewing. Several colour will be seen if the film has a non-homogeneous thickness[9].

Diffraction:

Diffraction (Figure 2.3f) is a particular case of the combined effect of scattering and interference. The behaviour of light in the edge of a material (e.g. a razor blade) is influenced by the sharpness of the edge. The light arriving the edge can be transmitted, scattered, or absorbed, reflected, or refracted depending on the relationship between its wavelength and the dimensions of the edge. If several edges exist the resulting scatter at the edges is subjected to interference effects. When daylight strikes such an assembly of edges, waves in phase are enhanced in different directions: a display spectral colours results when viewed from different angles[9].

2.2. Decorative coatings

Decorative coatings have been used for a considerable amount of time and were first applied in small consumer products such as writing instruments[5,17], eyeglass frames[1,3,5,17], wristwatch casings[1,3,17] and jewellery parts[5,17] and their commercial value keeps increasing[18].

In addition to enhance the appearance of surfaces, leading to attractive colours, the

decorative coatings are supposed to exhibit surface quality[17,18], skin compatibility[17,18], scratch resistance[1,5], high wear resistance[17,18] and protection against corrosion[5,17]. Thus, by proper selection of the coating methods and materials it is possible to protect the substrate to increase their service lifetime and, also, increase the commercial value of the products[19,20].

Decorative thin films have been mostly based on elemental materials, metal nitrides (TiN, ZrN, HfN) and titanium carbonitrides[3].

The main objective of this thesis is produce decorative intrinsic coloured films, so the focus will be placed in the origins of intrinsic colours in oxynitride thin films and study the influence of different deposition parameters and compositional and structural features in the films colour.

From a physical point of view, the production of intrinsic colour is caused by selective absorption of portions of the incident light together with transmission, reflection and scattering of the radiation that was not absorbed[14,21,22].

Light is absorbed by several absorption mechanisms before resulting in colour experiences. The absorption occurs due to the response of optical phonons and outermost electrons. The absorption processes are divided in four[22] :

1. Reststrahlen absorption
2. Interband transition
3. Absorption due to impurities
4. Free-carrier absorption

In Figure 2.4 it is possible to see the optical absorption spectrum as a function of the energy of the photons.

Reststrahlen absorption

Reststrahlen absorption occurs usually in the infrared region of the electromagnetic spectrum having no contribution in the colour effects[22]. In Reststrahlen mechanism light is selectively reflected from the surface of a transparent material when the frequency of the incident light is comparable to the vibration of the lattice[21,23]. The majority of the light that reaches the transparent solid is transmitted through it, and part of the light is absorbed, the remaining is reflected[23]. Light of certain frequencies (close to the frequency of vibration of the material) does not travel far into the material[23]. Part of this light is absorbed nearby the surface, being the energy of the light transferred to the vibrating ions of the solid, as some reflected as Reststrahlen[23]. Almost all the light of the right frequency that reaches the surface of the

material can be reflected in this selective way, the radiation that remains after multiple reflections is all essentially of the same frequency[23].

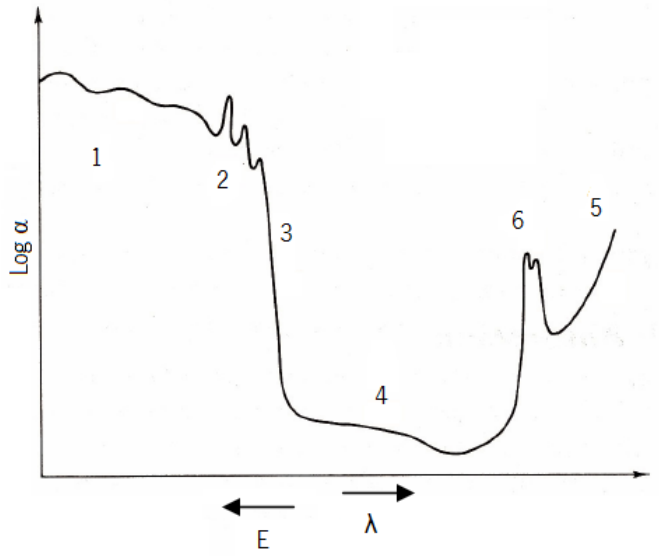

Figure 2.4 Types of optical absorption; (1) transition of high-lying bands, (2) excitons, (3) fundamental absorption, (valence band to conduction band transition), (4) impurity absorption, (5) free-carrier absorption and (6) Reststrahlen absorption.

Interband transition

When a photon with energy comparable to the energy gap impinges the material, the valence electrons at the ground state absorb photons of threshold energy and then cross the band gap to an empty conduction band[21,24]. In a perfect crystal, with a filled valence band and an empty conduction band, the absorption process is ruled by the interband transition mechanism[22,25]. Interband transitions can be either direct or indirect[25].

Colour is caused by the remaining light that was not absorbed[22]. Colour caused by this process depend on the magnitude of the band gap, if the band gap is larger than the higher energy of the visible region (3.5 eV), the materials are perceived as transparent since there is no absorption of visible light[21,22,26]. For its turn, materials with band gap smaller than the lower limit of the visible region of the electromagnetic spectrum (1.7 eV) are opaque and blackish once there is the absorption of the whole spectrum of the visible light wavelengths[21,22,26]. For band gaps lying in the visible region, particular threshold energies are absorbed and the materials present a characteristic colour[22].

Absorption due to impurities

In the case of imperfect crystals, extra energy levels are situated in regions around the defects. This extra energy levels cause that the valence electrons need less energy to go to higher energy levels when compared to the perfect crystals. Thus, colour arises from the absorption of photons in the visible range[21,22].

One example of this mechanism is the diamond (colourless) that becomes yellowish when doped with nitrogen[26]. Nitrogen acts as a donor, and creates an energy level at 1.4 eV above Fermi level, even though the energy necessary for a direct transition is 4 eV. Hence, energy ranging from blue to violet is absorbed and yellow and green is transmitted. If some boron is added, the element will act as an acceptor originating an empty state at approximately 0.4 eV above the Fermi level. The diamond is capable to absorb light in the red region appearing bluish[21,22,26].

Free-carrier absorption

The main absorption mechanism in zirconium nitrides is free-carrier absorption[22]. When electromagnetic radiation strikes a material with a partially filed valence band, the free carriers from the original ground states are excited to higher energy states located immediately above the Fermi level. Thus the free carriers absorb light with a wide range of energy, including in the visible region. The excited electrons can return to lower energy states by dissipating energy in the form of heat, due to collisions with the lattice, or in the form of photons. These photons leave the surface of the material as the observed reflected light. As result of selection rules, the electron paths going to higher energies and returning to the ground states may differ, and, thus, the observed colour may not correspond to the absorbed light[21,22].

2.3. ZrO_xN_y system: properties and applications

Nitrides consist in a group of modern ceramic materials of technological importance[5]. Their properties make them suitable for tribological applications (such as cutting tools, turbine blades, and other abrasive environments applications)[27,28], for protective applications (such as wear, diffusion and corrosion-resistant devices)[5], for optical applications (such as solar collectors devices)[19] and also for optoelectronics[29] and microelectronics[5].

Transition metal nitrides have been used successfully for the past years due to their optical and mechanical properties[1,19,30]. The combination of ionic, covalent and metallic

bonding[7] leads to promising properties. The covalent bonds lead to properties such as high hardness[5,7,19], chemical[5,7,19] and thermal stability[31], high melting point (Titanium nitride (TiN): 2950°; Zirconium nitride (ZrN): 2982°)[7,19,32], relatively low friction coefficient[19], wear[31] and corrosion resistance[7,19,32], and brittleness[31]. The metallic bonds lead to electrical conductivity and metallic reflectance[22].

More specifically, titanium and zirconium nitrides films are of great industrial interest due to their applications such as hard coatings[19,33,34], diffusion barriers in semiconductors technology[19,34,35], Josephson junctions[33,34], as superconductors[33] and optical applications in heat mirrors[19,32,36]. But, particularly, due to metallic properties (electrical conductivity and metallic reflectance), along with the aesthetic properties of the colorations in the visible wavelength region, make them very interesting in the field of decorative coatings[31,35].

The gold-like appearance of TiN and ZrN makes then interesting as gold substitutes for example on watches, with improved scratch resistance and being, obviously, less expensive coating materials[22,32]. This gold-like appearance is caused by the high reflectance of this materials at the red-end of the visible spectrum and low reflectance near the ultraviolet region[22]

Stoichiometric ZrN is the only stable phase, and presents a gold-like colour, other non-stoichiometric phases also exist such as Zr_2N, ZrN_2, Zr_3N_4 and Zr_4N_3[37]. ZrN_y thin films crystalize into a FCC NaCl structure type over a large chemical composition range ($0.7<y<1.2$)[37]. ZrN coatings have been produced by many techniques such as vacuum arc deposition, reactive magnetron sputtering, pulse laser deposition and ion beam-assisted deposition[38,39].

Despite all the remarkable properties of the transition metal nitrides thin films (TiN, ZrN...) the colour range achieved by them is limited to colours such as golden as well as brown and black[34]. Additionally, the demand for low cost products combined with reduced material resources is pushing the research to deposition techniques that allow to produce coloured films with minimum use of resources[5,8]. Likewise the continuous change in deposition procedure such as material targets and/or reactive gas changes to obtain different coloured films is unsuitable[5,8].

Considering these limitations, a new class of materials has been drawing attention when it comes to decorative applications, the metal oxynitrides[5,40]. The major advantage of this nitride and oxide combination is not only the possibility to have a range of different colours and physical properties, but, above all, the opportunity to have them from the same system: one target (Zr, Ti,...) and the same gas mixture (N_2+O_2), i.e. with the same system setup and by

varying the N_2/O_2 ratio it is possible to achieve a range of different colours[40].

Films based in zirconium oxides have a series of desirable properties. They are transparent in a wide wavelength range[41], have high refractive index[42,43], high melting point[42] high thermal stability[41], corrosion resistance[42], chemical resistance[41] and good adhesion[41]. For its turn, zirconium nitrides usually have optical properties of low variability and with the addition of a third element, in this case oxygen, structural changes can occur, with the possibility to tailor the properties of the materials in a much wider range[44]. When adding oxygen to the zirconium nitrides a synergy of properties occurs with the desirable properties of the metal oxides (optical and electrical properties) and nitrides (electrical, mechanical and tribological properties)[44].

The presence of oxygen allows tailoring the properties of the film between those of metallic nitrides and the correspondent insulating oxides, leading to unexpected and promising functional range of materials[8,40,45,46]. As was already referred MeO_x has excellent properties namely mechanical properties of oxide-based films along with good chemical stability, high refraction index and wide optical band gap[7]. Therefore, varying the oxide/nitride ratio allows to tune the band-gap[5,40], bandwidth[5,30,40] and crystallographic order[5,30,40,47], between oxide and nitride. As a consequence, the electronic and optical properties of materials can be modified and thus their colour properties could be tailored by elucidating the relationship between the corresponding physical, structural and mechanical properties[5,30,40].

Due to the higher reactivity of oxygen relatively to nitrogen, the addiction of oxygen to a growing transition nitride film induces the formation of ionic-metal-oxygen bonds in a matrix of metal-nitrogen bond[30]. This leads to the creation of a new structure with different properties, and the optical and decorative characteristics of these ceramic material may be enhanced[30]. Though a careful control of the oxygen flow is important once the final properties will depend on the N/O ratio[48].

Transition metal oxynitrides, more specifically zirconium and titanium oxynitrides, are of interest for several applications[46]. Titanium oxynitrides are used in applications such as sun collector components, solar selective absorbers, diffusion barriers, isolation films in metal-insulator-metal structures and in wear-resistant coatings[49]. On its turn, zirconium oxynitride thin films are suitable for electronic applications like gate dielectrics[46]. ZrO_xN_y has also been used as an element in temperature sensors and corrosion resistant coatings[46,50]. Lately ZrO_xN_y thin films have been used in decorative applications such as eyeglass frames, wristwatch casings and wristbands, besides the decorative effect, zirconium oxynitrides increase the

durability of the substrate by improving its hardness and its heat and corrosion resistance[46,51].

2.3.1. Film growth – Structure Zone Model of Growth

The film near the interface is influenced by the substrate and it requires a certain thickness before the films acquires a particular growth mode[64]. When a growth mode is established the morphology of the film can be described by a structure Zone model (SZM) (Figure 2.5). The SZM was first used in vacuum-deposited coating and latter extended to sputter deposited films[64].

In Zone 1 of the model the adatom surface diffusion is insufficient to overcome the geometrical shadowing[70]. In this Zone the film has high surface area and a ''mossy'' appearance[64]. The morphology developed is columnar and the columns can have different shapes depending on the crystallographic structure of the material[64,70]. The dimension of the columns ranges the microns but the grain size can be smaller than 1000 Å (0.1 μm), or be amorphous in the columns[64]. Once the columnar growth depends only of the surface geometry, angle of incidence, and adatom surface mobility, both amorphous and crystalline materials can develop columnar growth.

The angles of incidence of the adatom flux has major importance on the columnar growth. The columnar growth is intensified if the deposition flux orientation is off-normal once the valleys will get no flux. The off-normal angle of incidence can be related to a rough surface, or a smooth surface with off-normal deposition. In an off-normal incident flux, the columns grow towards the adatom source in opposition to the normal angle incidence, were the columns grow normal to the surface[64].

The Zone T of the model is characterized by a fibrous morphology, and represents a transition from Zone 1 to Zone 2[64,70]. The formation of the Zone T is caused by the bombardment of the substrate with high energy neutrals reflected from the target. The neutrals erode the peaks and fill the valleys partially[64].

In Zone 2 the growth of the films is ruled by adatom diffusion[64,70]. In this Zone the surface diffusion leads to the densification of the intercolumnar boundaries[64]. Thought the columnar remain, and the grain size increases[64].

In Zone 3, recrystallization, grain growth and densification occur as a consequence of the bulk diffusin[64,70]. The modified columnar structure is noticeable with single crystal

columns[64].

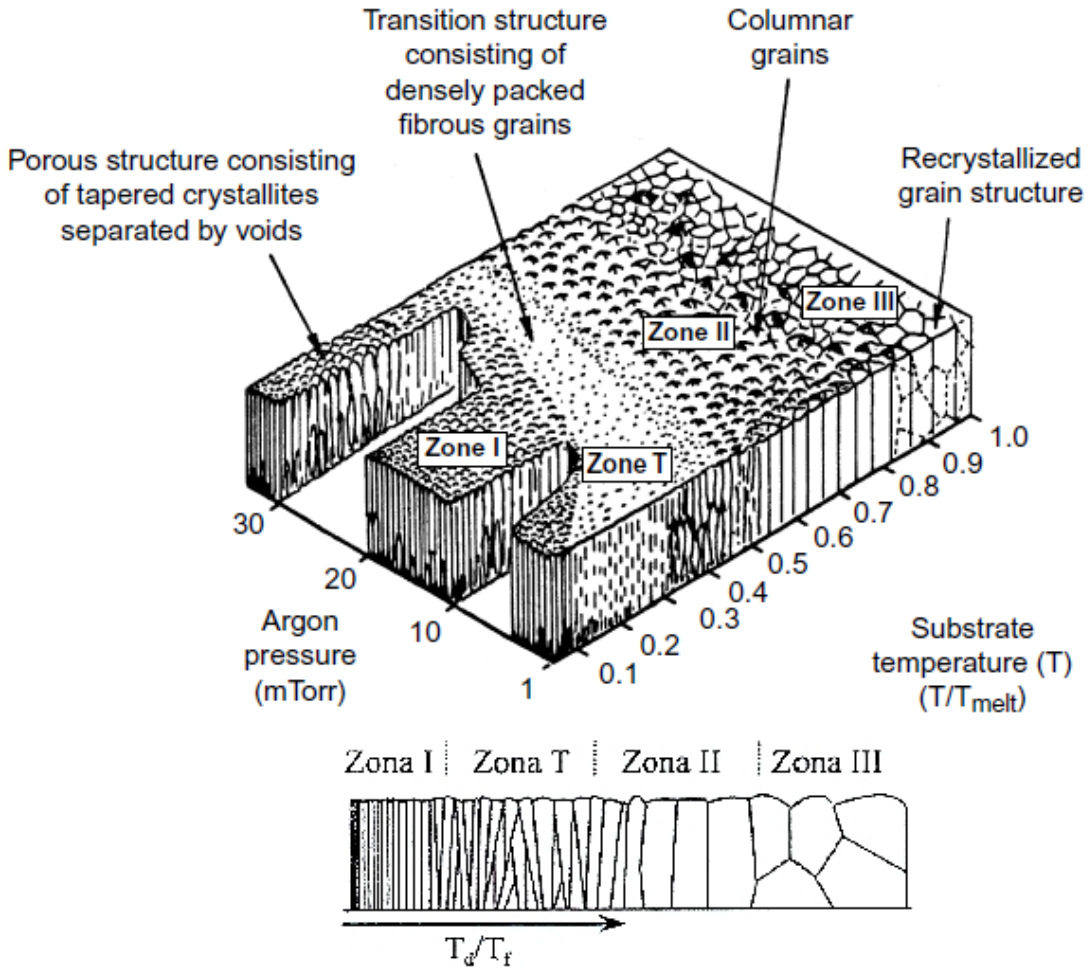

Figure 2.5 Representation of the structure Zone model for thin film growth[64]

2.4. ZrO_xN_y coatings deposited by physical vapour deposition

Physical vapour deposition (PVD) processes have been applied with success to several technological fields due to the wide range of material combinations and thus property gradients[7]. Examples of PVD's versatility include several types of optical filters, solar cells/collectors, structural components, automotive parts, among others[7].

PVD processes are widely used in the deposition of decorative coatings due to several characteristics of this process like the possibility of producing abrasion resistant coatings, the durability of the coatings and the controllability of the process[52,53]. Furthermore PVD is considered environmental friendly once chemical reactants are not used[52,54]. Various PVD techniques have been used to produce zirconium and titanium oxynitrides films like

radiofrequency reactive magnetron sputtering, direct current reactive magnetron sputtering, and reactive cathodic arc evaporation, among others[46].

Since the 1980's reactive sputtering of thin films as been deeply investigated because sputtering metallic targets in the presence of a reactive gas makes easy to form compound films such as nitrides, oxides, carbides and their combinations[55]. Additionally, reactive magnetron sputtering has the advantage over other techniques that it can easily be scaled from small sized laboratory targets to industrial applications on large area substrates[56,57]. Moreover, the deposition of zirconium oxynitrides by reactive magnetron sputtering has advantages like high deposition rate on large substrates[34,58], control of the film composition, small temperature variation in the substrate during deposition, better adhesion of the deposited film, and thickness uniformity[34].

There are several examples on the literature that report the colour tones obtained from processing zirconium and titanium oxynitrides thin films, some of which will be presented below and summarized in Table 2.2.

Carvalho et al.[6] deposited ZrO_xN_y thin films onto high-speed steel, stainless steel and silicon substrates by reactive dc magnetron sputtering. The gas atmosphere was composed of argon (working gas) and nitrogen + oxygen (reactive gas) with a 19:1 ratio. The working gas flow was kept constant (55 sccm), while the reactive gas flow ranged from 4 to 17.5 sccm. The samples were later characterized by means of ball cratering, x-ray diffraction (XRD) and spectrophotometry. The authors claim that the results evidence the influence of the reactive gas flow on film colour, which is directly correlated to the oxygen content. For low flow rates, with the increase of the flow rate from 4 to 5.5 sccm there is a colour change from bright yellow-pale to golden, the colour remains golden for flows as high as 7 sccm. For higher flow rates the film colour goes from red-brownish to dark blue at flow rates superior to 11 sccm.

Carvalho et al.[7] deposited ZrO_x, ZrN_y and ZrO_xN_y films on glass and silicon substrates by reactive dc magnetron sputtering. The atmospheres were composed of argon + nitrogen, argon + oxygen for the deposition of ZrN_y and ZrO_x respectively. The ZrO_xN_y were deposited with a nitrogen + oxygen reactive gas mixture (17:3 ratio) and argon as working gas. The argon flow was constant (60 sccm) for all depositions whereas the reactive gases flow varied. The samples were then characterized by Rutherford backscattering spectroscopy (RBS), particle induced x-ray emission measurements, ball cratering, x-ray photoelectron spectroscopy (XPS) and x-ray diffraction. Regarding the surface appearance, for flows below 10 sccm the colour shifts from metallic (silver like) to golden, characteristic of the change form metal-like to nitride-based

compounds. For gas flows between 10 and 14 sccm, the colours ranged from red brownish to dark blue. Above 15 sccm of gas flow the samples revelled interference like tones no longer presenting the characteristic intrinsic colours observed for lower flows.

Vaz et al.[5] produced ZrO_xN_y samples by reactive rf magnetron sputtering onto high-speed steel, stainless steel, silicon and glass substrates. The depositions were performed in an atmosphere with argon (working gas) and nitrogen + oxygen (reactive gas). The samples were prepared with a variation of the reactive gas from 0 to 6.5 sccm while the argon flow was constant. The bias voltage was also varied from -75 V to 0 V. The samples were then characterized by RBS, ball cratering, scanning electron microscopy (SEM) and atomic force microscopy (AFM). X-ray diffraction was also performed as well as spectrophotometry. Finally, the hardness of the samples was measured. Regarding to the coloration of the samples, the authors found out that with increase of oxygen content the colour vary from bright yellow-pink colour to red brownish at intermediate oxygen fractions to dark blue at highest oxygen fractions. The results suggest a strong dependence of the colour upon the oxygen content, and reveal that surface roughness also influences the colorations, since different waviness of the surface leads to different interaction of the radiation with the films surface leading to differences in the colour.

Table 2.2 Examples of the evolution of the colour in oxynitride systems whit the variation of reactive gas

Reference	System	System conditions	Evolution of the colour	Reactive gas (sccm)
Carvalho et al. [6]	ZrO_xN_y	Reactive dc magnetron sputtering Working gas: Ar (55 sccm) Reactive gas: N_2+O_2(4 to 17.5 sccm) (19:1)	Bright yellow-pale Golden Red-brownish Dark blue	4 5.5 to 7 7<x<11 ≥11
Carvalho et al. [7]	ZrO_x; ZrN_y; ZrO_xN_y	Reactive dc magnetron sputtering Working gas: Ar (60 sccm) Reactive gas: O_2 (0.5 to 15 sccm); N_2 (3 to 40 sccm); N_2+O_2 (6 to 40 sccm) (17:3)	Metallic silver like golden Red brownish Dark blue Interference like tones	2 to 10 10 14 15 to 30
Vaz et al. [5]	ZrO_xN_y	Reactive rf magnetron sputtering Working gas: Ar (100 sccm) Reactive gas: N_2+O_2(0 to 6.5 sccm) Bias: -75 V to 0 V	Bright yellow-pink colour Red brownish Dark blue	-

The Ph.D thesis of Carvalho, P.[21], carried out previously in our research group, was studied more thoroughly than the remaining literature. This is because it can be considered as the 'seed' of this present thesis, since the idea is to expand the colour palette obtained in that work by an extensive exploration of the deposition parameter space. In section 2.5 it will be presented an overview of the main results of Carvalho which will be of help for understanding the

results of this thesis.

2.5. Summary of the main results from the work of Carvalho et al.[21]

Carvalho's thesis main objective was to prepare ZrO_xN_y coloured-multifunctional thin films with a wide range of properties. His focus was the study of the influence of the processing conditions (gases partial pressures and bias voltage, among others) in the particular film's growth characteristics: composition, crystalline and electronic structure, and morphology and the subsequent changes in the properties of the coatings, namely the electrical, optical and functional ones.

2.5.1. Deposition conditions

Four Series of samples (Table 2.3) were produced by direct current reactive magnetron sputtering. The first Series of samples was deposited in static mode using a gas atmosphere of argon (working gas) and a mixture of N_2+O_2 (reactive gas) with a 17:3 ratio. The base pressure was bellow $2x10^{-4}$ Pa. The Series 2 was deposited with similar conditions of Series 1 but with a N_2+O_2 mixture with a 19:1 ratio. The remaining conditions were the same.

Table 2.3 Summary of the deposition parameters of the four series

		Series 1	Series 2	Series 3	Series 4
Target current density	[$A.m^{-2}$]	100	100	100	100
Argon Flow	[sccm]	60	60	60	60
Gas mixture ratio (N_2:O_2)		17:3	19:1	17:3	-
Gas mixture (N_2+O_2) flow	[sccm]	6 to 40	4 to 17.5	7.5 to 13.5	-
Nitrogen flow range	[sccm]	5.1- 34	3.8- 16.6	6.4- 11.5	10
Oxygen flow range	[sccm]	0.9- 6	0.2- 0.89	1.1- 2	0- 3
Bias Voltage	[V]	Grounded	Grounded	-70	Grounded
Period of the pulse (T)	[s]	-	-	-	3
T_{on}	[s]	-	-	-	0.5 to 2.5
$\tau_{mounting}$	[s]	-	-	-	-10
$\tau_{descending}$	[s]	-	-	-	0.1

Series 3 was produced with the same conditions of Series 1, but instead of grounded,

the substrates had a bias voltage applied of -70 V and the substrate holder was on rotation mode. Series 4 was produced with similar conditions to Series 1 but using a reactive gas pulsing process were the nitrogen mass flow was kept constant but the oxygen mass flow was modulated as a periodic function.

2.5.2. Structure

The four Series of samples were structurally characterized by x-ray diffraction (see section 3.4.1 for details of the technique). It was possible to observe distinct structural arrangements in the four series with the variation of the gas flow. Four different types of structures were observed in the films; Figure 2.6 summarizes which types of structures were found in each series and the gas flow ranges in which they appear.

The films in Zone I crystalized in an fcc NaCl-type structure typical of ZrN films. Regarding the films from Zone II, the results indicate de development of a crystalline structure different from de ZrN fcc, a smooth transition of the Zone I structure towards a new one was observed. The reduced number of diffraction peaks with a significant broadening does not allow an accurate indexing of the structure, but the structure was labelled as Zr_3N_4 with oxygen inclusions. In the films from Zones III and IV, which correspond to films with higher gas flow, the structures identified were mixtures of Zr_2ON_2 and ZrO_2 for Zone III and ZrO_2 in Zone IV.

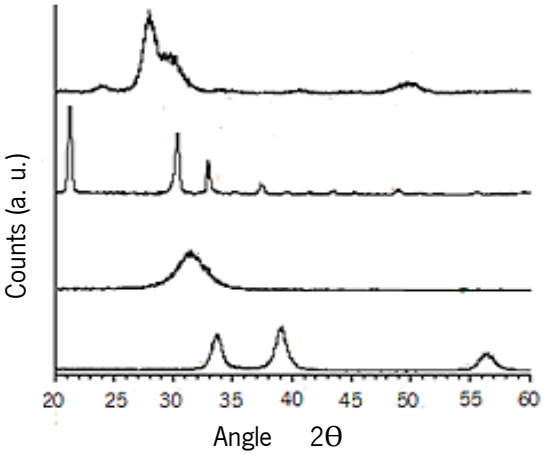

Series	1	2	3	4
Variable	N_2+O_2 Flow [sccm]			Ton/T
Zone IV	40	-	-	-
Zone III	15- 30	17.5	13.5	0.83
Zone II	10- 14	12.5-17.5	11-11.5	0.67-0.83
Zone I	6-12	4-12.5	7.5-10.5	0.17-0.5

Figure 2.6 Summary of the types of structures observed in the films and the correspondent gas flow ranges

2.5.3. Chemical composition

All the four series of samples were characterized by RBS in order to study the chemical composition of samples (see section 3.4.3. for details of the technique).

In Table 2.4 is possible to see the evolution of the atomic percentage of oxygen and nitrogen with the variation of the gas flow. The samples from Series 1 belonging to the Zone I have a small concentration of oxygen, indeed the first sample (6 sccm) has no oxygen which is in agreement with the indexed ZrN structure. With the increase of the reactive flow within Zone I the concentration of nitrogen increases and the oxygen concentration is still very low. In Zone II the concentration of oxygen and nitrogen are in agreement with a smooth transition from the ZrN structure towards a new one, Zr_3N_4. As the flow increases in Zone II the oxygen concentration increases and the nitrogen decreases. With further increase of the gas flow, Zone III, an abrupt increase of the oxygen concentration is observed. This increase is probably correlated to the formation of another structure, Zr_2ON_2. The films prepared with 40 sccm, Zone IV, have the highest oxygen concentration of the Series 1 samples and belong to a ZrO_2 structure.

Series 2, as was already referred, was prepared with a different gas mixture than Series 1. Although the two series presented a similar structural evolution. In terms of the chemical composition, samples within Series 2 present a higher concentration of nitrogen when compared to samples of Series 1 prepared with the same gas flow, which was expectable due to the higher N_2/O_2 ratio of the reactive gas mixture.

Table 2.4 Evolution of the atomic percentage of oxygen and nitrogen for the four structural Zones identified by XRD for the 4 series of samples

Series	1		2		3		4	
	C_O	C_N	C_O	C_N	C_O	C_N	C_O	C_N
Zone IV	64.2	0.0	–		-		-	
Zone III	47.1	11.9						
	14.7	44.5	12.9	47.0	23.0	40.0	19.2	37.1
Zone II	15.8	41.2	-	-	19.9	41.0		
	8.6	46.4	11.4	48.0	19.1	41.0	14.6	41.1
Zone I	5.1	43.0	10.1	47.9	16.0	44.0	14.2	41.3
	0.0	32.4	2.8	41.3	4.8	47,1	7,1	45.7

Series 3 was prepared with the same gas flow mixture than Series 1 but instead of grounded the substrate were biased with -70 V, and the samples were prepared in rotation mode. It was observed that although the samples from Series 3 were prepared using a bias voltage, the

structural evolution was similar to the observed in Series 1 and 2. Regarding the chemical composition, these conditions are equivalent to a deposition made with a higher reactive gas flow. With the increase of the reactive flow the chemical composition of the samples presented an evolution similar to the previous 2 Series.

Series 4 was prepared with the RGPP process as was already referred, and due to this the Series presented a smother increase in the oxygen content and also a smoother decrease in the nitrogen them the former Series. In Series 4 it was possible to observe that the structural evolution of the samples was similar to the evolution of the other 3 series. For the sample belonging to the Zone I, it is possible to see that the oxygen content is higher than the sample from Series 1, which could indicate that introducing oxygen in pulses may have a similar effect to a deposition with a higher gas flow.

The values of the chemical composition were plotted in a ternary diagram (Figure 2.7) in order to make it easier to visualise the evolution of the composition of each Series.

The first observation that can be made is that there is a concentration of the samples in a triangle formed by ZrO_2, Zr_3N_4 and $ZrNO_{0.43}$, which corresponds to a small area of the diagram. Moreover, all the samples appear to share a thin restricted 'band' of the diagram. This concentration can be due to the chosen reactive gas flows, once there is the intension to produce intrinsic coloured films, the flows were restricted to certain values. Additionally, the use of a reactive gas mixture composed of N_2+O_2 causes some composition restrictions namely due to the different chemical reactivity of the gases.

It is possible to see in the diagram that Series 1 goes from ZrN_y compounds (for low N_2+O_2 flows) to ZrO_x compounds. This leads to conclude that at low flows the kinetic of the reaction dominates, leading to the formation of ZrN_y, and with the increase of the flow the samples have increasing amounts of oxygen. If enough oxygen is available the thermodynamic of the reaction dominates leading to the formation of the ZrO_x.

Comparing the evolution of Series 1 and 2 similar tendencies were observed in the two series. It is possible to see in Figure 2.7 that the tendency of Series 1 and 2 have a similar shape but the main difference is that the evolution of Series 2 occurs in a much smoother way and with smaller variations. It was concluded that the lower oxygen content of Series 2 atmosphere plays a decisive role in the smother transitions even though the same tendencies were observed.

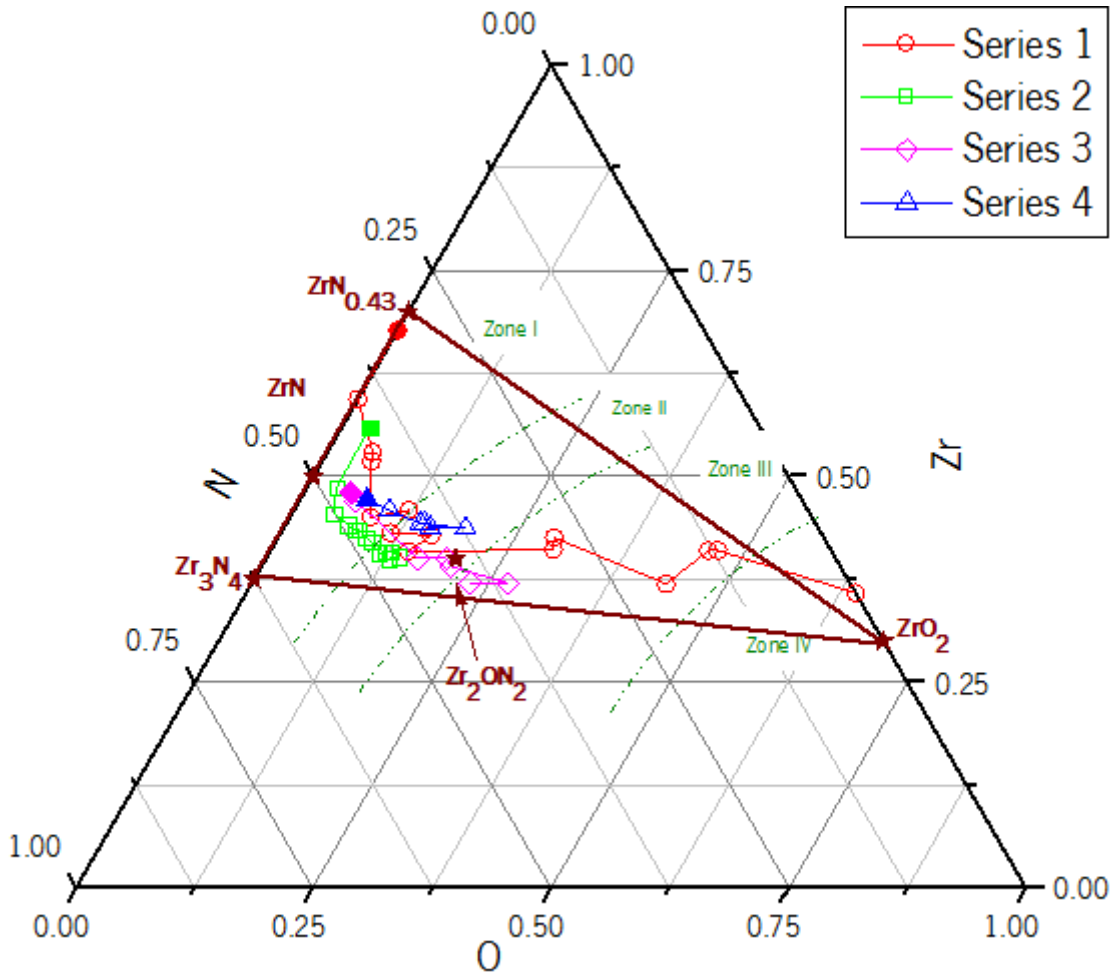

Figure 2.7 Plot of the chemical composition evolution of the four series of samples, the filled point in the series 1-3 represent the lower gas flow, and in the series 4 the lower Ton/T

Regarding the division of the diagram in Zone (Zones I-IV), the division was made based on the structural Zones (Figure 2.5), in order to verify any relation with the composition. In the case of Series 1 the division in Zones is the same of the division made in respect to the structure of the films. In the other 3 Series the limits of the Zones in the diagram are not exactly the same as the limits regarding the structure. This samples have very smooth composition variations from sample to sample, leading to very close points in the diagram. This makes difficult to draw an accurate line. So the division made in the diagram is an approximation once there are samples that in terms of chemical composition belong to one Zone but in terms of structure belong to other.

With Table 2.4 and Figure 2.7 it was possible to see that samples belonging to a certain Zone lay within a certain compositional range, exhibit roughly the same structure. So, even though the four series show differences in terms of composition and structure, those differences

are small and the results indicate a tight correlation between composition and crystalline structure, which in theory would allow to predict the crystalline structure by controlling the composition of the films.

2.5.4. Colour

As was already referred, the evolution of the chemical composition of Series 2, with the increase of the reactive gas, presents a similar tendency of the one observed in Series 1 but with smoother transitions and for different gas flows. In Figure 2.8b the elementary chemical compositions of the two series were overlapped, and the similarities are notorious. Even though the concentration of each element (Zr, N and O) is not exactly the same, it is clear that it follows the same trend and the concentration of each element is relatively similar in both series.

Figure 2.8a shows an overlap of the colour coordinates (see section 3.4.4 for details) of Series 1 and 2. This plot was done using the same shift as in Figure 2.8b. As it has been seen for the chemical composition, also the colour coordinates follow similar trends in both Series 1 and 2, which means that with the increase of the gas flow the evolution of the colour of the coatings is identical for both series.

For Series 3 similar plots were done. In Figure 2.9b it is possible to see the overlap of the elemental chemical composition of Series 1 and 3. In this case the resemblance in the evolution of the chemical composition is not as good as in the case of Series 2, which is particularly visible in the case of the oxygen.

The higher amount of oxygen in Series 3 may appear as an unexpected consequence of the use of bias, since O presents higher resputtering rate then N, due to the lower bond strength with Zr. But, unlike Series 1, Series 3 was prepared with the rotation of the substrate holder. Therefore, during the 'shadow Zone' (i.e. when the substrates are not in front of the target), there is a decrease in the Zr atoms arriving to the substrate, leading to a higher non-metal to metal ratio. Considering the higher chemical affinity of oxygen towards zirconium, the higher incorporation of oxygen in the coatings can be explained.

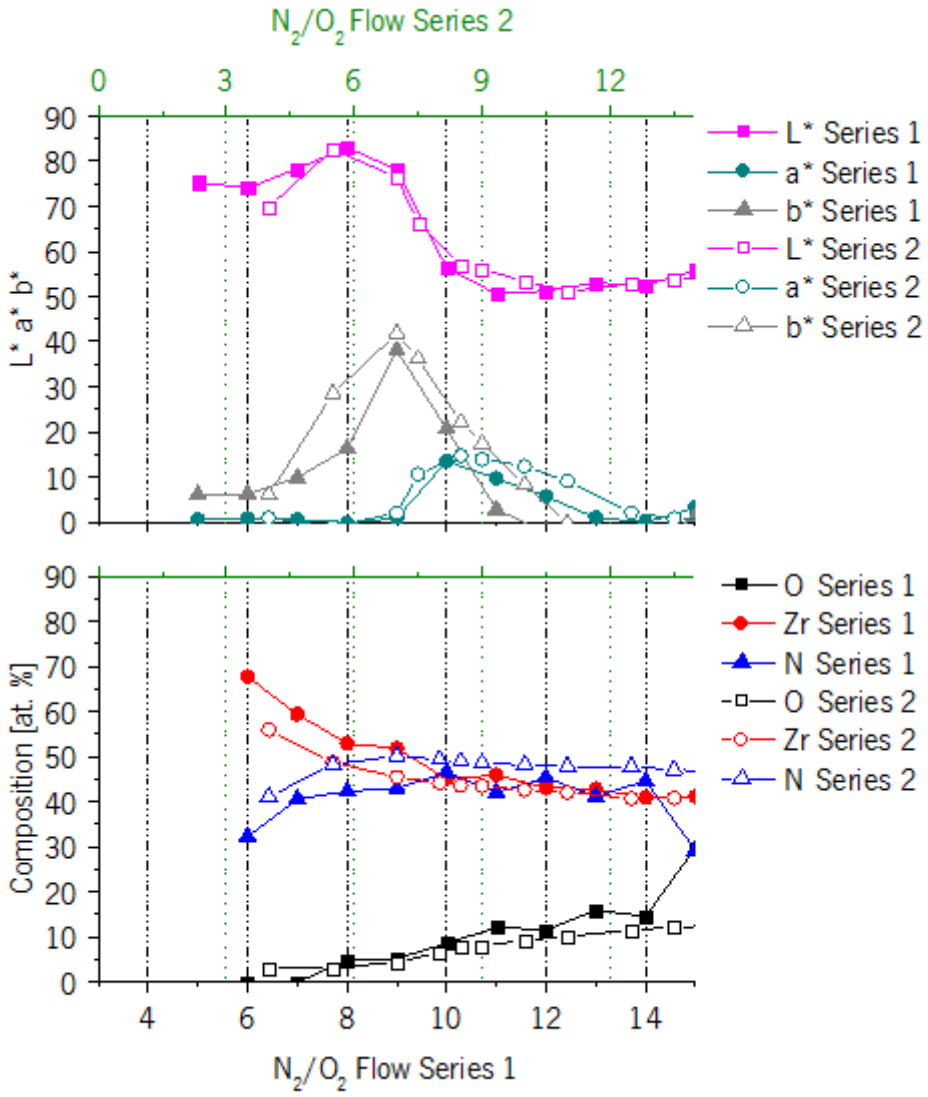

Figure 2.8 Comparison of the evolution of Series 1 and 2 elemental composition and colour coordinates with the deposition flow

In Figure 2.9a it is possible to see the overlap of the colour coordinates of Series 1 and 3. As in the previous case, the shift used in the plot of the chemical composition (Figure 2.9b) was the same used in this plot (Figure 2.9a). It is possible to see that, even though, the evolution is not exactly the same, they follow a similar tendency. The most notorious differences are verified when the chemical composition of the two series differs the most (flow of 10-12 in Series 1), indicating that when the chemical composition is similar the colour coordinates are also similar in the prepared coatings.

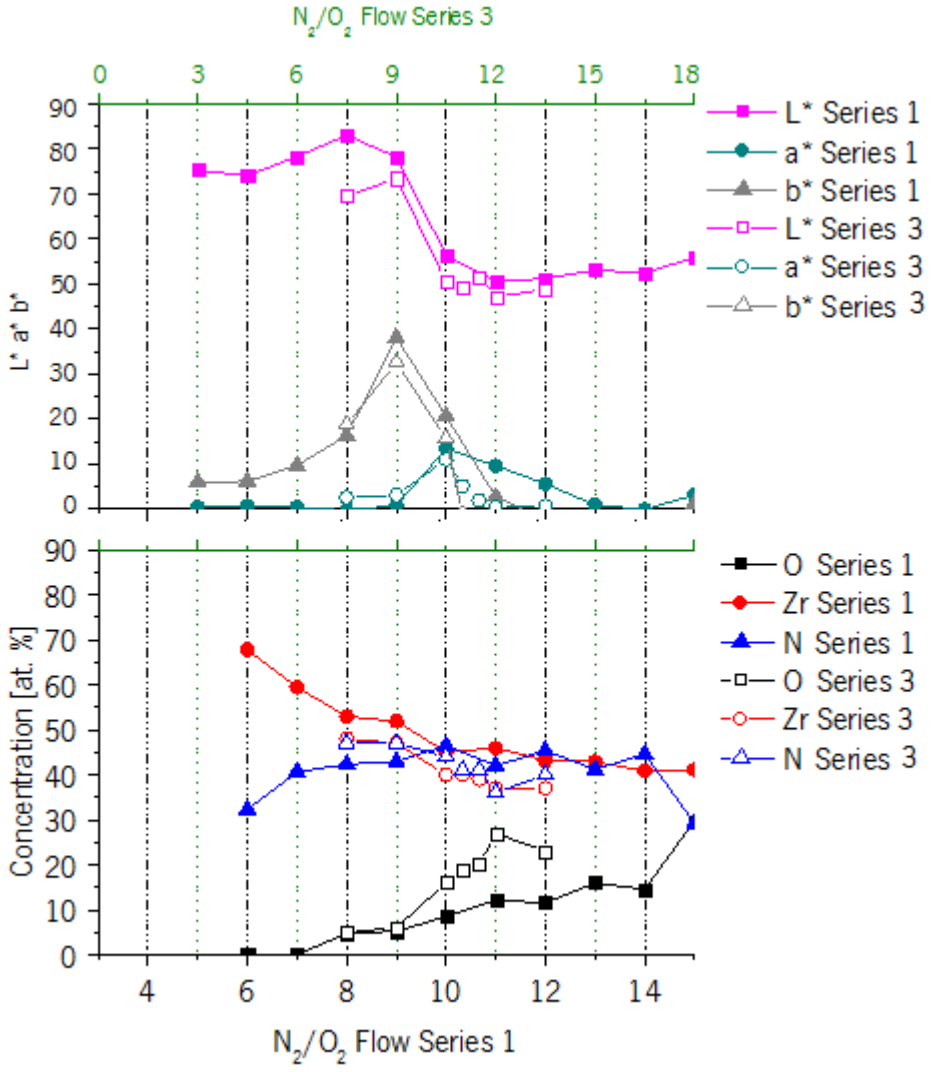

Figure 2.9 Comparison of the evolution of Series 1 and 3 elemental composition and colour coordinates with the deposition flow

It has been stated before that with the parameters used in the production of these films, a certain chemical composition range is correlated to a certain structure. The fact that the shift used to make the chemical composition overlap was the same used in the colour coordinates may lead to conclude that a certain composition is correlated to certain colour coordinates. The main observations made when analysing the plots of Figure 2.8 and Figure 2.9 were that films with similar chemical compositions presented similar colours. In other words, we could state that a certain chemical composition, is related to a certain structure and a certain colour. If this would be true, then this can be used in order to predict the colour of the films based on the chemical composition and structure.

The a* and b* colour coordinates of the four series were plotted in a colour wheel (Figure 2.10) in order to better visualize the evolution of the colour of these four series with the reactive

gas flow. It is possible to see that the evolution of the colour, starts with golden-yellow tones, and, as the flow increases, the colour shifts to red-brownish colours and finally to dark blue.

.

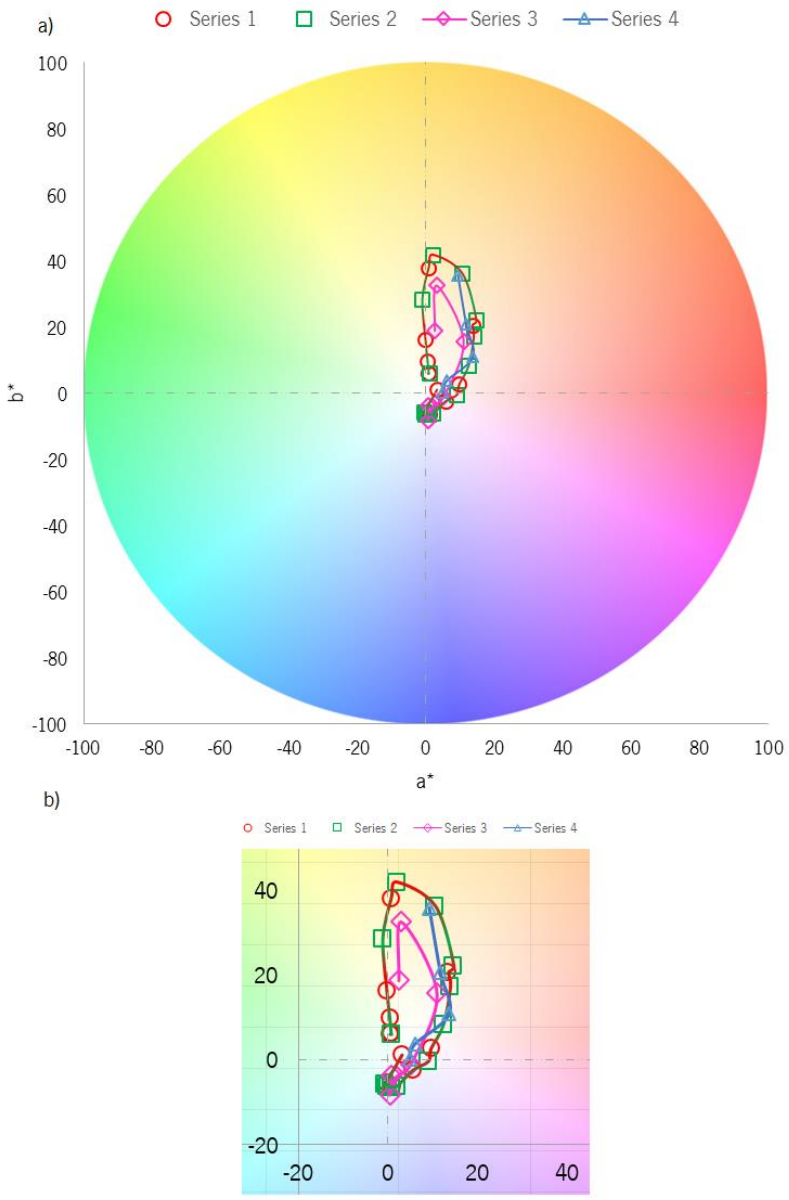

Figure 2.10 Colour coordinates of the four series of samples a) colour wheel b) zoom of the colour wheel

It can be seen that Series 1 and 2 have a very similar evolution of the colour coordinates, as was already seen in the previous plots. The tendency of the two series is so similar that they can be connected by the same tendency line. This similarity in terms of colour is probably related to the high resemblance in terms of chemical composition and structure that was seen previously.

In the case of Series 3 it is possible to see that, even though the evolution of the colour passes through the same colours (golden tones, red-brownish, dark blue), the series covers a

narrower area of the plot. This characteristic may be due to the differences observed in the chemical composition of Series 3 when compared to Series 1.

Series 4 shows a tendency considerably different than the others, but besides that the colour evolution is similar, the colour tones of the first samples are golden but very close to the red Zone of the wheel, and the samples of Zone II and III evolve to red-brownish colours and finally dark blue ones.

It was possible to observe that, as for the ternary diagram (Figure 2.7) the area of the colour wheel covered by the samples is considerably small (less than 3% of the total area). Once more, this is probably due to the limitations imposed to the deposition parameters in order to obtain intrinsic colour and due to some composition restrictions such as different chemical reactivity of the gases. Therefore, one of the objectives of the present investigation is to explore other regions of the composition diagram, and as a consequence reach other regions of the colour wheel

CHAPTER 3

Experimental details

3.1. Introduction

In this work ZrO_xN_y films (some of which doped with titanium) were deposited onto high-speed steel, glass and silicon (100) substrates, by reactive direct current magnetron sputtering in a laboratorial-size deposition equipment. The base series was prepared with varying reactive gas flows and in the following ones, several other parameters were varied (Figure 3.1) in order to understand the influence of each one of them in the characteristic and properties of the coatings, namely the optical ones.

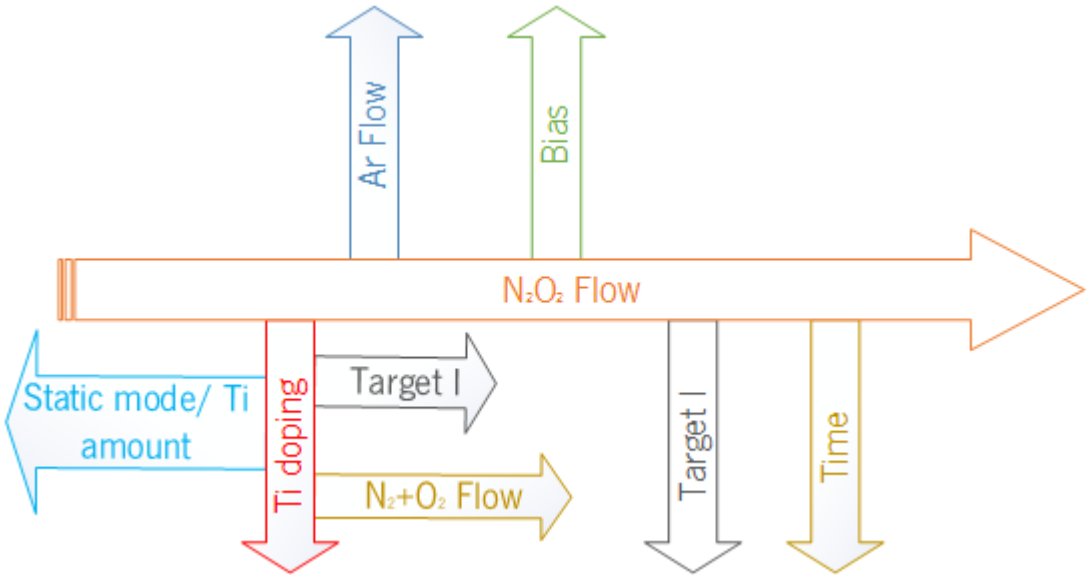

Figure 3.1 Representative scheme of the several parameters changed in the films

The purpose of this thesis was to deposit new coloured coatings for decorative applications. Therefore, ZrO_xN_y coatings were deposited in several batches and then characterized according to the methodology of Figure 3.2 prior to the deposition of the next batch. This sequential approach was used to adjust properly the parameters for the next batch of samples.

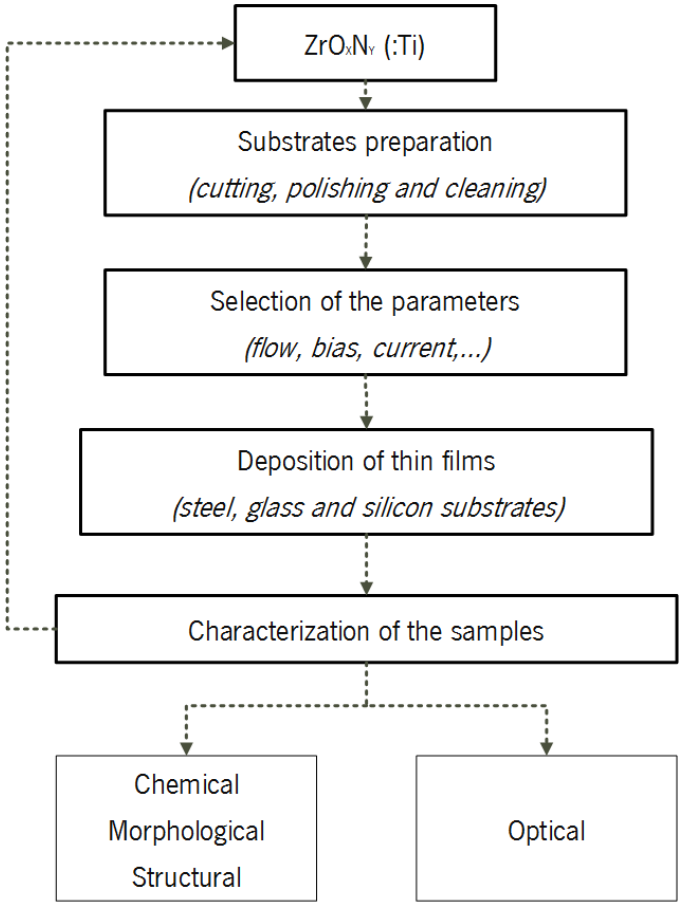

Figure 3.2 Flowchart which summarize the methodology used in this thesis

Before the depositions took place, the preparations of the substrates was performed. The steel substrates (one per deposition, cylinders and with approximated dimensions of 3 cm in diameter and 0.5 cm in height) were mirror-polished and silicon and glass substrates were cut into pieces (five and two per condition, respectively, and with approximated dimensions of 1.5x1.5 cm). Afterwards, all the substrates were sputter etched in a Plasma System Zepto commercialized by Diener equipped with a 40 KHz/100 W generator. The power used was 100 W and the Ar pressure was approximately 80 Pa. Finally, the samples were clamped in the substrate holder, and placed in the deposition chamber.

3.2. Deposition: Reactive magnetron sputtering

Sputtering techniques are among the most used in the deposition of thin films. Sputtering industrial importance ranges from areas such as semiconductor processing, surface finishing and jewellery, among others. The basic sputtering process consists on the acceleration of ionized atoms towards a surface in order to eject atoms from that surface which are latter

condensed onto a sample as a thin film. The same process can be used to remove unwanted material from a surface, a process named sputter etching[59].

Figure 3.3 illustrates the sputtering process. In the sputtering the target is the source of the coating material, and the substrate is placed in the chamber facing the target. The system is then evacuated until pressures in the range of 10^{-6} to 10^{-10} Pa are reached. Argon is typically used as the working gas. The substrate is maintained at ground potential (or biased in some cases). The target is then subjected to a potential (Direct current power – DC in this case) of 0.5-5 KeV in order to produce an electrical discharge[60]. This discharge ionizes the Ar particles giving rise to a plasma[54,60]. The target is negatively biased so the surface is bombarded by argon ions from the plasma and remove target atoms by momentum transfer. The ejected species proceed in the direction of the substrate and are deposited as a thin film. Electrons released during Ar ionization are accelerated to the anode substrate and will collide with Ar atoms, creating more ions and free electrons in the process, continuing the cycle [60].

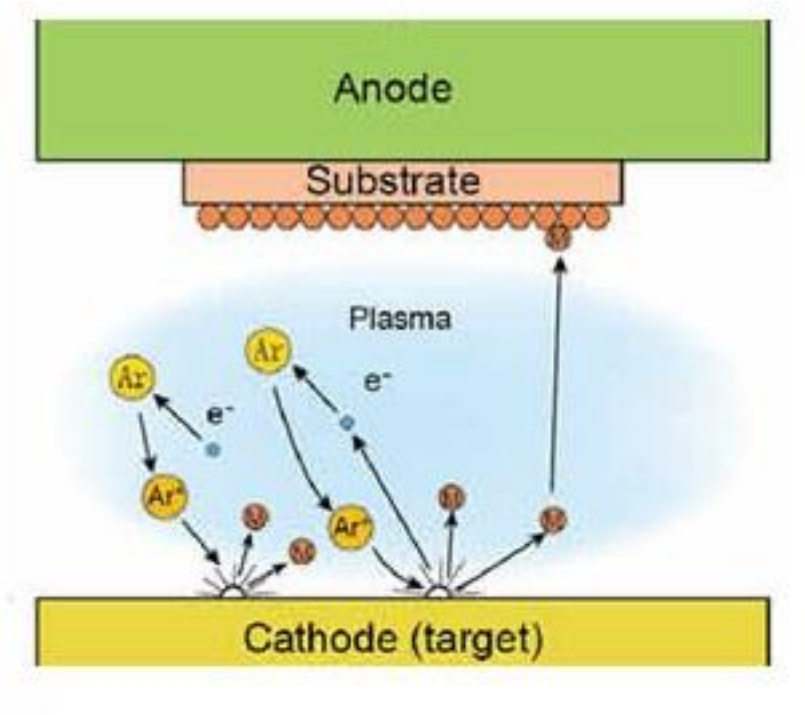

Figure 3.3 Representation of the sputtering process[61]

Initially, sputtering was less used then other possibilities due to the low deposition rates of the process. The ionization efficiency was low and the film usually had inferior properties and substrate heating was common[62].

These limitations were overcome with the development of the magnetron sputtering. Magnetron sputtering consist in imposing a magnetic field near the target. This field limits the

motion of secondary electrons to the neighbourhood of the target and increases their residence time in the discharge. This leads to a higher plasma density at lower reactive gas pressures leading to an increase in the process efficiency, namely in the deposition rate and in the quality of the deposited films[62].

Planar magnetron sputtering has become the most used sputtering configuration, because of the higher quality deposition rate of the films obtained, particularly, when depositing metals in direct current (DC). One of the drawbacks of magnetron sputtering is the non-uniformity of the plasma over the target surface. This can lead to a non-uniform deposition in terms of thickness and film morphology, which creates the necessity to add motion to the substrate with respect to the target. Additionally, the non-uniform plasma also lead to the non-uniform erosion of the target (Figure 3.4), where only 30% of the material is being used in some cases, leading to the known 'race track'[62].

Figure 3.4 Non-uniform erosion of the target – 'race track'[63]

In order to deposit compounds a variation of magnetron sputtering is often used – reactive magnetron sputtering. In reactive magnetron sputtering a reactive gas (e.g. oxygen, nitrogen, methane, and even combination of gases) is inserted in the chamber in addition to the working gas. The material sputtered from the target can react with the reactive gas which is chemically activated by the plasma. A wide range of materials can be produced and the composition can be adjusted, for instance, by the amount of the added reactive gas. This process can be done in two deposition modes, sputtering in metallic mode, with low amount of reactive gas which usually leads to stoichiometric films, and sputtering at high reactive gas amount, which lead to stoichiometric or over-stoichiometric compounds[60,62]. In the transition between these two modes, some process characteristics such as discharge voltage, deposition rate, reactive gas pressure and film composition can present a complex behaviour. This behaviour is

caused by the 'target poisoning', which consist in the deposition of the coating not only in the substrate but also in the surface of the target. This results in a considerable reduction of the sputtering yield and influences other process parameters, making difficult the preparation of intermediate compounds[60,62]. The simplest way to avoid the 'target poisoning' is to insert only enough reactive gas into the chamber to react with the sputtered atoms at the substrate[64].

The deposition system used in the production of the samples studied in this work consisted of a laboratorial size equipment. The depositions were performed in an atmosphere with argon as working gas and a mixture of nitrogen and oxygen as reactive gas, and with a zirconium target 99.6 at. % purity with 10×20 cm of dimension. The base pressure of the depositions was always below 2.0×10^{-5} Pa. The films were prepared with the substrate holder positioned at 75 mm from the magnetron and with a rotational speed of 5 rpm. The discharge parameters (target potential, applied current and work pressure) were monitored during deposition, using a Data Acquisition/Switch Unit Agilent 34970A, with a multifunction module. This unit uses a RS-232 interface and the data acquired with a Benchlink Data Logger III software.

Titanium doping configuration

The samples doped with titanium were not prepared by gluing titanium pieces on the target, which is the typical approach, in order to avoid damaging and contaminating the Zr target for future depositions without Ti doping. Thus, the titanium was introduced by placing two Ti bars in the 'race track' of the zirconium target, according to the scheme depicted in Figure 3.5.

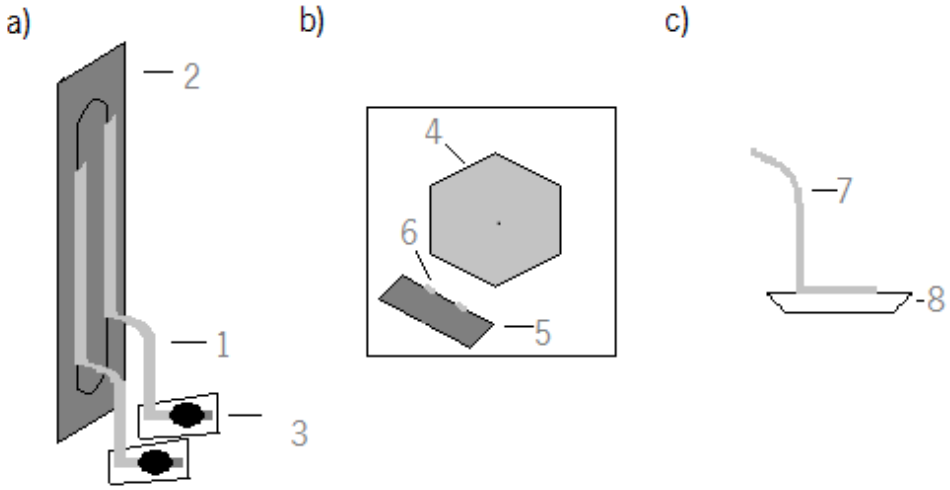

Figure 3.5 Schematic representation of the titanium introduction: a) 1 Titanium bars, 2 Zirconium target and 3 Pieces of glass; b) Top view of the deposition chamber: 4 Substrate holder, 5 zirconium target and 6 Titanium bars; c) 7 Titanium bar, 8 Glass

The bars were placed above a piece of glass in order to isolate them from the chamber and keep them at the same potential as the target. Small heavy steel pieces were placed over them in order to keep them stable. The geometry of the glasses corners (Figure 3.5c) was beneficial in order to avoid film deposition that would connect the bars to the chamber and could lead to shortcuts. The depositions were carried out with the same basic conditions as the ones without titanium, as it will be described in the following section.

3.3. Deposition conditions of the coatings

The conditions used to deposit each batch will be described with detail below. In Figure 3.6 and Figure 3.7 are depicted schemes that illustrate the different parameters used in the deposition of ZrO_xN_y and $Ti:ZrO_xN_y$ samples, respectively.

Table 3.1 summarizes the parameters of the ZrO_xN_y samples produced with different parameters. The nomenclature chosen for the samples starts with letters, which stand for the parameter that is being tuned (RG – Reactive gas; TC – Target Current; WG – working gas; B – bias voltage and T – time), followed by a number that identifies the value of the parameter, and at the end (for all the Zr-N-O samples except the RG series) the value of the reactive gas flow used, in order to easily know to what sample of the base series the sample in question is comparable to. The percentages of N_2+O_2 and Ar flows indicates the percentage in respect to the maximum flow in sccm of the respective flowmeter, which are 50 sccm for the reactive gas mixture and 500 sccm for the working gas (Ar). Although these values only indicate the gas flows in an indirect manner, they were used for convenience, since this was the notation used internally during the realization of this work and a redundant labelling could induce errors. The correspondence between the internal notation used in this thesis and the values of flow in sccm is indicated in Table 3.1.

The RG samples constitute the 'base' series. All the other parameters will be tuned using the base conditions of samples from this series. For example samples TC 1.5 8.5% were produced with the same parameters as RG 8.5%, but with different target currents.

In all the depositions the reactive gas mixture was composed by 85% nitrogen and 15% oxygen (17:3 ratio). The base series was deposited with N_2+O_2 flows ranging from 5% to 30 (2.5 to 15 sccm). The Ar flow was constant at 5% (25 sccm), the deposition time was 60 minutes (except for the samples of 6.25 and 15 sccm), the target current was of 2 A and the samples were grounded.

Table 3.1 Summary of the deposition conditions of the ZrO_xN_y samples. The varied parameters are highlighted in bold.

Sample	Flow of gases				Time	I	Bias
	Ar		N_2+O_2		[min]	[A]	[V]
	[sccm]	%	[sccm]	%			
RG 5%	25.0	5	**2.5**	**5**	60	2.0	0
RG 7.5%	25.0	5	**3.8**	**7.5**	60	2.0	0
RG 8%	25.0	5	**4.0**	**8**	60	2.0	0
RG 8.5%	25.0	5	**4.3**	**8.5**	60	2.0	0
RG 9%	25.0	5	**4.5**	**9**	60	2.0	0
RG 9.5%	25.0	5	**4.8**	**9.5**	60	2.0	0
RG 10%	25.0	5	**5.0**	**10**	60	2.0	0
RG 10.5%	25.0	5	**5.3**	**10.5**	60	2.0	0
RG 11%	25.0	5	**5.5**	**11**	60	2.0	0
RG 12.5%	25.0	5	**6.3**	**12.5**	30	2.0	0
RG 30%	25.0	5	**15**	**30**	30	2.0	0
TC 1.5 7.5%	25.0	5	3.8	7.5	60	**1.5**	0
TC 1.5 8%	25.0	5	4.0	7.5	60	**1.5**	0
TC 1.5 8.5%	25.0	5	4.3	8.0	60	**1.5**	0
TC 2.5 8.5%	25.0	5	4.3	8.8	60	**2.5**	0
WG 8% 8.5%	**40.0**	**8**	4.3	8.5	60	2.0	0
WG 2% 8.5%	**10.0**	**2**	4.3	8.8	60	2.0	0
B -40 8.5%	25.0	5	4.3	8.5	60	2.0	**-40**
B -30 8.5%	25.0	5	4.3	8.8	60	2.0	**-30**
T 30 9%	25.0	5	4.5	9.0	**30**	2.0	0
T 120 9%	25.0	5	4.5	9.0	**120**	2.0	0
T 30 10%	25.0	5	5.0	10	**30**	2.0	0
T 120 10%	25.0	5	5.0	10	**120**	2.0	0

Table 3.1 indicates the deposition characteristics of all the ZrO_xN_y series, and the varying parameter is highlighted in bold. Thus, the TC# samples were deposited with the same basic conditions as the series RG#, with the exception the target current. This parameter ranged from 1.5 A to 2.5 A. The WG# samples were deposited with the same conditions then RG# samples but with Ar flow ranging from 10 to 40 sccm. The samples B# were produced with bias voltages of -40 and -30 V, the other parameters were the same used in the RG#. The samples T# were produced with different depositions times then the RG# samples, with times ranging from 30 to 120 minutes. The dashed lines in Table 3.1 indicate the samples of the RG# series that serve as references. Figure 3.6 helps visualizing the different parameters used.

Table 3.2 summarizes the deposition parameters of the Ti:ZrOxNy films. This samples

were deposited using titanium as a dopant with the configuration explained previously (see Section 3.2). In this batch, 10 different samples were deposited in order to study the influence of titanium doping in the properties of the coatings. The nomenclature of the samples is similar to the one used before. All the samples start with 'Ti' to identify the presence of titanium. The first sample Ti RG 9.5% has the same conditions of the RG 9.5% sample thus the nomenclature chosen. The samples TiTC were deposited with different reactive gas flow, similarly to the RG# series but with 1.5 A, similarly to the RG# series, this sample can be seen as the 'base' deposition conditions of the Ti:ZrOxNy samples. The samples highlighted at yellow were deposited with different target current (2 A). Finally, the samples Ti 1b 8.5% and Ti 1b static 8.5%, besides the different target current, were deposited with less titanium then the others (only one bar), and the latest was done in static mode.

Table 3.2 Deposition parameters of the Ti:Zr-O_x-N_y samples

Samples name	Flow of gases				Time	I	Bias	Ti Bars
	Ar		N2+O2		[min]	[A]	[V]	
	[sccm]	%	[sccm]	%				
Ti RG 9.5%	25.0	5	4.8	9.5	60	2.0	0	2
Ti T30 8.5%	25.0	5	4.3	8.5	30	2.0	0	2
Ti TC1.5 5%	25.0	5	2.5	5.0	60	1.5	0	2
Ti TC1.5 7.5%	25.0	5	3.8	7.5	60	1.5	0	2
Ti TC1.5 8%	25.0	5	4.0	8.0	60	1.5	0	2
Ti TC1.5 8.5%	25.0	5	4.3	8.5	60	1.5	0	2
Ti TC1.5 9.5%	25.0	5	4.8	9.5	60	1.5	0	2
Ti 1b 8.5%	25.0	5	4.3	8.5	60	1.5	0	1
Ti 1b static 8.5%	25.0	5	4.3	8.5	30	1.5	0	1 static

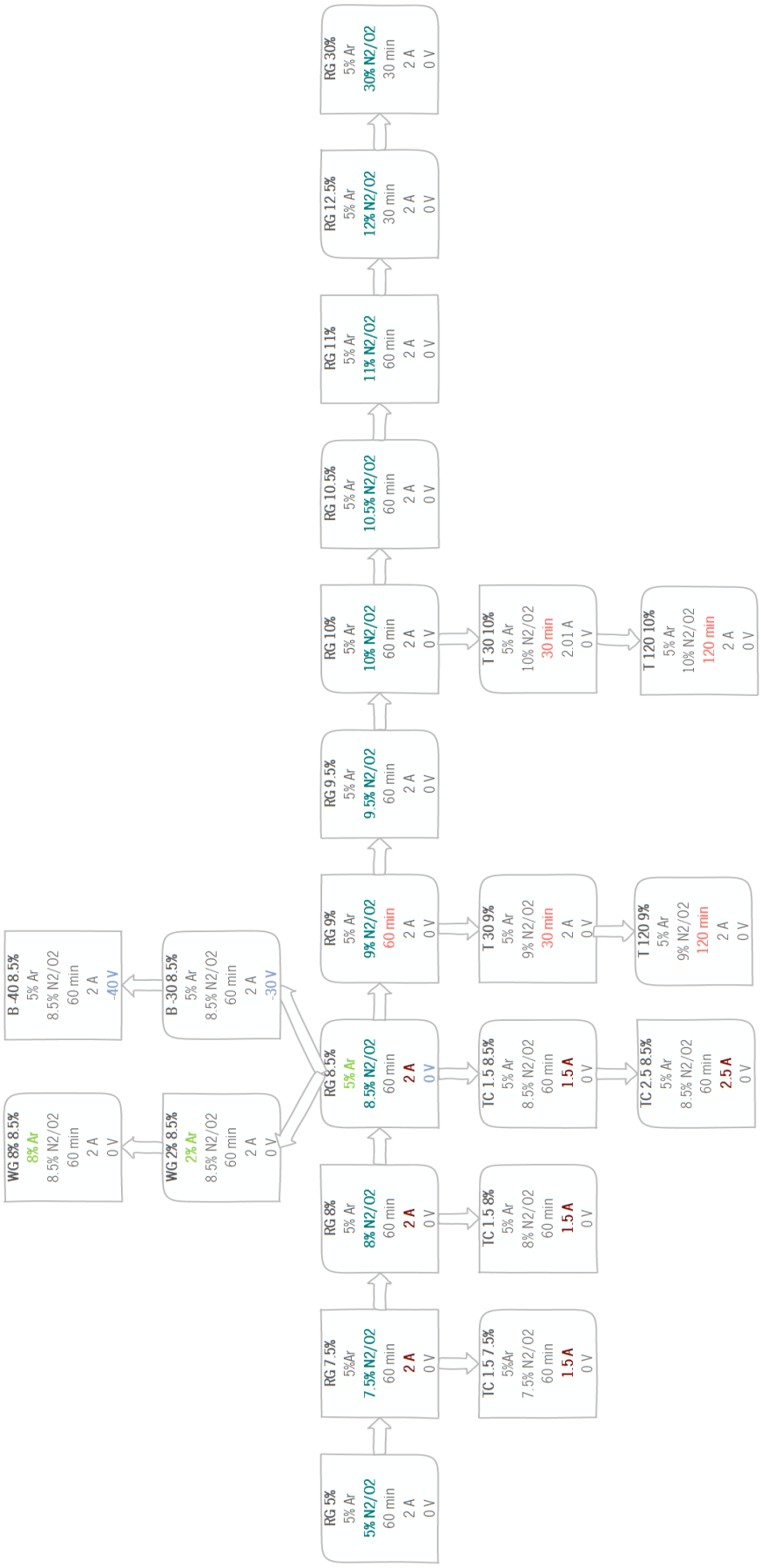

Figure 3.6 Schematic representation of the ZrO_xN_y samples deposited with different parameters

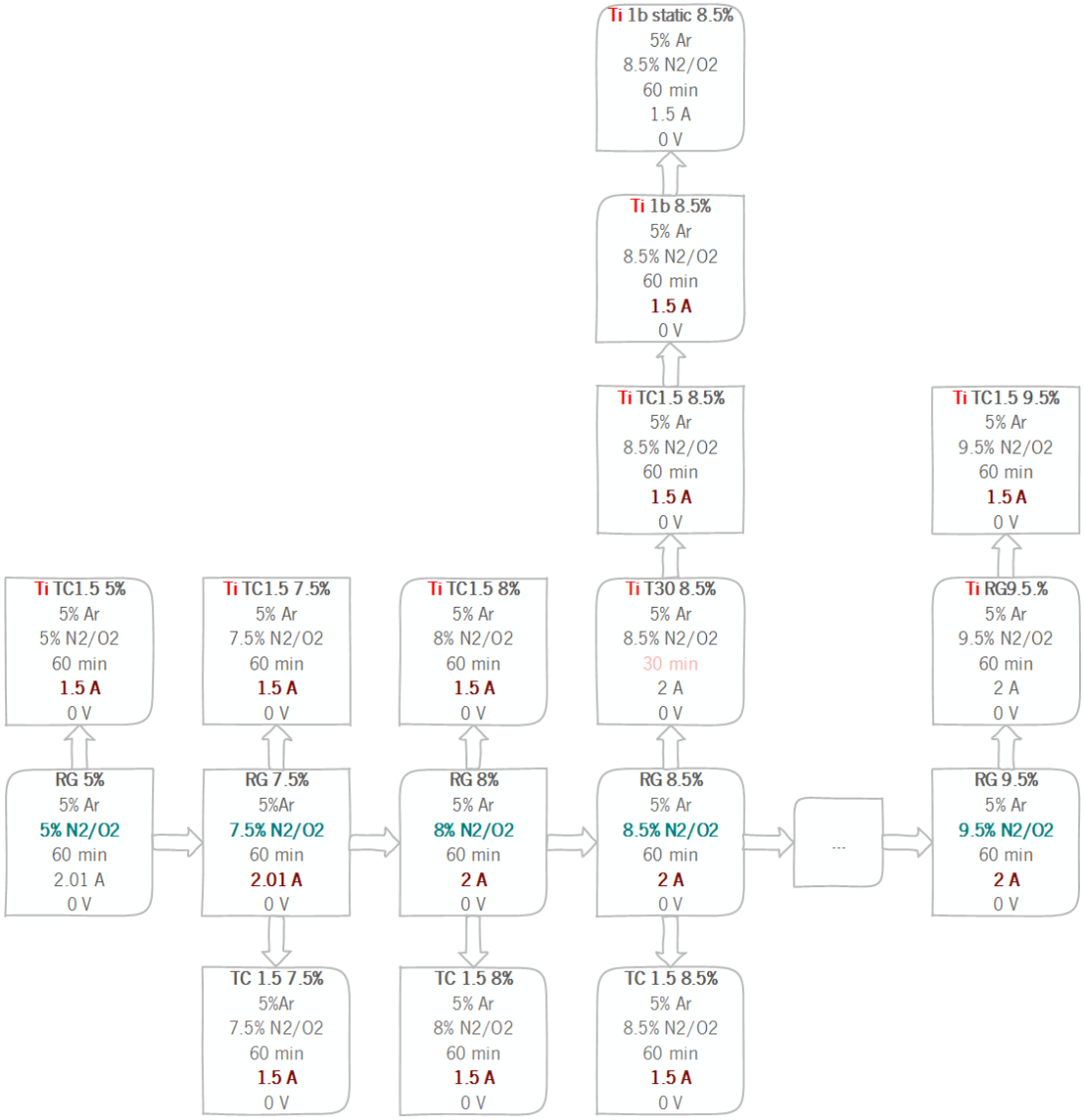

Figure 3.7 Schematic representation of the Ti:Zr-O_x-N_y samples deposited with different parameters

3.4. Characterization techniques

In this section the characterization techniques used in this work will be briefly described as well as the experimental parameters used.

3.4.1. X-ray diffraction

In X-ray diffraction a beam of x-rays is focused on a specimen and it is then diffracted by the crystalline planes present in the sample. The pattern of diffraction is characteristic of each compound (except very few cases), which allows to identify the crystallographic phase. The diffractometer (Figure 3.8) has three main components, the x-rays source, the sample holder, and the detector[65].

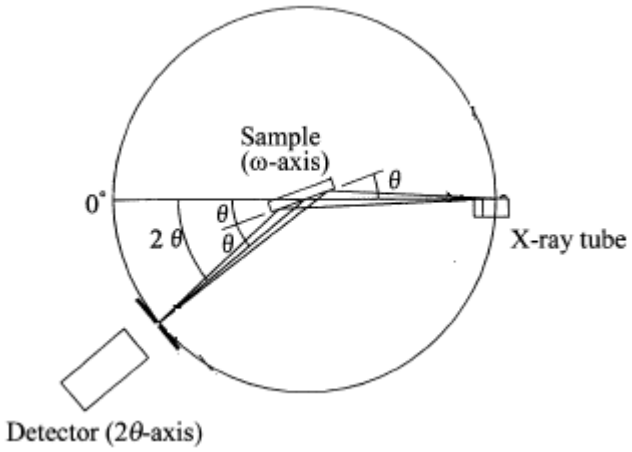

Figure 3.8 Representation of the diffractometer configuration[65]

In this work, in addition to the Bragg Brentano (BB) geometry, the samples were also measured in grazing incidence (GI) at Θ=1º and Θ=4, once in this configuration the x-ray beam is confined within the film due to the lower penetration caused by the low angle incidence of the beam[66]. A comparison between the diffractograms of one of the samples deposited in this work acquired at these three geometries is plotted in Figure 3.9.

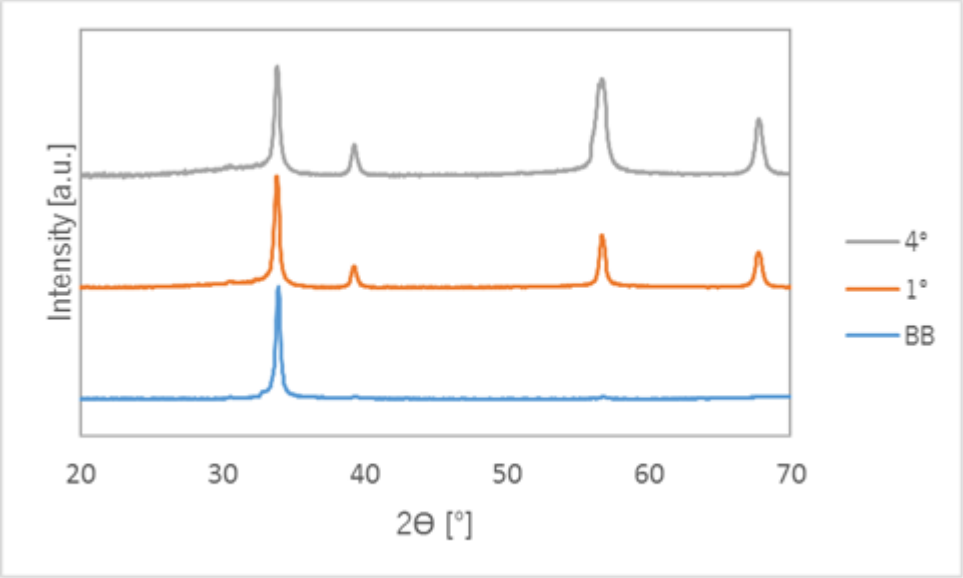

Figure 3.9 Example of the results obtained on the same specimen using the three different geometries explored in the XRD measurements

For this sample and the other it was possible to see that at BB configuration the amount of information obtained from the diffractogram is lower than in the other two geometries. This is

because the thin film nature of the samples under analysis, which causes the beam to penetrate not only the film, but also the substrate. In addition, the crystallographic texture present in thin films due to preferential growth of certain planes may cause to certain peaks to disappear in the BB condition. For both GI geometries it was verified that, even though the results were very similar, the 4° incidence presented in general more pronounced peaks and lower higher signal-to-noise ratio. Therefore, this was the geometry selected to analyse the structure of the samples.

In addition, some of the specimens were subjected to 'in situ' heating during XRD measurement, in order to study the evolution of the structure of the films. The measurements were performed in a vacuum atmosphere with pressures around 10^{-4} mbar – 10^{-5} mbar. The films were then heated from room temperature (r.t.) up to 1000 °C with a heating rate of 20 °C/min, and kept at each temperature for 60 min. The measurements were performed, in grazing incidence, at r.t., 500 °C, 600 °C, 700°C, 800 °C, 900 °C and 1000 °C. Finally, the samples were measured, again, at r.t. after the heating.

In this thesis, x-ray diffraction, including the 'in situ' measurements, were was carried out in MATEIS Laboratory-INSA of Lyon using a x-ray diffraction Brucker D8 Advance System apparatus equipped with Cu Kα radiation (λ = 0.154 nm).

3.4.2. Scanning electron microscopy

Scanning electron microscopy (SEM) is a useful technique in the analyses of topography of materials. In SEM, electrons thermionically emitted from a tungsten or LaB_6 cathode filament are drawn to an anode and focused by two condenser lenses placed one after the other. Scanning coils in the objective lens deflect the beam into the sample(Figure 3.10) [67].

The volume under examination is impinged with a focused electron beam which can be static or dynamic, swiping the sample. The types of signals produced by the incidence of the beam in the surface include secondary electrons, backscattered electrons, characteristic x-rays, and photons of various energies[68]. This signals are obtained from specific emission volumes (Figure 3.11) and collected with appropriated detectors in order to provide information about several characteristics of the sample such as surface topography and crystallography[68,69].

In SEM the signals of greatest interest are the secondary and backscattered electrons, once those vary with the variation of the surface topography. The secondary electrons allow a higher resolution image once they are confined to a volume near the beam's impact area and so they constitute the most common imaging mode[67,68].

In this work, SEM was performed in order to analyse the cross section of the samples namely the growth (dense, columnar) of the films and its thickness.

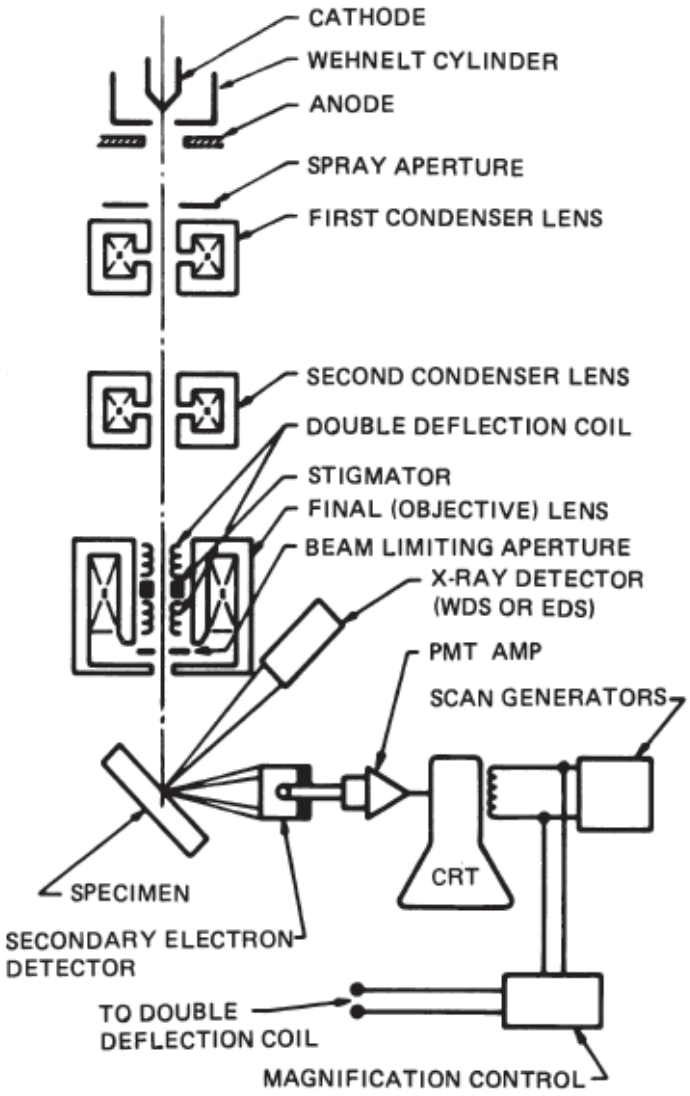

Figure 3.10 Schematic representation of the Scanning electron miscroscope[68]

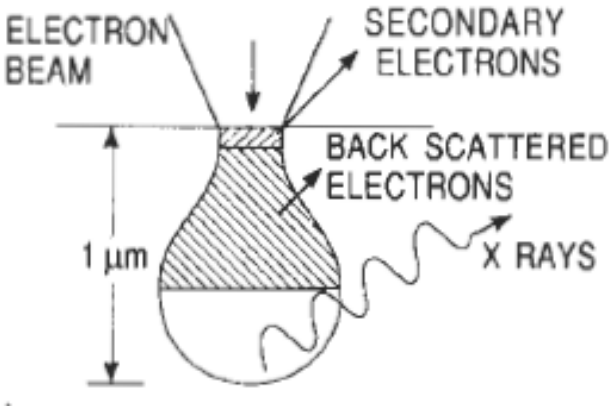

Figure 3.11 Electron beam impingement and signal emission from the sample surface[67]

3.4.3. Rutherford Backscattering Spectroscopy (RBS)

Rutherford backscattering spectroscopy uses a beam of very energetic hydrogen or helium ions to probe the samples[64]. This technique takes advantage of the energy losses of the beam when it collides with the atoms of the sample and is backscattered. The backscattered helium particles are analysed regarding their number and energy, allowing to determine atomic mass and elemental concentration versus the depth bellow the surface[64,67,69].

In this work the atomic composition of the samples was measured in the Centre of Nuclear Sciences and Technologies/ Plasma and Nuclear Fusion Institute of IST – University of Lisbon in the CTN/IST Van der Graaff accelerator in a small chamber were three detectors are installed: standard at 140°, and two pin-diode detectors located symmetrical each other, both at 165° (detector 3 on same side as standard detector 2). Spectra were collected for 2 MeV $^{4}He^{+}$ and for 2.3 MeV $^{1}H^{+}$. The angle of incidence was 0° (normal incidence). The composition profiles (Figure 3.12) for the samples were determined using the software IBA Data Furnace NDF v9.6d.

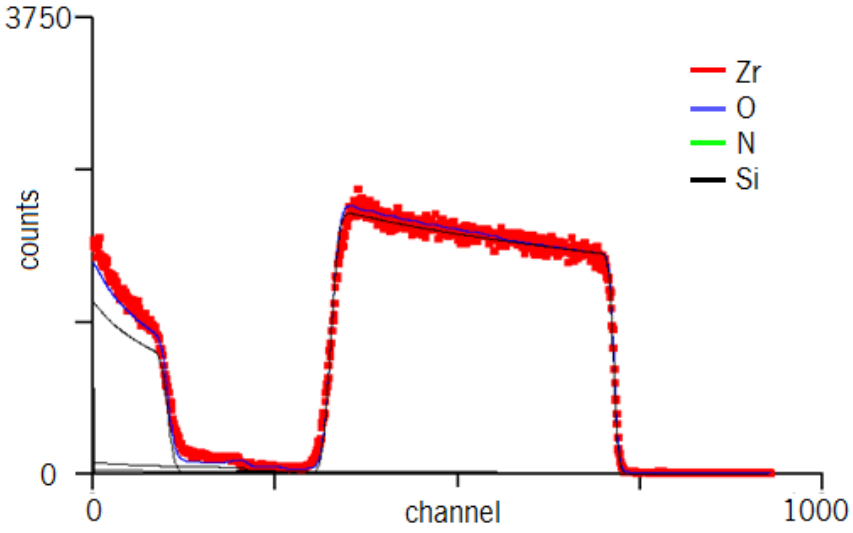

Figure 3.12 Example of a composition profile

3.4.4. Colour spectrophotometry

The spectrophotometer (Figure 3.13) works by focusing a beam of light through the sample, and then measures the ratio of reflected to incident light (reflectance) from the sample at several points through the visible spectrum[14].

The light is then reflected of the sample back to the spectrophotometer to a highly efficient colour analyser which consists of a number of interference filters. Each filter allows a specific wavelength to pass, the spectrophotometer measures the individual wavelengths and

then calculate L*, a* and b* values[14].

Spectrophotometry was performed using a commercial Minolta CM-2600d portable spectrophotometer (wavelength range: 400–700 nm) in order to quantify the colour of the samples according to CIELAB colour space.

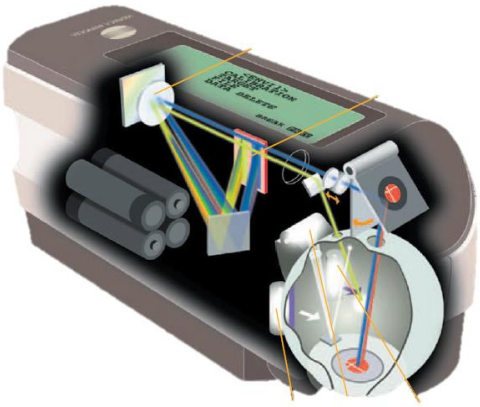

Figure 3.13 Illustration of the spectrophotometer functioning [71]

CIELAB colour space (Figure 3.14) was established in 1976 for application on non-self-luminous colours. CIELAB is a tree dimensional colour space (Figure 3.14) based on three colour values[10]:

- L*: lightness or black-to-white contribution
- a*: red-to-green contribution
- b*: yellow-to-blue contribution.

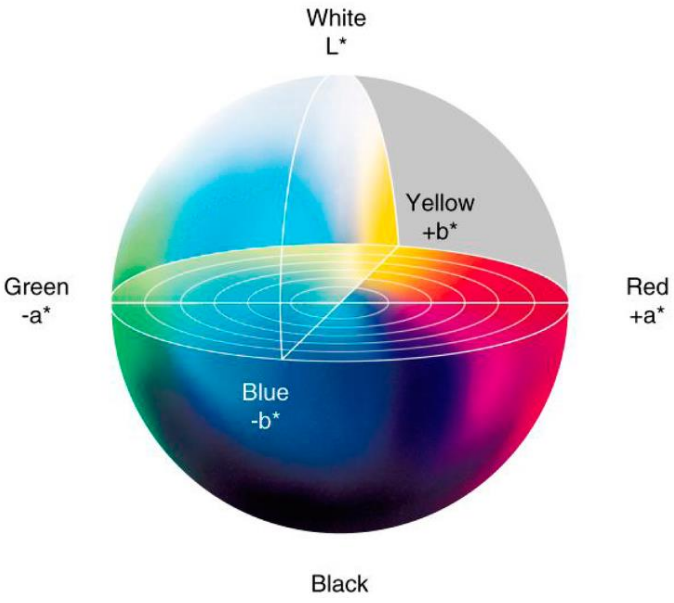

Figure 3.14 Representation of the CIELAB colour space

Using these parameters a particular colour can be described by a unique L*a*b*

coordinates. The system is formed by three orthogonal axes. The L* values range from 0 (ideal black) to 100 (ideal white). The a* and b* coordinates range from -100 to 100 and represent the chromatic part of the colours space. The further way the colours are from the lightness axes, the more chromatic and saturated they are. The colours lying on the axis are called achromatic colours[10].

CHAPTER 4

Variation of the N_2+O_2 flow

In this chapter, the characterization of the films belonging to the reactive gas series, will be presented and discussed in order to understand the behaviour of the system with the increase of the reactive gas flow. The main idea is to evaluate the degree of reproducibility of the work from Carvalho et al. (see section 2.5) in our deposition system. The coatings belonging to RG# series were deposited with the same base conditions as Carvalho's Series 1 i.e. varying the reactive gas flow (see Table 2.3 and Table 3.1: where the conditions used by Carvalho and our conditions are summarized).

4.1. General overview

One of the main findings from Carvalho was the division of samples in three different Zones depending on the N_2+O_2 flow. Therefore, we have performed a similar analysis, in order to find out if the same behaviour was observed in our case, and if so, determine if the characteristics of each Zone are comparable.

To distinguish the different regions, the evolution of three different parameters with the N_2+O_2 flow was considered (see Figure 4.1): deposition rate, target potential and elemental chemical composition.

It is possible to see that the films can be divided in three Zones. The first Zone corresponds to reactive gas flows until 7.5%. This Zone englobes the coatings with the higher deposition rates (> 1.4 μm/h) and lower voltage (< 280 V). Here, with the increase of the reactive gas flow from 5% to 7.5%, a decrease in the deposition rate was observed, and the voltage increased slightly. In terms of chemical composition this Zone corresponds to the coatings deposited with the lowest reactive gas flows, this films have a very low amount of oxygen (~1%) and the highest amount of Zr (> 68%). The N/O ratio is higher than 10.

In the third region (reactive gas flows above 9%) the three samples present a similar deposition rate (around 600 nm/h), considerably lower than the values of the first Zone. In terms of the target potential, the increase of the reactive gas flow causes an increase in the target potential, from values around 307 V to values around 362 V.

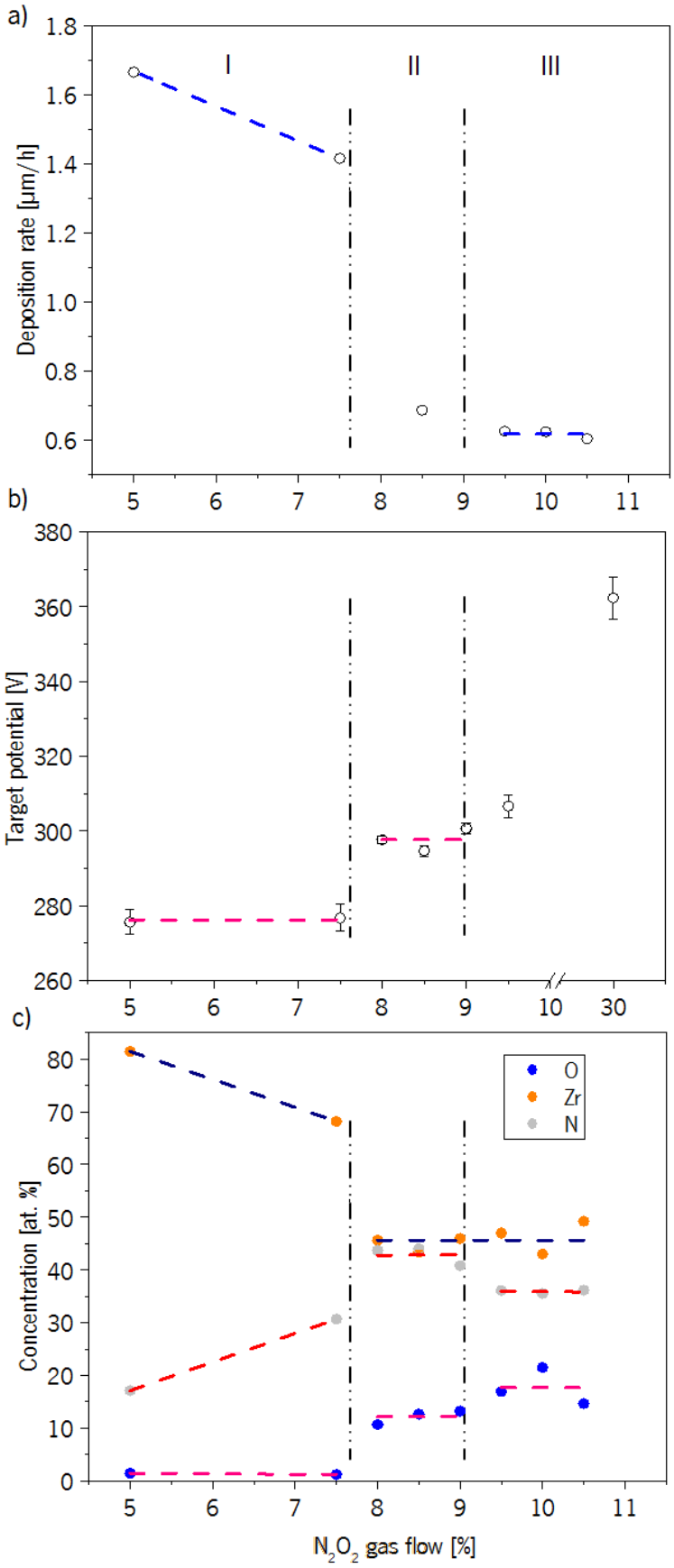

Figure 4.1 Variation with the increase of the reactive gas flow of the: a) Deposition rate; b) Target potential (Equilibrium values - steady state); c) Elemental chemical composition

In this Zone the oxygen concentration has values around 18±3%. The Zr concentration present values of 46±3. And the nitrogen values of 36±1%. The N/O ratio is below 3.

In the second Zone (reactive gas flows between 7.5% and 9%) only one sample was analysed, in terms of deposition rate, so it is not possible to establish a tendency. Nevertheless, the value of the deposition rate was considerably lower than the value of Zone I and slightly higher than the values of Zone III. The voltage in the Zone II is more and less constant (~ 300 V). In this Zone the concentration of oxygen has a value of 12±1%, which is considerably higher than the concentration of the Zone I and slightly lower than the concentration of Zone III. The zirconium content is 44±1% which is considerably lower than the concentration of Zone I and very similar to Zone III. The nitrogen, for its turn, shows higher values than in the other two Zones, with values of 43±2%. The N/O ratio has values lower than 3, similarly to Zone III.

In the literature (Figure 4.2) it is possible to find models of the deposition rate variation in reactive sputtering processes with the increase of the reactive gas partial pressure[21]. The deposition rate is related to the atmosphere present in the deposition chamber and allows to differentiate the films as metallic-like, oxide-like, etc.

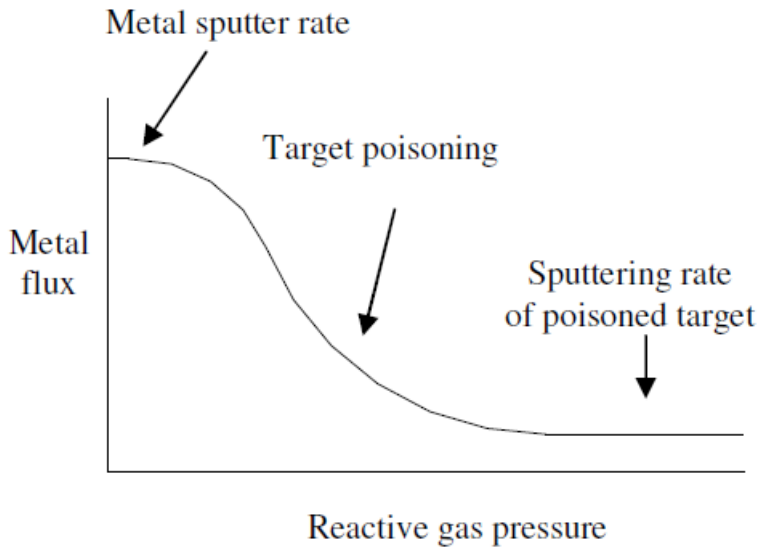

Figure 4.2 Model of the Evolution of the metal flux as a function of reactive gas pressure[21]

At low gas flows the cleaning sputtering rate overcomes the poisoning rate, and a metal flux arrives to the substrate leading to higher deposition rates. When the poisoning rate is higher than the cleaning rate a partial poisoning of the surface of the target occurs. Once the sputtering yield of metal atoms from the poisoned surface is smaller than the non-poisoned surface, the

metal flux from the target decreases with the increase of the reactive gas pressure until the entire poisoning of the target.

The variation of the deposition rate with the reactive gas flow (Figure 4.1a) resembles the model from Figure 4.2 and so it can be concluded that Zone I corresponds to metallic-like coatings produced with higher deposition rates, leading to the ticker samples. In this Zone, the cleaning rate is higher than the poisoning rate, and a high metal flux is expected. At the substrate, for low reactive gas pressure, the formation rate of the film is limited by the impact rate and the used of reactive gas atoms. Even though oxygen is more reactive with zirconium than nitrogen, the N_2/O_2 ratio in this zone is very high; this is because the low concentration of oxygen in the reactive atmosphere (15% of O_2 in the reactive gas mixture, together with the low gas flow of the reactive mixture) and the high rate of metal atoms arriving to the substrate the kinetics of the reaction is dominant over the thermodynamics, leading to the formation of ZrNy–type compounds. This phenomenon is visible in the chemical composition that, as it was seen, has a high amount of Zr and very low O.

In Zone II the target potential shows a more and less linear increase congruent with an increase in the target poisoning, meaning that the target has to work at higher potential in order to overcome this effect. Thus, in this Zone the poisoning rate starts to get higher than the cleaning rate leading to the poisoning of the target. As a consequence, the samples from Zone II were deposited with lower deposition rate than the previous Zone. The decrease of the zirconium concentration relatively to the previous Zone can be related to the increase of the reactive gas amount, since more reactive gas is available to react it is expected an increase in the non-metal incorporation in the coatings with a decrease in the Zr content. In addition, the rate of sputtered Zr decreases. Under these circumstances, a mixture of behaviours with the thermodynamic of the reaction starting to play a role together with the kinetics is expected.

Zone III is consistent with an increasingly higher state of poisoning of the target. It was expected that the value of the potential reached a maximum which would be similar among the samples of this Zone, indicating a completely poisoned target This behaviour was verified for the deposition rates, which were very similar in the three samples of this Zone, but the target potential presented a continuous increase which suggests that a total poisoning of the target was yet to be reached, but that will eventually be the case with a continuous increase in the reactive gas flow. It is expectable that the thermodynamics of the reaction has an increasing role in the formation of the films, leading to a higher incorporation of O with further increase of the reactive gas flow at expenses of both nitrogen and zirconium concentrations, and, eventually, reach

composition characteristic ZrO_x-type films. Such behaviour is indeed observed in Figure 4.1c.

4.2. Chemical composition

Table 4.1 summarizes the elemental chemical composition and thickness of the films deposited with different values of the reactive gas flow. In Figure 4.3 those values (which were previously shown in Figure 4.1c were plotted in a ternary diagram in order to observe the general tendency of the chemical composition with the reactive gas flow and compare with the overall behaviour of the coatings deposited by Carvalho (Figure 2.7)

Table 4.1 Chemical characterization and thickness of the RG# samples

Sample	Zr [at. %]	O [at. %]	N [at. %]	Thickness [µm]
RG# 5%	81.4	1.4	17.1	1.39
RG# 7.5%	68.1	1.2	30.7	1.18
RG# 8%	45.6	10.7	43.7	-
RG# 8.5%	43.4	12.6	44.0	0.69
RG# 9%	45.9	13.2	40.8	-
RG# 9.5%	47.0	16.9	36.1	0.63
RG# 10%	43.0	21.5	35.5	0.62
RG# 10.5%	49.2	14.6	36.2	0.60

It is possible to see that the samples are restricted to a small area of the diagram, in good agreement with the results of Carvalho (see section 2.5.3). This is a consequence of the parameters selected to obtain intrinsic coloured coatings, which lead to composition restrictions caused by the different chemical reactivity of the gases.

In this diagram (Figure 4.3), the three different Zones identified previously are indicated with dashed lines.

The overall tendency of the elemental concentration presented the expected evolution. It is also possible to see that the evolution of the composition seen on Figure 4.3 resembles the evolution of Carvalho's Series 1 (Figure 2.6) which was deposited with the same basic condition and reactive gas flow mixture then the RG# Series. The main difference between both tendencies is that RG# Series is located in a narrower place of the diagram then Carvalho's Series 1. This is, probably, due to the reactive gas variation range which was between 2.5 and 5.25 sccm in

opposition to the range of 6 to 40 sccm used by Carvalho.

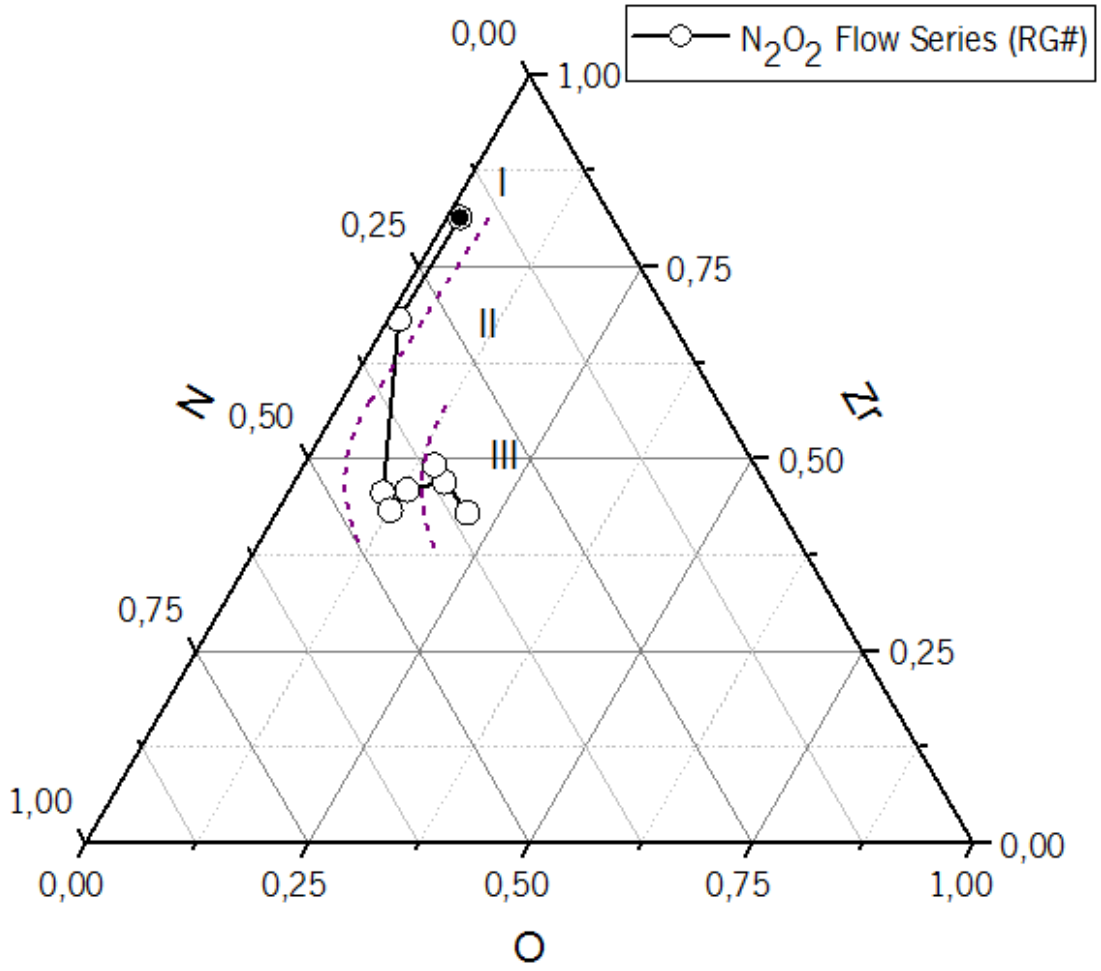

Figure 4.3 Ternary diagram of the composition evolution of the samples with the increase of the reactive gas flow. The filed dot corresponds to the samples with the lowest reactive gas flow.

In Table 4.2 it is possible to see the elemental chemical composition of each region limit samples for both the RG# Series and Carvalho's Series 1. The samples of both series were organized in terms of the chemical composition (namely O concentration). It can be seen that the compositional ranges of both series in each Zone is very similar, so a parallelism between each Zone of the two series can be established. The main difference are the flow ranges that limit each Zone. It is possible to see that the RG# Series presents similar composition as Carvalho's Series 1 for lower N_2+O_2 flows. Even though the N_2/O_2 ratio was the same in the two series, the samples from Carvalho were deposited in static mode, while the RG# samples were deposited with substrate rotation. During the 'shadow Zone' (when the substrates are not facing the target) there is a decrease in the amount of Zr arriving to the substrate leading to a higher non-metal content in the films. In other words, for the same N_2+O_2 flow a sample from the RG# Series will present less Zr than the corresponding sample from the Carvalho's Series 1. In addition, since

the oxygen has higher reactivity with zirconium than nitrogen, this effect can lead to a higher amount of oxygen in the coatings.

Table 4.2 chemical composition of each Zone limits for RG# series and Carvalho's series 1

Zones	N_2+O_2 Flow (RG# samples)	Zr	O	N	N_2+O_2 Flow (Carvalho's series 1)
I	5%	81	1	17	
		68	0	32	6%
	7.5%	68	1	31	
		52	5	43	9%
II		45	9	47	10%
	8%	46	11	44	
	9%	46	13	41	
		43	16	41	14%
III		41	15	44	15%
	9.5%	47	17	36	
	10%*	43	21	36	
		41	47	12	30%
IV		36	64	0	40%

4.3. Microstructure

The SEM cross section micrographs of the several RG# series samples are depicted in Figure 4.4 , and the measured thickness of the films are summarized in Table 4.1.

The samples from Zone I (RG 5% and RG 7.5%) have a considerably higher thickness then the other samples being the RG 5% film the thickest. As indicated previously (Figure 4.1) these samples have the highest deposition rates. The remaining samples from both Zone II and III have similar deposition rates which are considerably lower than that from Zone I.

The microstructure of the films of the RG# Series can be better appreciated on Figure 4.5, which shows the SEM cross section at higher magnification than in Figure 4.4. The first two samples (Figure 4.5a and b) are the ones that were previously indexed to Zone I.

Both samples reveal a columnar morphology, which is typical in films deposited by PVD. In addition, with the increase of the reactive gas flow from 5% to 7.5%, the columns appear to become narrower and more defined. Regarding the indexation to the Thornton's Zone model (Figure 2.5), both samples seem to be located in the Zone T.

The sample from Zone II (Figure 4.5 c) also presents a columnar morphology which is similar to the latest sample from Zone I although the columns seem to be narrower. Therefore, it can be also classified in the Zone T according to the Thornton's model.

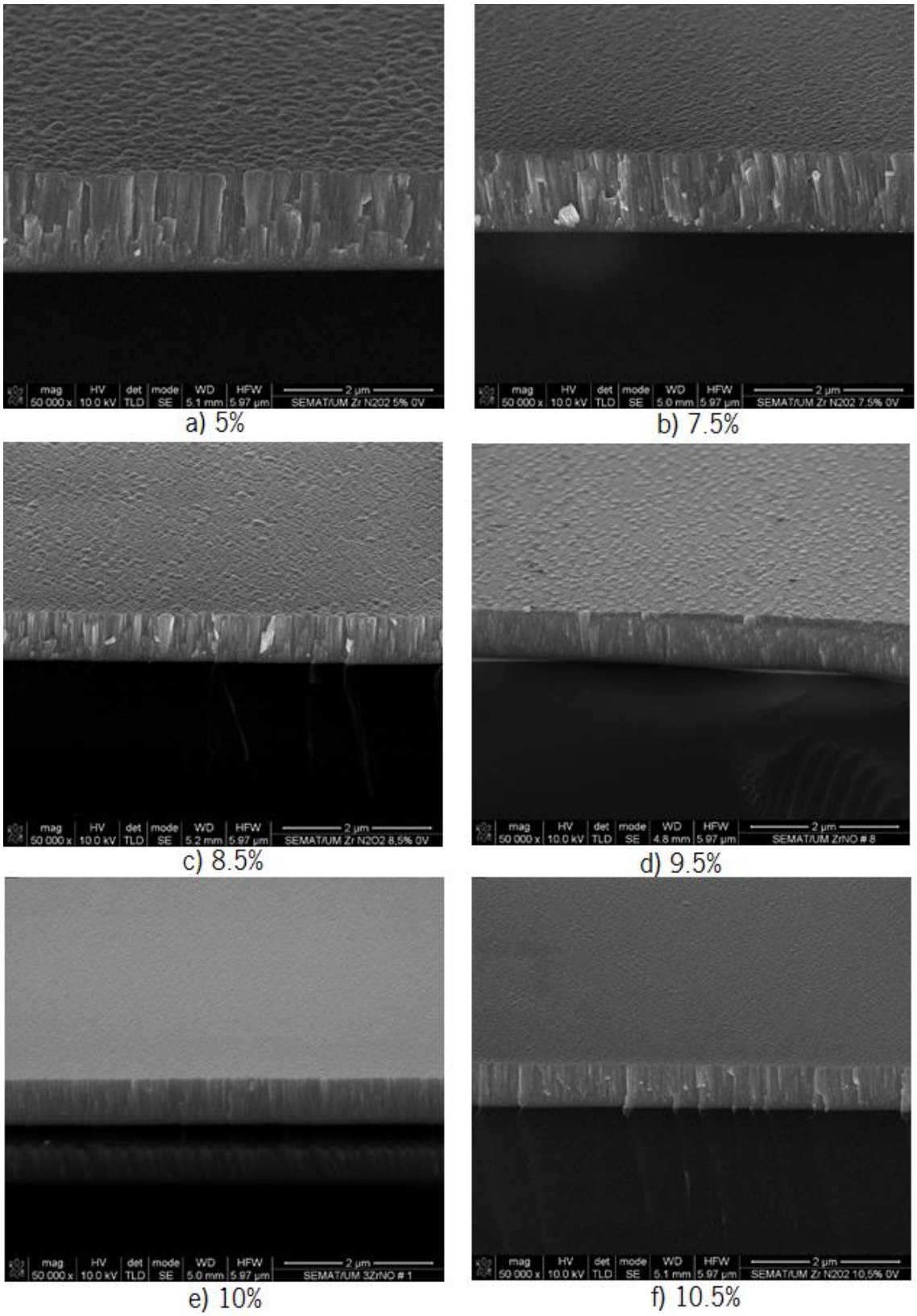

Figure 4.4 SEM cross section images of films prepared at different reactive gas flows: a) RG 5%; b) RG 7.5%; c) RG 8.5%; d) RG 9.5%; e) RG 10%; f) RG 10.5%.

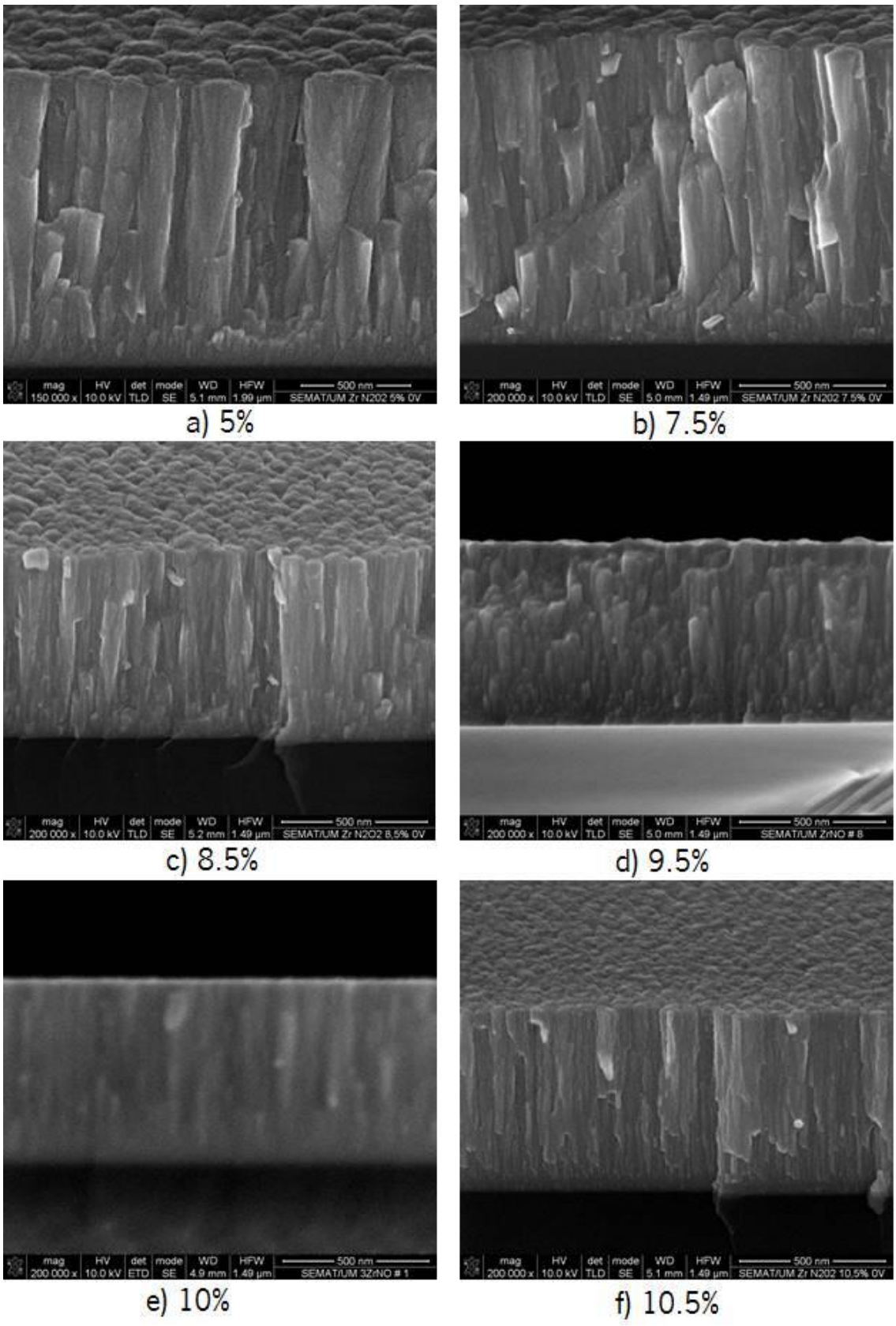

Figure 4.5 SEM cross section images at higher magnification of samples prepared at different reactive gas flows: a) RG 5%; b) RG 7.5%; c) RG 8.5%; d) RG 9.5%; e) RG 10%; f) RG 10.5%.

In the coatings from Zone III (Figure 4.5 d to f) it is possible to appreciate a change in the microstructure. The columnar structure starts to vanish (in Figure 4.5d, the columns start to appear interrupted) and the films start to present a more dense structure. With further increase in the gas flow (Figure 4.5f) the compact structure becomes even more obvious and the coatings exhibit a more featureless microstructure. Regarding to the Thornton's Zone model, the samples from Zone III can be index to a transition between Zone T and Zone I.

The overall morphology of the RG# Series reveal columnar features characteristic from PVD films. It was possible to see that the main difference with the increase of the reactive flow is the narrowing of the column size that ends with almost featureless samples.

4.4. Crystallographic structure

Representative samples were selected in order to study the influence of the different deposition parameters in the structural features of the samples.

Figure 4.6 shows the XRD diffractograms acquired at GI of 4° of the RG# series with reactive gas flows between 5% and 10.5%.

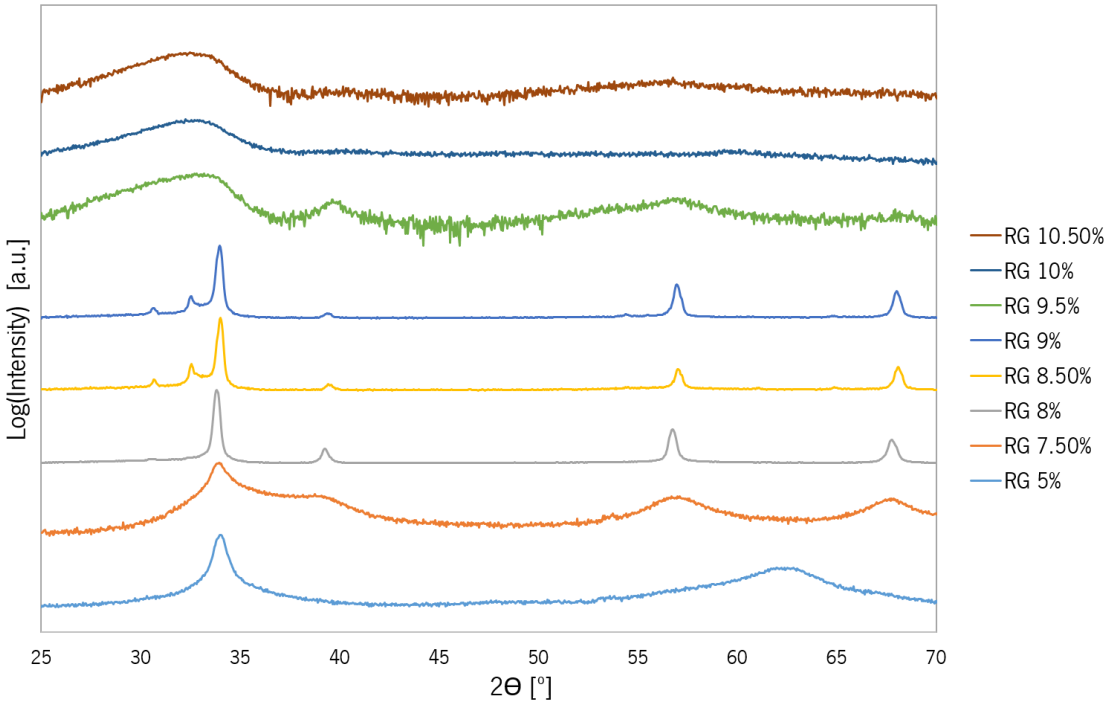

Figure 4.6 Diffractograms at 4° GI of the films prepared at different values of the reactive gas flow

It can be seen that the samples can be divided into 3 Zones in terms of structural features. Zone I is formed by the samples RG 5% and RG 7.5% (N_2+O_2 flow below 8%), the Zone II

contains the samples RG 8% to RG 9% (flows between 8 and 9%), and Zone III is composed by the samples RG 9.5% to RG 10.5% (flows above 9%). This division is in agreement with what described in Section 4.1. The three structural Zones will be analysed with detail below.

4.4.1. Zone I

The diffractogram of samples belonging to Zone 1 are presented in Figure 4.7 with the respective phase identification. Both samples present broad peaks consistent with an amorphous structure. It was possible to verify that the samples crystalize in a FCC structure characteristic of the ZrN films. The identification of these samples as ZrN-Type phase is in agreement with their chemical composition, which has very low oxygen content. As a consequence, no oxygen-containing phases were identified. It was also possible to notice that the sample RG 5% presents a peak consistent with a Zr phase. As indicated before, this coating has the highest deposition rate and the lowest flow of reactive gases. Thus, some Zr was probably deposited without reacting with the O and N.

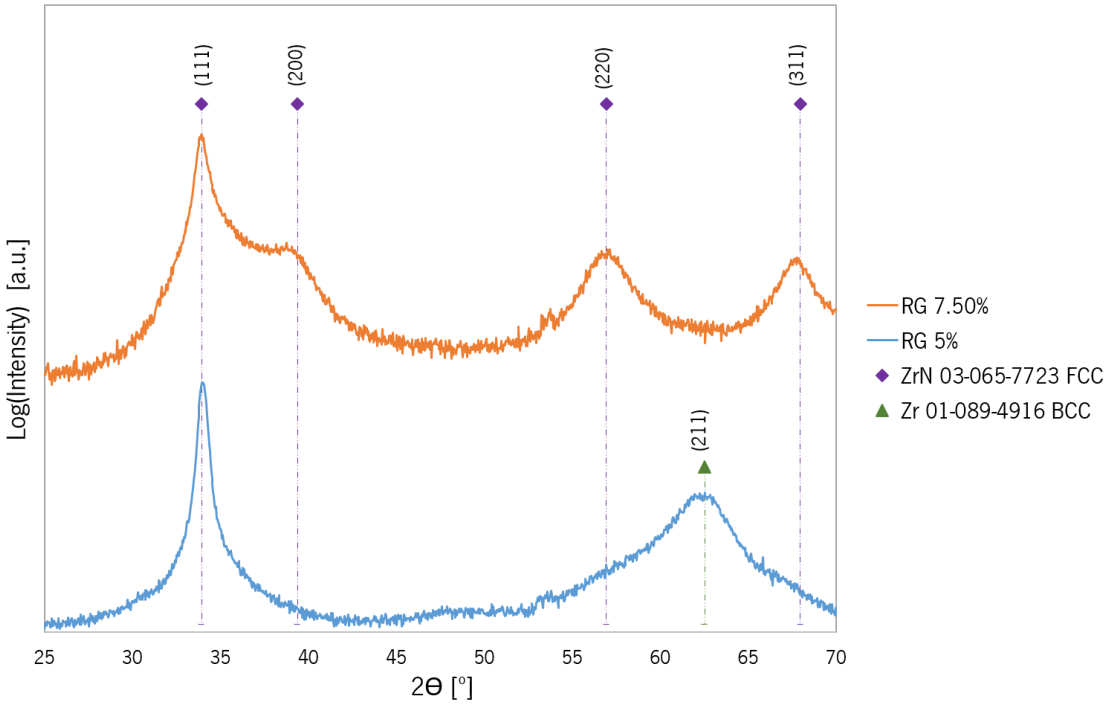

Figure 4.7 Diffractogram of the films belonging to Zone 1, with the respective indexed crystallographic phases

It is possible to see that with the increase of the gas flow from 5% to 7.5%, the preferred orientation of the film growth starts to change from (111) to the other crystallographic planes (200), (220) and (311).

These results are similar to what has been studied in literature for reactively sputtered ZrN_y films[21], results indicate that the preferred orientation is determined by the lowest energy plane, such process consists on a competition between the lowest strain energy (which comes from (111) plane and the lowest surface energy (plane (200)). The ZrN_y films deposited under similar conditions as in this work show strong (111) preferred orientations (as in the case of the RG 5% sample) and for N/Zr ratios approaching stoichiometry the (200) peak has a higher intensity. Thus, further increasing in the reactive gas flow inside Zone I should lead to a higher intensity of the (200) peak as the N/Zr ratio approaches the stoichiometry.

4.4.2. Zone II

The diffractograms at 4° from the samples identified as belonging to the Zone II are depicted in Figure 4.8. The three samples have very similar structure, being the main difference the relative intensity of the peaks. These samples have much more shaper peaks than films of Zone I, which indicates a better crystallinity and larger grain size.

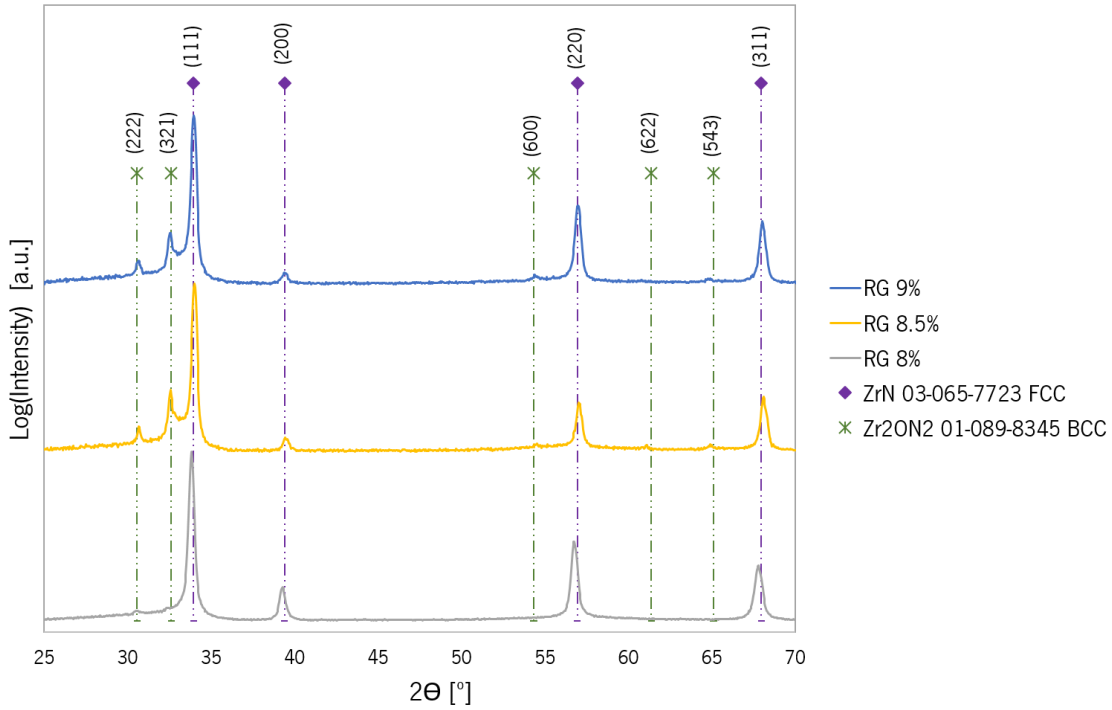

Figure 4.8 Diffractogram of the films of Zone II with the respective indexed crystallographic phases

The samples from Zone II present all the characteristic peaks from ZrN, being the (111) the most intense peak.

With the increase in the reactive gas flow from Zone I to Zone II the composition shows

an abrupt increase in the oxygen content (Table 4.1). This change is correlated with the formation of a new structure which is observed in the diffractograms from Figure 4.8. This structure was identified as Zr_2ON_2.

The first sample from Zone II presents a very low intensity of the Zr_2ON_2 peaks, which increases slightly for the sample with 8.5% and remains more or less constant for the sample with 9%.

4.4.3. Zone III

The diffractograms obtained at 4° for the samples of Zone III are included in Figure 4.9. The three films have similar structures with an initial broad peak located between 30 ° and 35 ° and other smaller broad contributions.

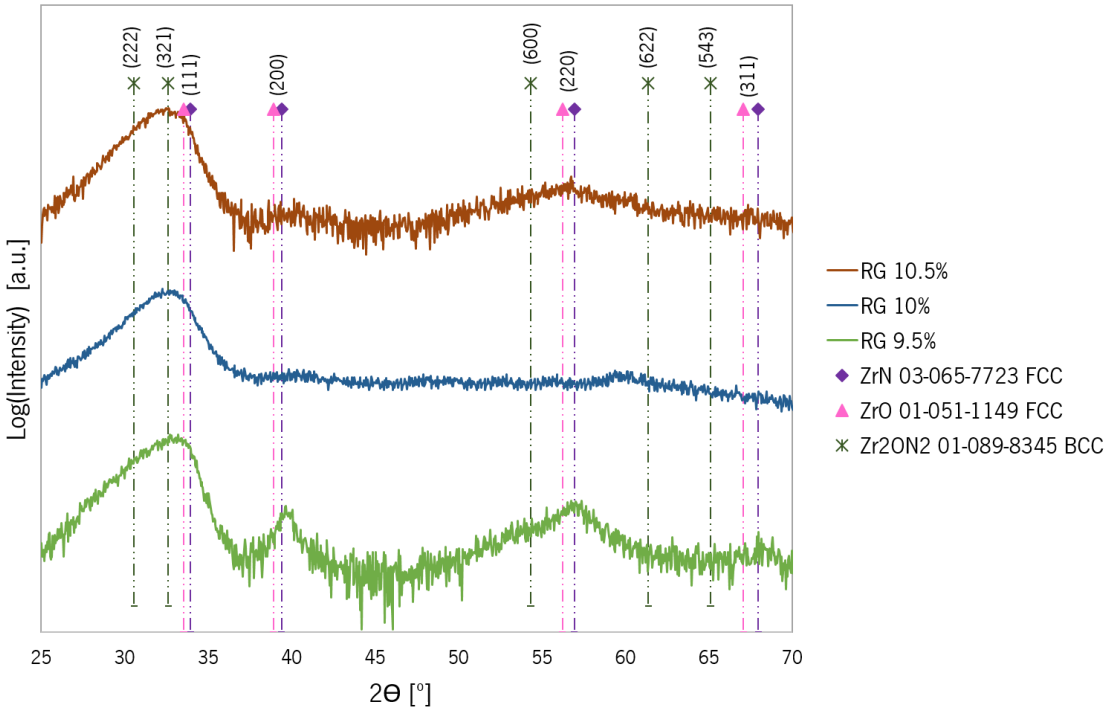

Figure 4.9 Diffractogram of the samples belonging to Zone III with the respective indexed crystallographic phases

The increase in the oxygen content is followed by a loss of crystallinity, leading to films which are practically amorphous. The loss in crystallinity is related to the increase in the oxygen content promoted by the increase in the reactive gas flow. The increase of the oxygen content above supersaturation reduces the possibility of crystallization, mainly the crystallization of ZrN. The incorporation of oxygen in the Zirconium nitride structure, forming a Zr-N-O phase (ZrN and ZrO are isostructural), can occur and will cause its deformation and the number of defects promoting the amorphization. This oxygen perturbation explains the broadening of the peaks. In

fact, the first peak is not centered around the position of the ZrN or ZrO, but also covers the area of the peaks of the Zr_2ON_2 phase that appeared for the films belonging to Zone II. Therefore, it is likely that these films are composed by a combination of FCC (ZrN and ZrO-like) and FCC (Zr_2ON_2-like) Zr-N-O quasi-amorphous phases.

4.4.4. Comparison with the results of Carvalho [21]

Figure 4.10 compares the types of structure from Carvalho's Series 1 and from RG# Series. In both cases, Zone I corresponds to ZrN-type films, although in Series 1 the structure is better developed. The structure from Zone II in the Series 1 presented broad peaks and was indexed as Zr_3N_4 with oxygen inclusions. In contrast, Zone II from RG# series presents ZrN and Zr_2ON_2 peaks. The Zone III from series 1 corresponds to a structure with mixture of Zr_2ON_2 and ZrO_2. In the case of the RG# series the structure was identified as a combination of Zr-N-O quasi-amorphous phases.

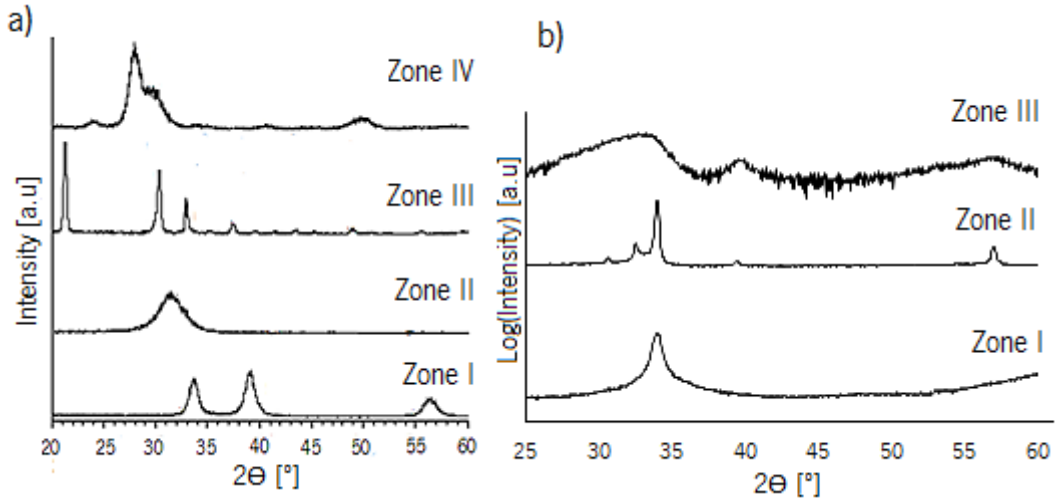

Figure 4.10 Structure types of the different Zones from a) Carvalho's series 1 and b) RG# series

Even though some similarities were found between Carvalho's Series 1 and RG# Series in terms of chemical composition, the structural evolution of both series in different Zones presents some differences. The structures from the Zones I of both series are similar, but in the case of the other two Zone that is not the case. It looks like the Zone II from Series 1 resembles the Zone III from RG# Series, both formed by ZrN –type structure with oxygen inclusions. And the Zone III of Series 1 presents some similarities with Zone II of RG# series, Zr_2ON_2 and ZrO_2 peaks (Series 1) and Zr_2ON_2 and ZrN peaks (RG# Series)

4.4.5. Evolution of the crystallographic structure with the temperature

As explained in the Section 3.4.1, the thermal stability of the samples was studied through XRD measurements while 'in situ' heating. Before and after the heating process, the crystallographic structure was evaluated at room temperature (RT) with a different setup (diffractograms identified as 'Before heating' and 'After heating'). The 'in situ' heating took place between the diffractograms labelled as 'RT' and 'RT cooled'. In fact, the measurements 'Before heating' and 'RT' and the measurements 'After heating' and 'RT cooled' are basically the same, but performed in different setups.

Figure 4.11 shows the diffractograms of four representative samples of the base series acquired at several temperatures. Thus, samples prepared at 5% and 7.5% of N_2+O_2 (Figure **4.11**a and b) belong to the structural Zone I, the film deposited with 8.5% (Figure 4.11c) belongs to the Zone II , and the coating grown at 9.5% (Figure 4.11d) belongs to the Zone III.

The evolution of the structure of the samples deposited with 5% and 7.5% of reactive gas flow (Figure 4.11a and b) with the temperature is quite similar. As was explained in the previous section both present peaks indexed as ZrN. Nevertheless, this phase is more developed in the film deposited at 7.5% of N_2+O_2, while in the specimen prepared at 5% the presence of metallic Zr can be detected.

For the sample deposited at 5% it is worth mentioning that both initial diffractograms are very similar, except for the presence of a narrow peak at 57° in the RT measurement, which is also present in all the measurements. Since there was no change in the sample between both initial measurements (both were carried out at RT prior to any heating), it can be concluded that this peak is an artifact of the measurement. In fact, such peak disappears in the measurement 'After heating'. At 500 °C, the ZrN peak (ca. 34 °) is still present in the sample, while the Zr one (ca. 63 °) disappeared. In addition, two oxygen-containing phases start to develop, whose peak position fits with ZrO and $ZrO(NO_3)_2$ patterns. The former one disappears at 700-800°C, while the latter can be detected up to 1000°C. The measurements performed when the sample cooled down, 'RT cooled' and 'after heating', are very similar, and reveal the formation of oxide phases, particularly ZrO_2.

In case of the film RG 7.5% it is possible to see that the initial measurements 'Before heating' and 'RT' are very similar, and contain peaks of the ZrN phase. At 500°C the ZrN phase is still present, but the development of ZrO has also started. Between 600°C and 800°C the ZrO phase is reinforced at expenses of the ZrN. At 800°C, two peaks whose position fit with the

$ZrO(NO_3)_2$ and ZrO_2 phases start to appear. At higher temperatures, these three contributions are present with different relative weight. After cooling, the observed peaks can be justified by oxide phases, particularly ZrO_2, as in the case of the RG 5% sample.

In Figure 4.11c the evolution of the structure of the RG 8.5% sample with the heat treatment is depicted. Before the heating, the film presents a structure with ZrN and Zr_2ON_2 peaks. Surprisingly, the 'RT' measurement only presents ZrN peaks, which might be caused by a different sensitivity of the measuring setups. Up to 600 °C the diffractogram is kept more or less invariant, although small peaks of ZrO and ZrO_2 start to appear. These phases gain weight at higher temperatures at expenses of the ZrN peaks, which lose intensity. The measurements taken after the samples cooled down are very similar and only present peaks related to Zr oxides phases.

In Figure 4.11d the diffractograms of the heating of the RG 9.5% sample can be seen. It is possible to see that up to 500°C the film presents a structure characteristic of the Zone III. Between 700 °C and 1000 °C, the structure is pretty constant, but very far from the previous one, since it is formed by zirconium dioxide phases. At 600°C, the intermediate situation between both cases can be appreciated. After cooling, the diffractogram does not change too much, and it is again formed by several zirconium oxides.

Figure 4.12 compares the situation of all these films at room temperature before and after the heating. It is possible to see that before the heating (Figure 4.12a) all the films have a distinct structure, which was analysed previously (see Section 4.4). However, after the heat treatment, the four samples present very similar structures, which are formed by zirconium oxide and dioxide phases. In addition, in general, in all the samples subjected to the heat treatment it is possible to see an increase in the crystallinity (higher amount of diffraction peaks which are sharper than before the heating). This oxidation of the samples can be due to the combination of different processes namely the stress relaxation induced by the reduction of defects, including segregation of O and N atoms from the interstitial sites to grain boundaries. The stress relaxation will lead to a decrease in the disorder of the crystallites and a rearrangement of Zr, O and N or the development of ZrO and ZrO_2 phases.

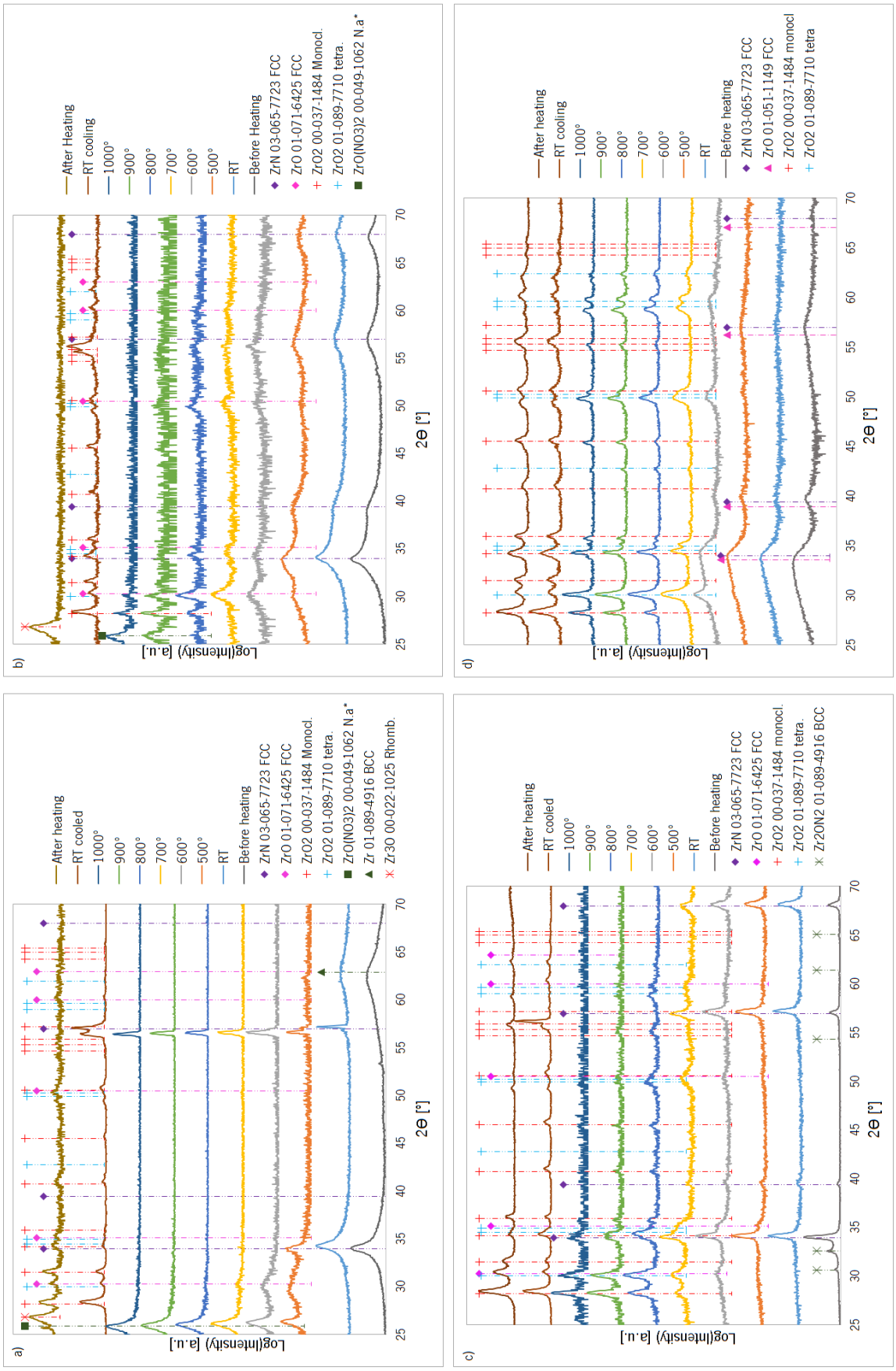

Figure 4.11 Diffractograms of RG# series samples with the heating of the samples a) RG 5%; b) RG 7.5%; c) RG 8.5% d) RG 9.5%

Another explanation for the oxidation of the four samples subjected to the heat treatment is the oxidation caused by the residual oxygen present in the XRD chamber. This explanation is more credible once the four initial coatings are very different among them in terms of structure and chemical composition, and after the heating they reach a very similar structure. Additionally some of the samples (namely the RG 5% and RG 7.5%) have very low oxygen contents which is not congruent with an oxidation caused by an internal rearrangement of the structure because there is not enough oxygen present in the film.

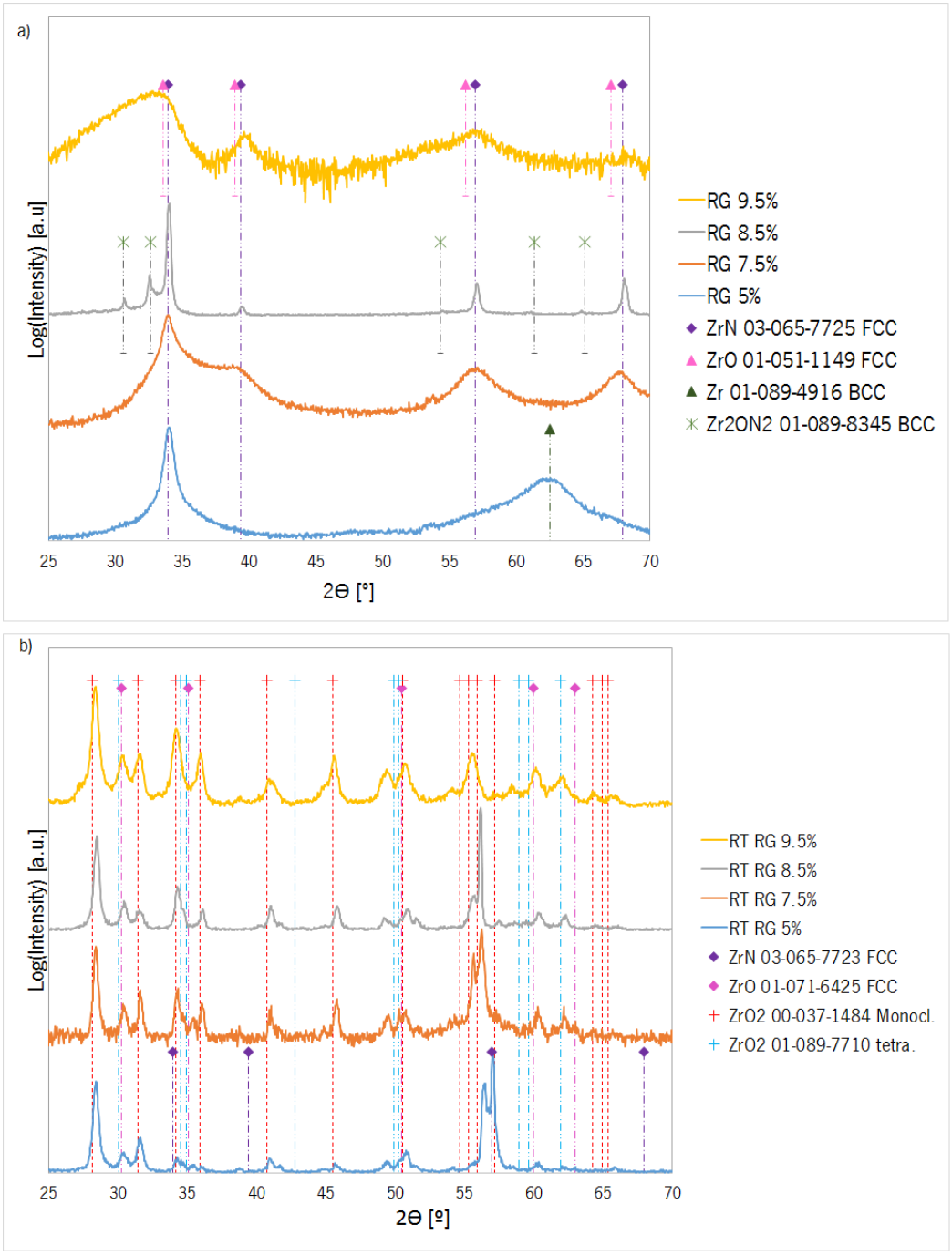

Figure 4.12 Diffractograms of RG# series samples before (a) and after (b) the heat treatment

4.5. Colour

Figure 4.13 illustrates some of the RG# series coloured films obtained with the same base conditions and different amounts of reactive gas flow.

Figure 4.13 Films obtained with the variation of the reactive gas flow in the different substrates (silicon, glass and steel) – RG# series

Figure 4.14 shows the L*a*b* coordinates for the samples deposited with different reactive gas flows. Similarly to what has been done in Section 4.1, the first analysis was the division of samples in groups according to the measured colour coordinates.

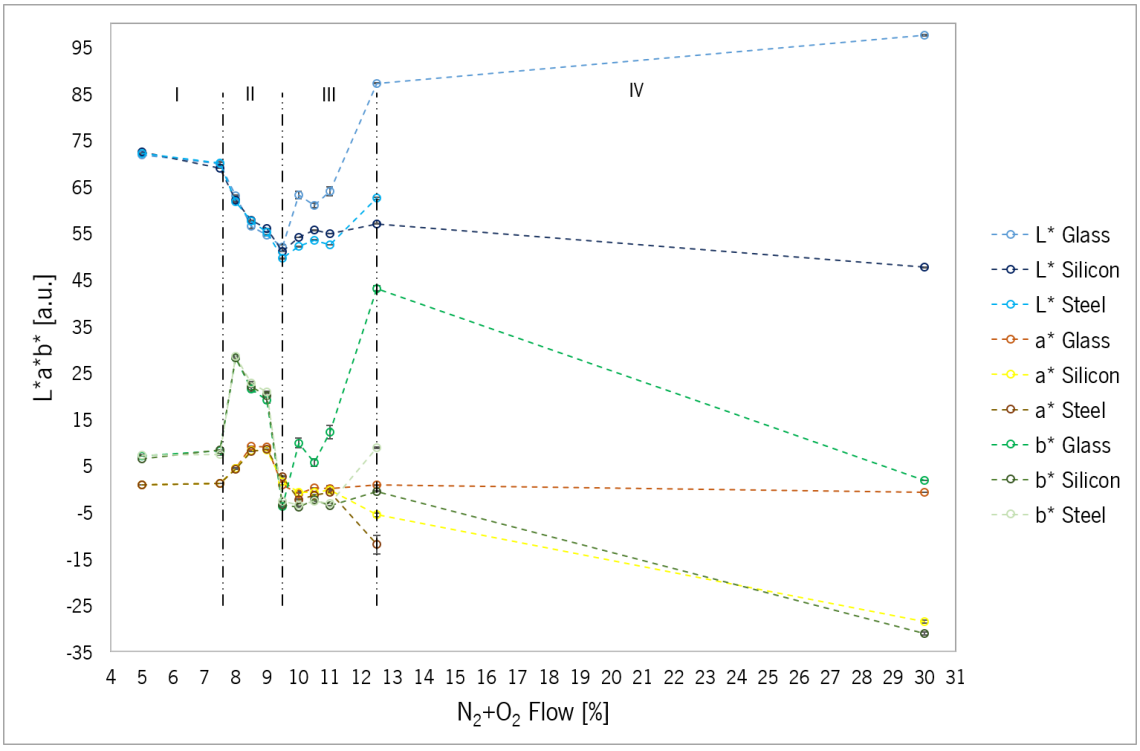

Figure 4.14 L*a*b* coordinates for the samples depending on the flow of reactive gas - RG# series

From Figure 4.14 is easy to see that the samples can be divided into four groups, which are represented by vertical lines. The first Zone is characterized by more or less constant values of the colour coordinates. The second Zone shows a decrease in the L* and b* coordinates, while a* increases. In the third Zone the L* and b* (for Glass substrate) coordinates increase considerably, and the values of a* and b* (Silicon and Steel substrates) are low and constant.

Finally, in the last Zone, the chromatic coordinates have very low values, and L* has values between 45 and 95. The three first Zones are consistent with those described before regarding the chemical composition and the structure of the films, which indicates a tight relation with the colour of the samples.

Nevertheless, the purpose of this work is the production of intrinsic coloured coatings for decorative applications. Thus, it was necessary to separate the intrinsic coloured samples from the others. This process can be made visually, but that is a quite subjective method. Since films with intrinsic colours should exhibit similar value of the colour coordinates (L*a*b*) independently of the substrate (silicon, glass, steel), a statistical method has been developed in order to distinguish the intrinsic coloured samples from the interference-like ones (see Appendix I for details). This formula calculates the standard deviation (SD) in the colour coordinates for the three types of substrates deposited in the same batch. As can be seen in Figure 4.15, each sample was deposited in glass, silicon and steel substrates. For each substrate, several measurements of colour were performed, which results in an average and a standard deviation for each parameter and substrate. The formula calculates the standard deviation of a colour coordinate (L*, a* or b*) taking into account the average and the stand deviations of that colour coordinate measured in each substrate. The output of this formula is the standard deviation of the colour coordinate among different substrates. If the colour is intrinsic the value of the deviation should be close to zero.

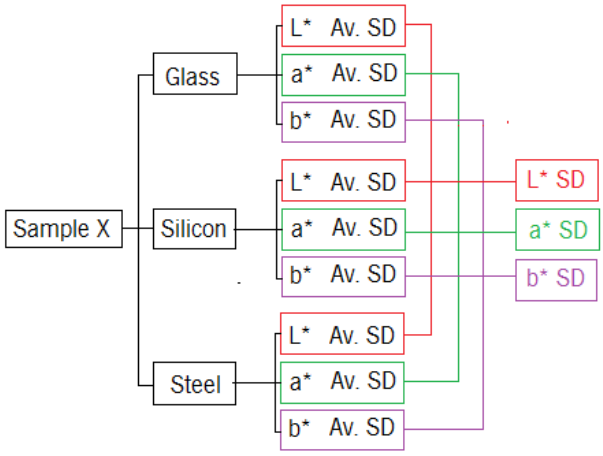

Figure 4.15 Schematic representation of the calculation of the standard deviation of the colour coordinates from substrate to substrate

Figure 4.16 shows the values of the overall SD's resulting of the application of that

formula. It can be seen that the values can be divided into three regions; the first one (reactive gas flows below 9.5%) corresponds to SD<1. This region englobes the Zones I and II of the RG series. The low values of the SD's indicate intrinsic coloured coatings, and these results are in agreement with the observation of the samples. The sample deposited with 9.5% starts to present SD value around one and represents the boundary between intrinsic coloured coatings and interference ones.

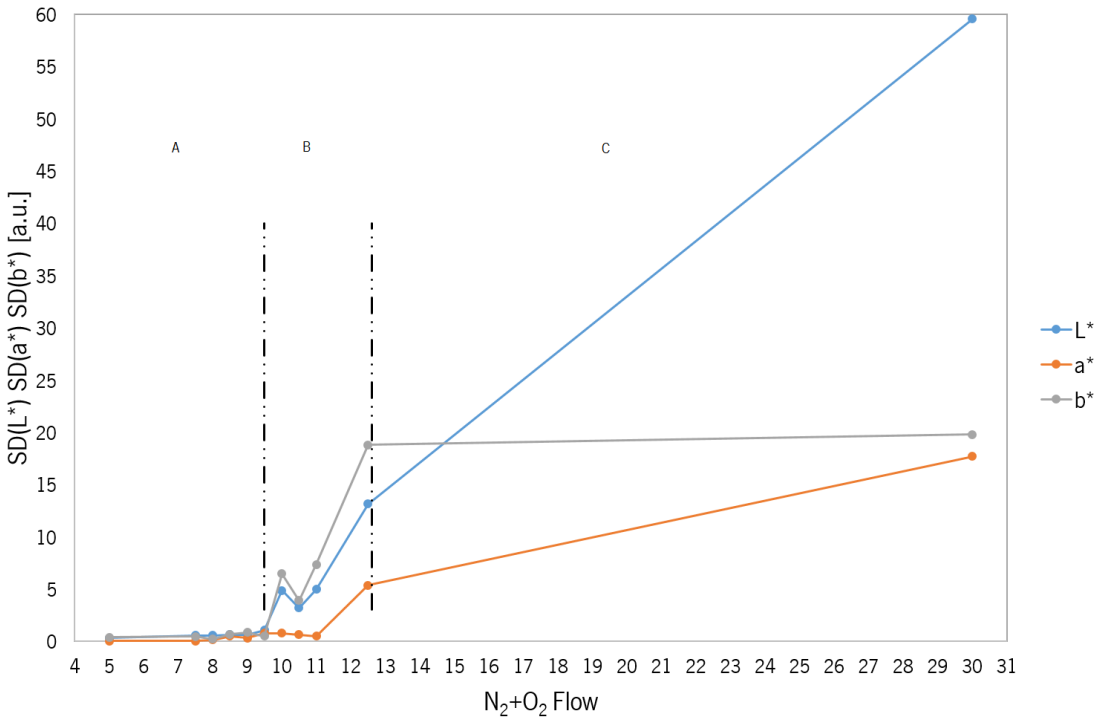

Figure 4.16 Standard deviations of the colour coordinates for the samples deposited with different reactive gas flows (RG# series)

In the second region it is possible to see that the L* and b* coordinates start to have very different values from substrate to substrate, and for flows higher than 12% the a* coordinate also shows high values of SD. The coatings from the second region show a coloured transparent appearance, while in the third Zone the appearance of this coatings is transparent and colourless. Figure 4.17 shows a scheme of the three regions described above. It can be seen that the deviation increases as the film is getting transparent.

Whit the application of this formula it is possible to see that the intrinsic coloured coatings have differences in the L*a*b* coordinates from substrate to substrate inferior to 1.

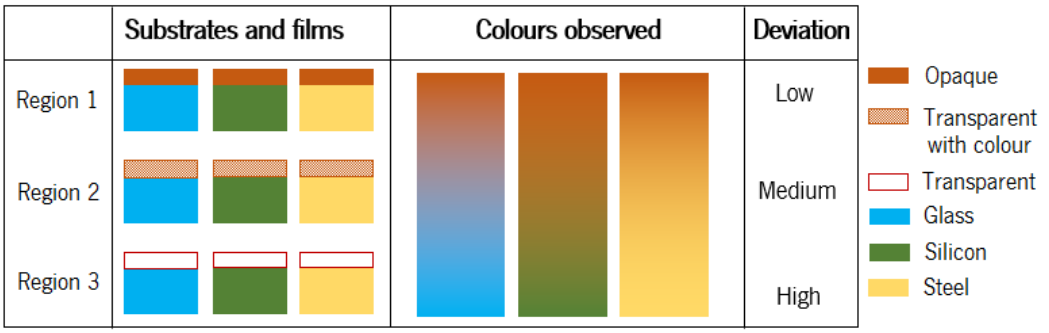

Figure 4.17 Scheme of the three regions distinguished in the samples in terms of colour with the increase of the SD

Figure 4.18 illustrates the evolution of the colour coordinates of the intrinsic coloured samples with the increase of the reactive gas flow, which corresponds to the Zones I and II of the RG# series. Samples deposited with 5% and 7.5% of reactive gas flow (i.e. belonging to Zone I), have very similar colour coordinates, with high values of L*, around 70 and values of a*~0 and b* ~8. The low values of the chromatic coordinates a* and b* of these samples together with the high values of L* lead to the silver colours characteristic of metallic-like coatings as can be seen in the CIELAB colour space from Figure 3.14. This result is in good agreement with the chemical composition of these films (very rich in Zr), and with the observed structure (disordered ZrN peaks and presence of metallic Zr in the sample deposited with 5% of N_2+O_2).

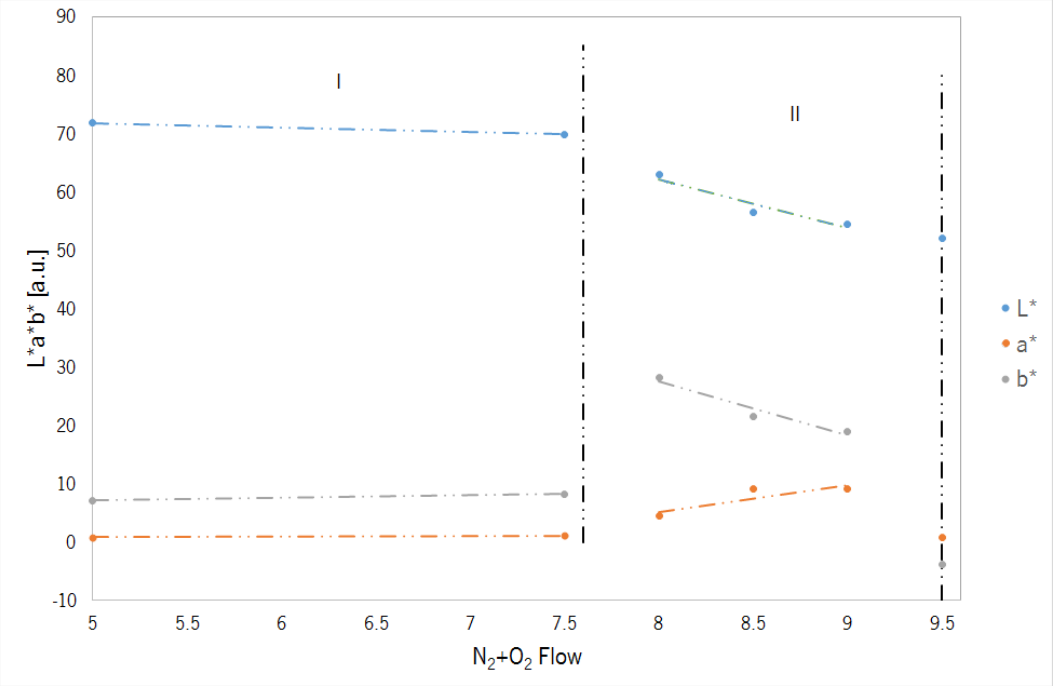

Figure 4.18 Variation of the L*a*b* coordinates for the intrinsic coloured samples with the flow of reactive gas

With the increase of the reactive gas flow (Zone II), there is a decrease in the brightness

(L*) comparing to Zone I, and inside the zone two there is a continuous decrease in this coordinate. The a* value is slightly higher in Zone II than in Zone I and presents an increase in this zone. The b* coordinate is relatively higher than in the previous Zone, and with the increase of the gas flow in Zone II presents a continuous decrease. This increase in the b* coordinate in comparison to Zone I, within positive values means an increase in the yellowness of the samples leading to golden-yellow coatings as can be seen in the Figure 4.19.

It is possible to see that the samples are restricted to a small area of the colour wheel, which is probably due to the restriction of the chemical composition to a small area of the ternary diagram (Figure 4.3)

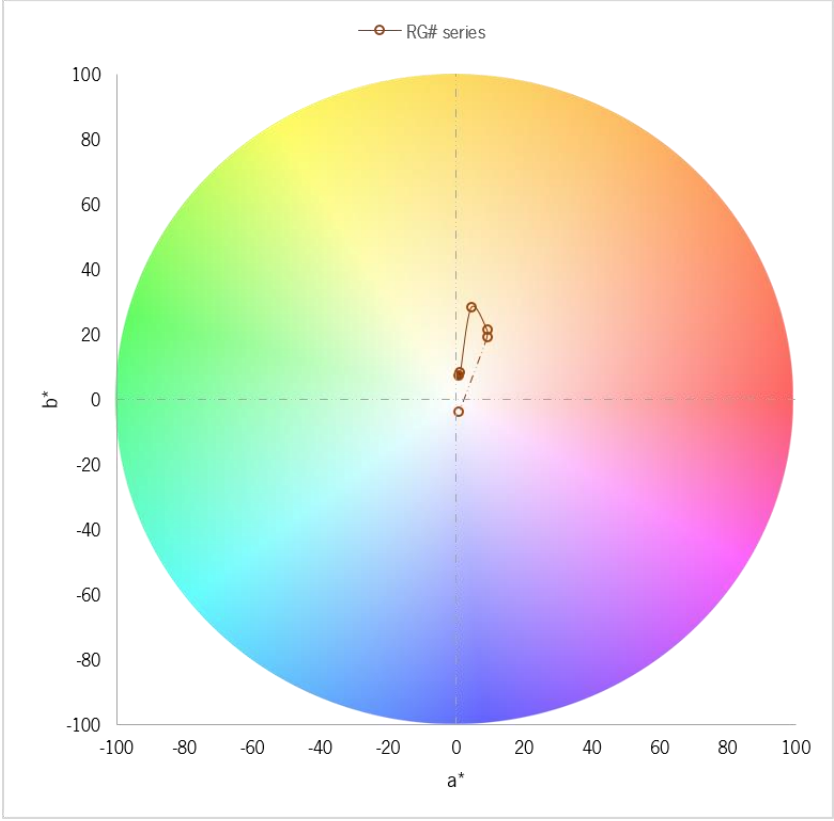

Figure 4.19 Colour wheel with the a* and b*colour coordinates from the RG# series intrinsic coloured coatings. The sample with the filed dot corresponds to the sample deposited with the lower reactive gas flow. The dashed line indicates the transition between intrinsic and interference colours

This confinement agrees with the results from Carvalho (Figure 2.10). In that case, silver and golden-yellow coloured samples were also observed. Nevertheless, when increasing the reactive gas flow, red-brownish and dark blue colours were achieved in the intrinsic domain. While the samples from RG# series with the increase of the reactive gas flow from 9% to 9.5% change from intrinsic golden-yellow colours to interference ones. This difference in the colours is

characterized by a different path over the colour wheel observed in the samples deposited by Carvalho, which move around a wider area of the diagram (Figure 2.7) although start in a very similar point (silver-coloured samples). This is probably connected to the different crystallographic phases observed in both works.

A second difference with the samples deposited by Carvalho (particularly the Series 1, which was deposited with the same reactive gas mixture than RG# series), is about the different N_2+O_2 flows that are used for obtaining each colour. Thus, the samples from Carvalho only exhibited interference colour at N_2+O_2 flows higher than 14 sccm, while for the RG# samples for flows over of 4.75 sccm (9.5%) the samples are already in the interference Zone. Also, in the case of Series 1, the metallic-like coatings extend until flows of 10 sccm, while in the RG# series only samples deposited below 4 sccm (8%) are metallic-like. This discrepancies in the flows at which similar behaviours are identified, namely the appearance of interference coatings at flows above 9.5% seems to indicate that the samples of the RG# series have an excess of O compared to the Carvalho Series 1. In fact, similar results were already discussed (see section 4.2). This excess of oxygen is leading to the passage of the sample from golden-yellow to interference colours without exhibiting red-brownish and dark blue colours observed by Carvalho. Therefore, in order to obtain those colours, the region between 9% and 9.5% of reactive gas flow would need additional exploration. Alternatively, depositions with slight modifications of the reactive gas mixture (i.e. O_2/N_2 ratio) would probably help tuning the colours in that region.

4.6. Conclusions

In this chapter three main conclusions can be drawn:

1. The samples deposited with different reactive gas flows can be divided into three Zones characterizes by the deposition rate, the target voltage, the chemical composition, the structure, the growth mode of the films and the colour coordinates. In Table 4.3 it is possible to see the resume of the previously referred parameters for each of the three Zones.
2. When comparing the samples from RG# series with Carvalho's Series 1, there is an agreement from the chemical point of view, the samples occupy the same region of the ternary diagram. This agreement is not verified in terms of structure once different diffractograms were observed. Moreover, the N2+O2 flows at what each region occurs are different, the possible reason for this discrepancy is the use of

substrate rotation in this work, in opposition to the static mode used in Carvalho's work.

Table 4.3 Resume of the characteristics of the Zones depending on each parameter

Zones	Deposition rate [µm/h]	Target voltage [V]	Chemical Composition [a.t. %] Zr	O	N	Structure	Growth/ Colour
I	> 1.4	<280	82-68	<2	17-31	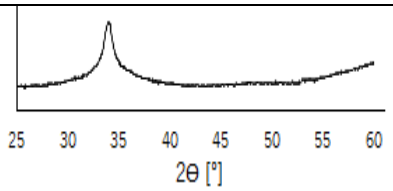	Columnar morphology – Zone T / Silver
II	~0.680	~300	~46	11.9 ±1.3	42.3 ±1.2	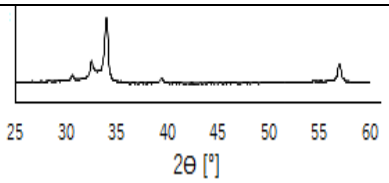	Columnar morphology – Zone T/ Golden- Yellow
III	~0.600	307<V< 362	48.1 ±1.1	15.8 ±1.2	36.1 ±0.1	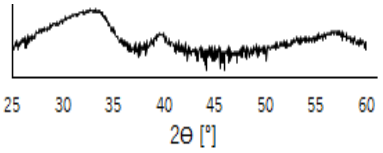	Dense morphology – Transition Zone T – Zone 1/ Interference

3. The films are confined in restricted areas of the chemical composition and colour (Figure 4.3 and Figure 4.19). These areas agree with the regions observed by Carvalho (Figure 2.7 and Figure 2.10). Therefore, a thigh connection between both parameters can be inferred. Thus, it is likely that a chemical variation out of that region would modify the colour observed. This will be the goal of Chapters 5 and 6.

CHAPTER 5

Exploration of the deposition parameter space

In this chapter the influence of the modification of several deposition parameters of Zr-N-O films will be analysed and compared with the RG# base series. The main goal is to 'escape' from the confinement observed in the chemical composition and colour observed in the previous chapter and in the work of Carvalho et al.

Table 5.1 shows the different parameters varied in relation to the base series, and the value of the varied parameter as well. The chemical composition evaluated by RBS and the deposition rate of the samples are also included.

Table 5.1 Parameters varied in respect to the base series, chemical composition and deposition rate

Parameter under study		Sample code	N_2+O_2 flow		Chemical composition [at. %]			Deposition rate [μm/h]
Parameter	Value		[sccm]		Zr	O	N	
Bias [V]	0	RG 8.5%	4.3	8.5	43	13	44	0.686
	-30	B -30 8.5%	4.3	8.5	53	7	40	-
	-40	B -40 8.5%	4.3	8.5	52	11	37	0.707
Deposition time [min]	30	T 30 9%	4.5	9	52	14	34	-
	60	RG 9%	4.5	9	46	13	41	-
	120	T 120 9%	4.5	9	50	5	45	-
	60	RG 10%	5	10	43	22	36	0.624
	120	T 120 10%	5	10	-	-	-	0.570
Target current [A]	1.5	TC 1.5 8.5%	4.3	8.5	36	30	34	-
	2	RG 8.5%	4.3	8.5	43	13	44	-
	2.5	TC 2.5 8.5%	4.3	8.5	55	9	36	-
	1.5	TC 1.5 7.5%	3.25	7.5	42	24	34	0.418
	2	RG 7.5%	3.25	7.5	68	1	31	1.416
Ar flow [sccm]	4	WG 2% 8.5%	4.3	8.5	47	13	40	-
	4.25	RG 8.5%	4.3	8.5	43	13	44	-
	10	WG 8% 8.5%	4.3	8.5	56	7	37	-

5.1. Chemical composition

The chemical composition of the samples deposited with different parameters is summarized in Table 5.1. Figure 5.1 includes the ternary diagrams showing the evolution of the chemical composition with the different parameters in comparison with the evolution of the base series.

The influence of the bias voltage is depicted in Figure 5.1a. It is possible to see that the samples with bias lay in the Zone of the diagram previous defined as Zone II, together with the

grounded sample (RG 8.5%). With the application of the bias voltage from 0 V to -30 V a vertical shift towards higher concentrations of zirconium at expenses of O and N is seen. A further increase in the bias voltage (-40 V) causes a horizontal displacement, which indicates that the oxygen concentration increases while the Zr in kept constant.

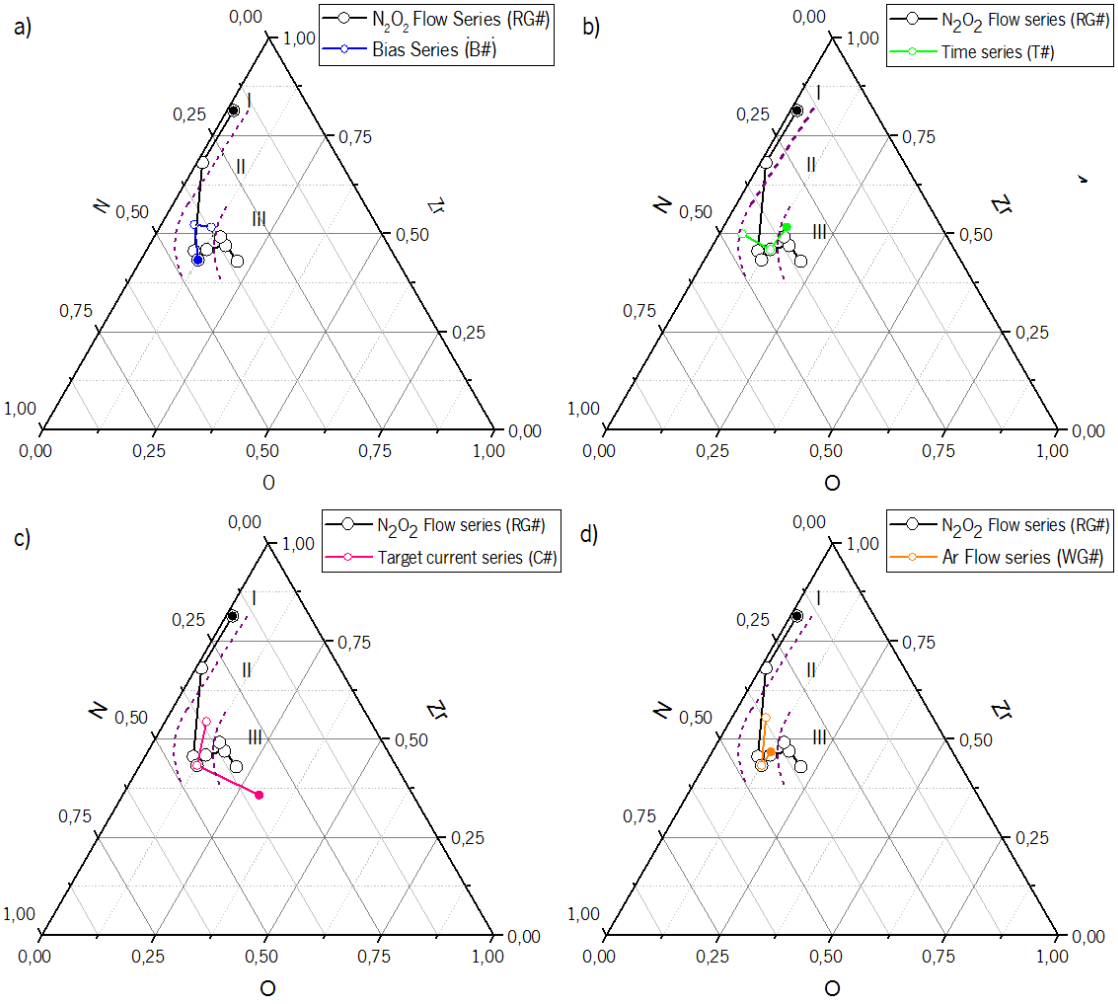

Figure 5.1 Evolution of the chemical composition for samples prepared to explore the deposition parameter space in comparison with the base Series a) Bias voltage; b) Deposition time; c) target current; d) Ar flow. The filled points correspond the lower value of the parameter under study (cf. Table 5.1)

Figure 5.1b shows the influence of the deposition time. The sample deposited with 30 min (T 30 9%) lays in the Zone previously classified as Zone III near the samples of the base series deposited with higher reactive flows. In contrast, the sample deposited with 120 min appears in the Zone II, as the sample deposited with 60 min. In general, a reduction of the deposition time leads to a decrease of the nitrogen concentration. When reducing the deposition time from 120 to 60 min, a clear O increase is observed at expenses of Zr and N equally. A further reduction from 60 to 30 min leads to a second decrease of N, while O is constant.

Figure 5.1c shows the influence of target current in the chemical composition. The sample deposited with lower target current (1.5 A) is located in the Zone III of the diagram with a considerable shift to a more oxygen-rich composition than the samples from the base series. The same behaviour is observed for the sample deposited at 7.5% (see Table 5.1). In contrast, the sample deposited with 2.5 A is located in the Zone II, but at higher Zr concentrations than the sample deposited with 2 A. It can be seen that the increase in the target current has a similar effect than a reduction of N_2+O_2 flow, since the trend observed for the three films where the Zr current was varied resembles the trend of the base Series. This is because a reduction of the target current has a similar effect on the poisoning than the increase of N_2+O_2 flow, since less Zr atoms are ejected and the poisoning of the target is favoured.

Figure 5.1d shows the ternary diagram with the evolution of the chemical composition with the variation of the flow of working gas. All the samples are located in the Zone II of the diagram. The sample with 2% Ar is located near the boundary between Zone III, while the film with 8% Ar is closer to Zone I. It is possible to see that for the former specimen (WG 2%) the chemical composition is very similar to the sample prepared at 5% Ar. In contrast, the sample deposited with 8% of working gas flow shows a considerable increase in the concentration of zirconium at expenses of oxygen and nitrogen. These differences are related to the increase of the deposition rate that will be discussed in the next section. This result is similar to what was observed when increasing the target current or when applying bias.

5.2. Microstructure

Figure 5.2 shows the SEM cross section micrographs of the RG 8.5% (0 V) and B -40 8.5% (-40 V). The sample deposited with bias voltage (B -40 8.5%) shows a slight increase in the deposition rate in comparison with the grounded sample. However, the variation is relatively low, and it can concluded that the applied bias voltage does not appreciably affect the deposition rate. The applied bias is probably too low to present any major effect in the deposition. For higher voltages, the expected behaviour was a reduction in the deposition rate; the coatings would become thinner due to phenomenon as the resputtering of O (lower bonding energy toward zirconium than N) caused by the increase of the ion bombardment of the growing films at the substrate. As can be seen in the micrographs the samples have similar thickness due to the similar deposition rate. In addition, it can be seen that both samples possess a columnar morphology which is very similar, maybe with narrower columns formed in the biased sample.

Similarly to the RG 8.5% coating, the B -40 8.5% sample can be indexed to the Zone T of the Thomton's Zone model.

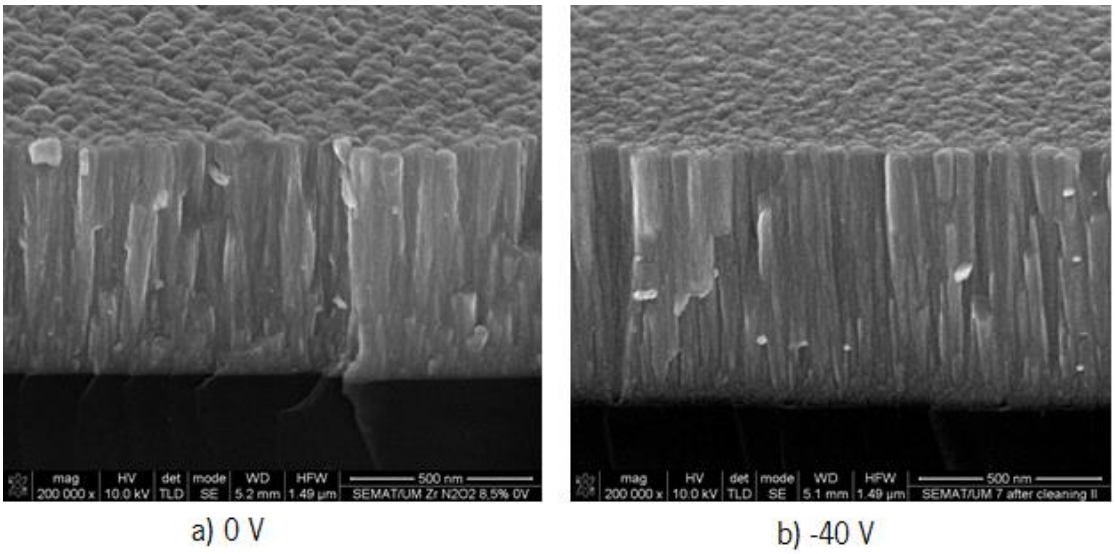

Figure 5.2 SEM cross section micrographs of the samples used to study the influence of bias: a) sample RG 8.5% – 0 V; b) sample B -40 8.5% -40 V

Figure 5.3 shows the SEM cross section micrographs of the RG 10% sample (60 min) and the T 120 10% samples (120 min). The most notorious observation is that the sample prepared with 120 min is considerably ticker then the one prepared with 60 min. This increase in the thickness was expected once the sample had twice the deposition time. However, the sample deposited with higher deposition time (T 120 10%) shows a deposition rate slightly lower than the deposition rate of the sample deposited with 60 min (RG 10%). This variation indicates that deposition rate slightly decreases with longer process times.

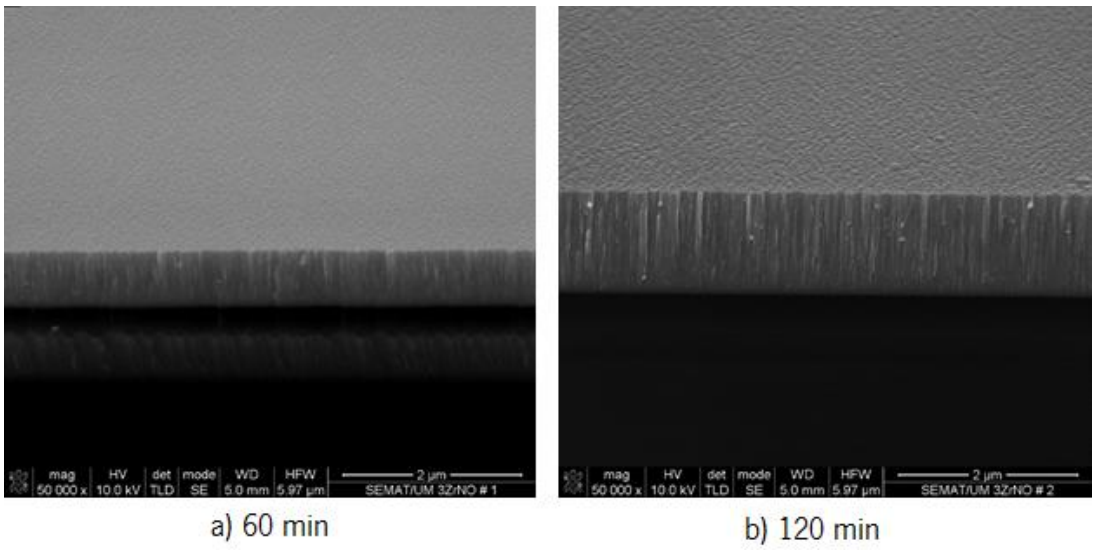

Figure 5.3 Cross section micrograph of the samples prepared with different deposition times: a) sample RG 10% – 60 min; b) sample T 120 10% - 120 min

As expected, both films show similar microstructure, which can be indexed to the T Zone of Thomton's Zone model

In Figure 5.4 the SEM cross section micrographs of the RG 7.5% sample (2 A) and the TC 1.5 7.5% (1.5 A) sample can be seen. The difference in the thickness is obvious, being the sample deposited with 2 A of target current considerably thicker than the one deposited with 1.5 A. The sample deposited with lower target current (TC 1.5 7.5%) presents a deposition rate considerable lower than the deposition rate of the sample deposited with 2 A (RG 7.5%). This is because a lower target current leads to a decrease in the ionized Ar atoms and a subsequent reduction of the sputtering and deposition rates.

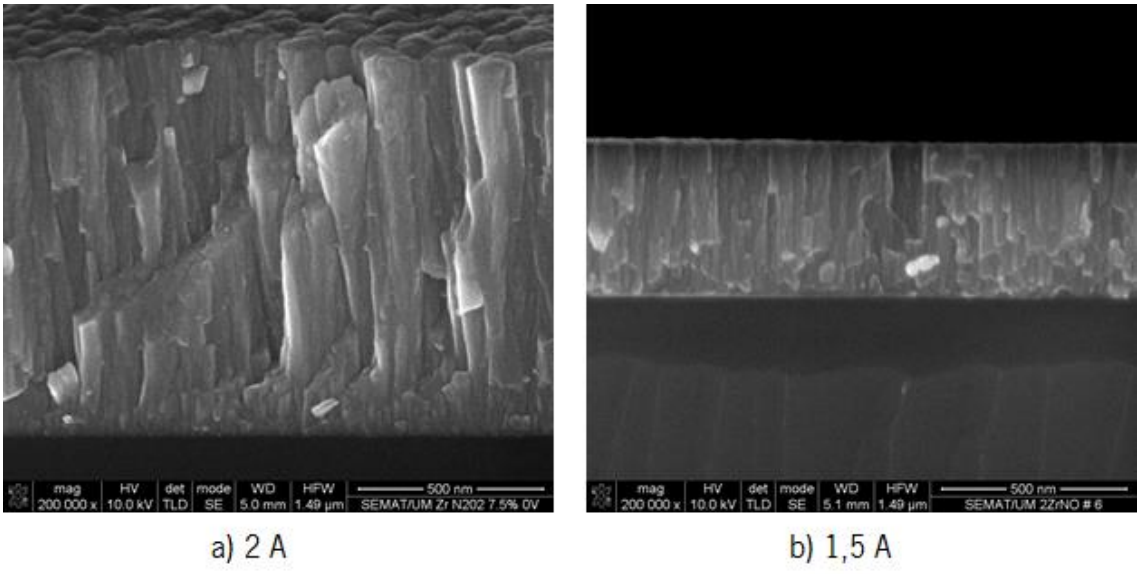

Figure 5.4 Cross section micrograph images of the samples with different target currents: a) sample RG 7.5% – 2 A; b) sample TC 1.5A 7.5% - 1.5 A

Regarding the morphology of the films, it is possible to see a difference between both samples. The sample deposited with 2 A has a columnar morphology indexed previously to the T Zone of the Thornton's model (see Section 4.3). In contrast, the sample produced with 1.5 A starts to lose the columnar growth and the columns appear 'interrupted'. This behaviour is similar to the structure developed for the samples of the RG# series deposited with higher reactive gas flows (cf. Figure 4.5), particularly to the sample deposited at 9.5% (Figure 4.5d). Therefore, this sample can be indexed to a transition Zone between Zone T and Zone I of the Thornton's Zone model.

The samples with different working gas flows were not subjected to SEM analysis. Either way, it is expectable that the decrease in the Ar flow would lead to similar results than the decrease in the target current. Thus, less amount of Ar ions would be impinging the target and,

hence, lower Zr sputtering rate and higher degree of poisoning would be obtained, leading to a reduction in the deposition rate. The increase of the Ar flow should present the opposite behaviour.

5.3. Crystallographic structure

Figure 5.5 shows the diffractograms for the samples deposited with different bias voltages. The sample deposited with 0 V (RG 8.5%) belongs to the structural Zone II, and it presents diffraction peaks from two crystalline phases ZrN and Zr_2ON_2, as discussed before.

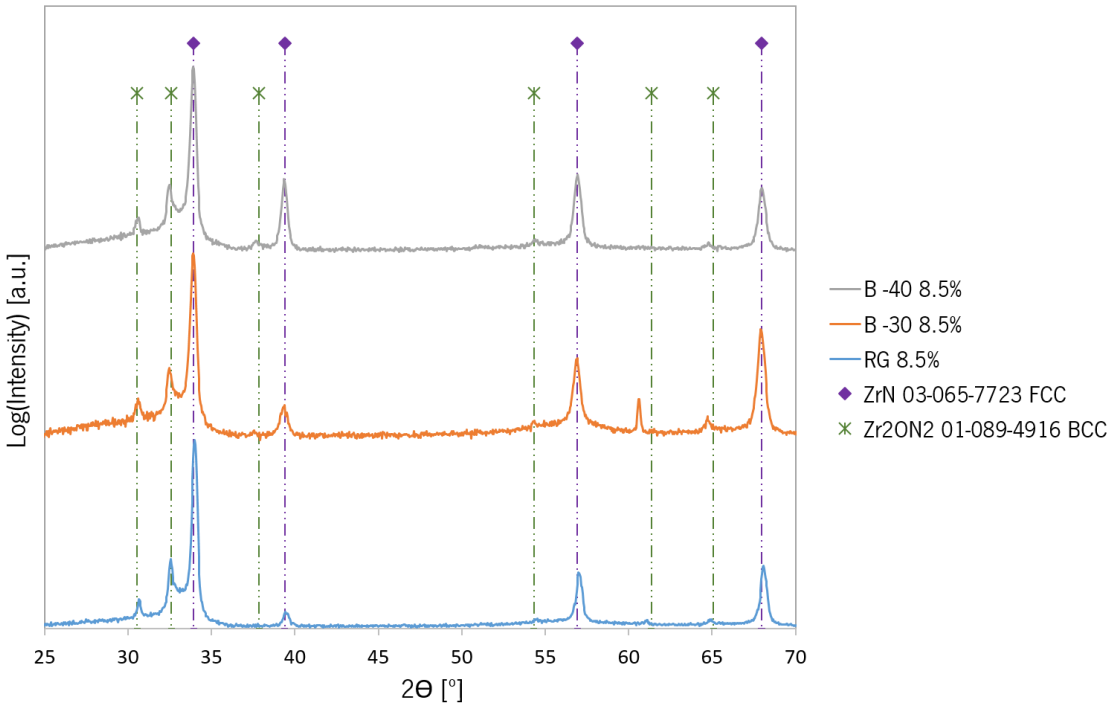

Figure 5.5 Diffractograms of the samples deposited with different bias with the respective indexed crystallographic phases

The other two samples, which were deposited with -30 V and -40 V, have similar diffractograms. The main differences between the samples with bias is the relative intensity of the peaks and the shift of the Zr_2ON_2 peaks located at ~61 and ~65 towards lower angles.

The shift of the diffraction peaks towards lower angles observed in the biased samples could be related to the internal strains in the sample caused by the bombardment of the growing film with the Ar ions, or any atom replacement in the Zr_2ON_2 phase. However, the ZrN do not present any observable shift. It is remarkable that the peaks located at ~61 and ~65 are only

observed for the sample deposited with bias voltage of -30 V, which is the one with the lowest O content (Table 5.1 and Figure 5.1a). This may indicate that the reduction of O contributes to a better crystallinity of the Zr_2ON_2 phase.

The B -30 8.5% and B -40 8.5% samples can be indexed to the structural Zone II as the RG 8.5% sample. In general, in agreement with what observed previously for morphology and chemical composition, the application of bias does not appear to affect the structure of the samples considerably.

Figure 5.6 shows the diffractograms at 4° for the samples deposited with different depositions times. The sample prepared with 60 min (RG 9%) was previously index to the structural Zone II. Both films with lower deposition time show very similar diffractograms, which can be considered as belonging to Zone II, although the sample with shorter deposition time was near the boundary with Zone III in terms of chemical composition.

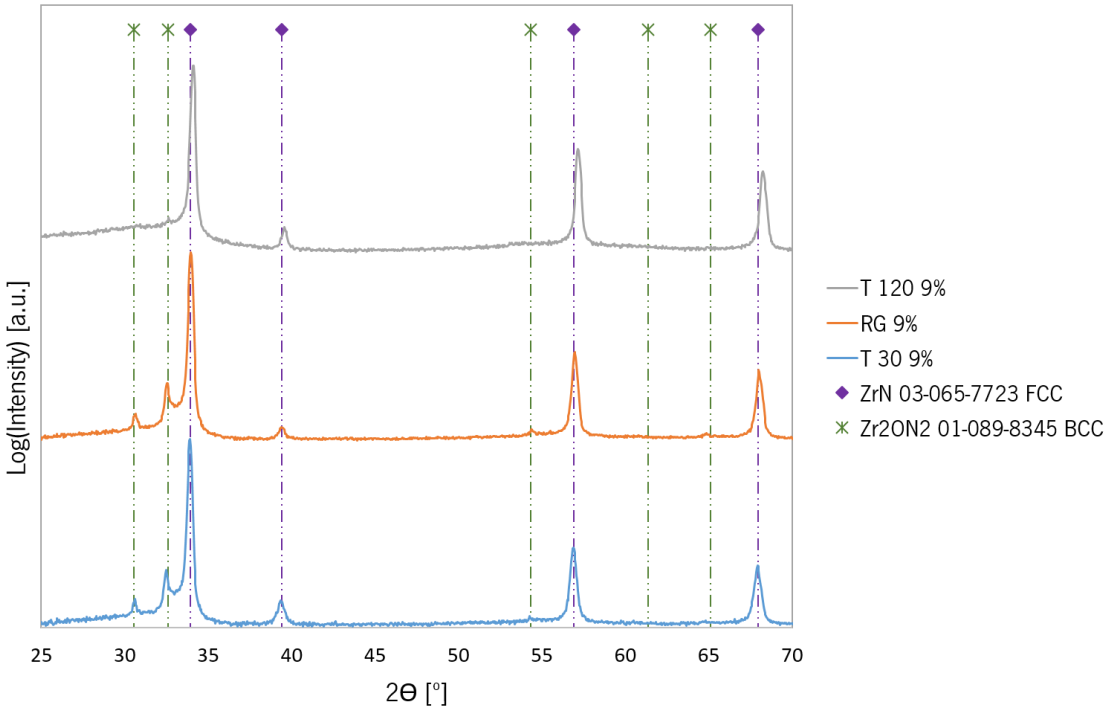

Figure 5.6 Diffractogram of the samples deposited with different deposition times with the respective indexed crystallographic phases

Nevertheless, the film deposited with longer time does not present a clear development of the Zr_2ON_2 phase. In addition, the ZrN peaks present shift towards higher angles. This differences are probably related to the decrease in the oxygen concentration in this sample compared to the others samples (Table 5.1). This causes a displacement of this sample too far

away to the left from the position of the Zr_2ON_2 phase in the ternary diagram (Table 5.1b). This film probably had insufficiency of oxygen to form the Zr_2ON_2 phase. Instead, the oxygen contained in this sample is likely located in the interstitial sites of the ZrN, which leads to the increase of the lattice parameter and explains the deviation of the ZrN peaks towards higher angles. Therefore, the sample deposited with 120 min is structurally belonging to Zone I, and it is located in the transition between Zone I and II in the ternary diagram.

In Figure 5.7 the diffractograms at 4° of the samples deposited with different target currents are depicted. The sample deposited with 2 A (RG 8.5%) was previously indexed as belonging to the structural Zone II.

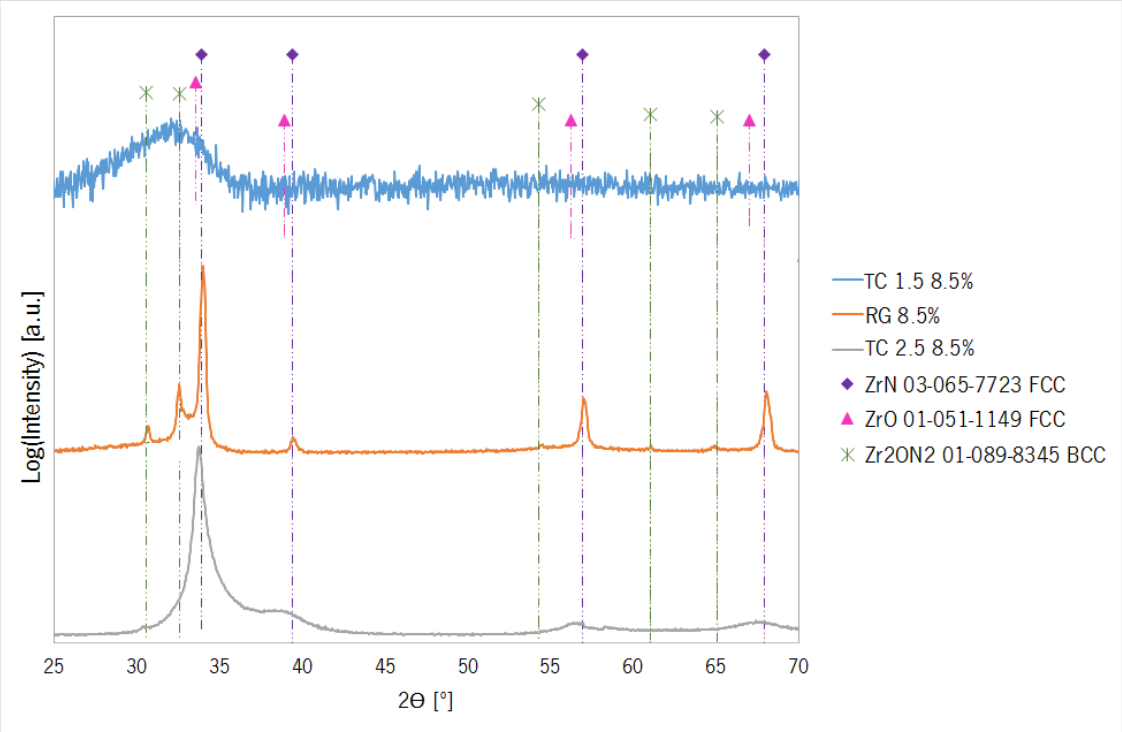

Figure 5.7 Diffractogram of the samples deposited with different target currents with the respective indexed crystallographic phases

The general evolution resembles the behaviour depicted in Figure 4.6. In the one hand, the sample deposited with 1.5 A presents a structure characteristic of an amorphous sample and similar to the structure of the samples indexed to the Zone III (Figure 4.9). So, similarly to the samples from Zone III, the amorphous structure of this sample can be due to the incorporation of oxygen atoms in the ZrN matrix, which hinders the crystallization of the phase and leads to broad peaks (the location of this sample in the ternary diagram is in the region with high O concentrations, cf. Figure 5.1c). For the samples deposited at 7.5%, a similar behaviour was

observed, although in this case the evolution was from Zone I (sample prepared at 2 A, cf. Figure 4.7) to Zone III (result not shown).

In the other hand, the sample deposited with 2.5 A does not present a clear development the phase Zr_2ON_2. Additionally the ZrN peaks present a broadening comparing to the sample with 2 A. As observed before (Table 5.1), this sample presents increased Zr concentration and lower O content, which explains the appearance of the ZrN peaks. The reduction of O probably impedes the formation of the Zr_2ON_2 phase, but its incorporation in the ZrN matrix explains the broadening of the peaks. This sample can be probably indexed to Zones I (see the similarity with diffractograms in Figure 4.7).

Finally, Figure 5.8 collects the diffractograms at 4° of the samples deposited using different flows of working gas. The sample deposited with 5% of Ar flow (RG 8.5%) was previously indexed to the Structural Zone II.

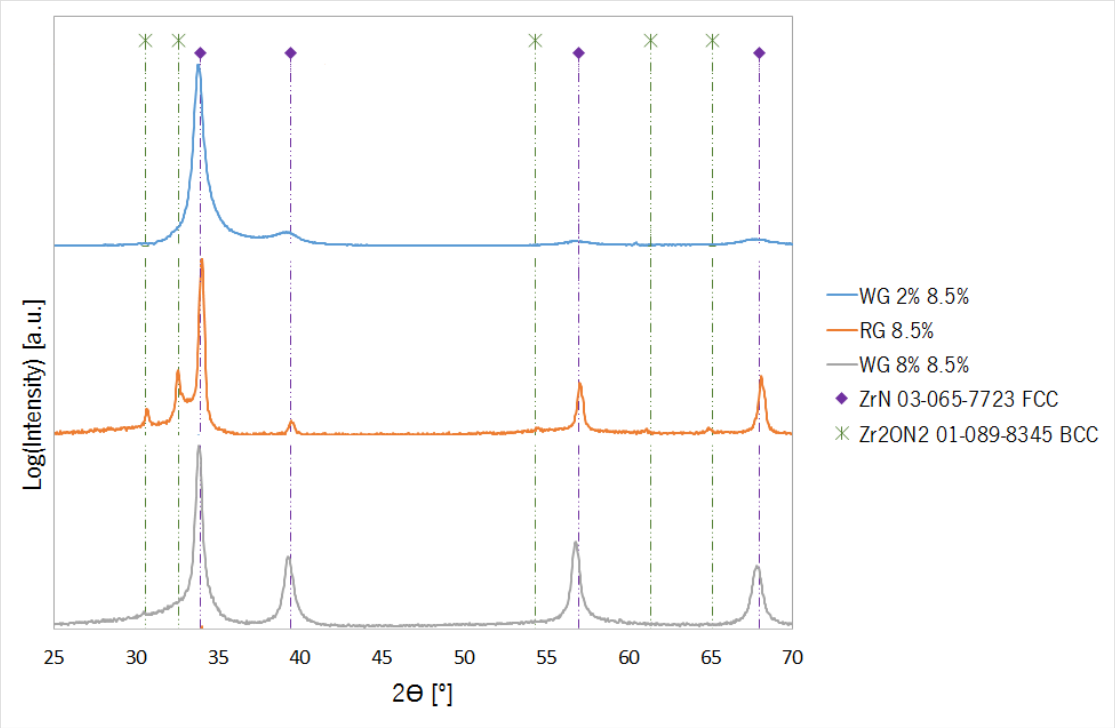

Figure 5.8 Diffractogram of the samples deposited with different working gas flow with the respective indexed crystallographic phases

The sample deposited with the lowest Ar flow, 2% (WG 2% 8.5%), presents broad ZrN peaks. In terms of chemical composition the samples deposited with 5% and 2% of Ar are very similar (Table 5.1, Figure 5.1). But contrary to the sample with 5%, the sample with 2% does not present a clear development of the Zr_2ON_2 phase. The differences in the chemical composition,

even though small, may have been enough to change the stoichiometry, not allowing the development of the Zr_2ON_2 phase. Instead, the oxygen present would be located in interstitial sites of the ZrN phase causing the broadening of the peaks. Thus, this sample would be located in a structural transition Zone between Zones II and III; the interstitial oxygen is starting to compromise the crystallinity of the sample. With further increase of the oxygen content the sample should present a structure similar to the Zone III structure (Figure 4.9). In contrast, the sample deposited with 8% of Ar flow presents diffraction peaks identified as ZrN and appears to show a slight development of the Zr_2ON_2 phase, so, similarly to the samples deposited with 2.5 A (Figure 5.7) and the sample deposited with 120 min (Figure 5.6) this sample would be located in the limit between the Zones I and II.

5.3.1. Evolution of the crystallographic structure with the temperature

In Figure 5.9 it is possible to see the diffractograms of the heat treatments of the samples prepared at 8.5% of N_2+O_2 with and without biasing of -30V.

Sample B 30 8.5% reproduces extremely well the results of the unbiased sample up to 700°C. From this point, the biased sample presents ZrN peaks through the heating and also after the heating, while in the case of the unbiased one the ZrN peaks start to loss intensity from temperatures above 700°C.

Other differences can be observed regarding the oxide phases present, for instance at 900°C. At this temperature, the biased sample does not show peaks of the Zr dioxide that are present in the unbiased sample (peak at 28°). In contrast, more peaks of the Zr monoxide are detected in the biased specimen (peaks at 35, 50, 60 and 63°).

In short, the biased sample keeps signs of existence of ZrN during the whole heating, and oxidizes more preferentially to Zr monoxides instead the oxides observed in the unbiased film. In other words, the biased sample seems to be more resistance against oxidation, which may be a consequence of a certain degree of densification of the structure caused by the application of biasing.

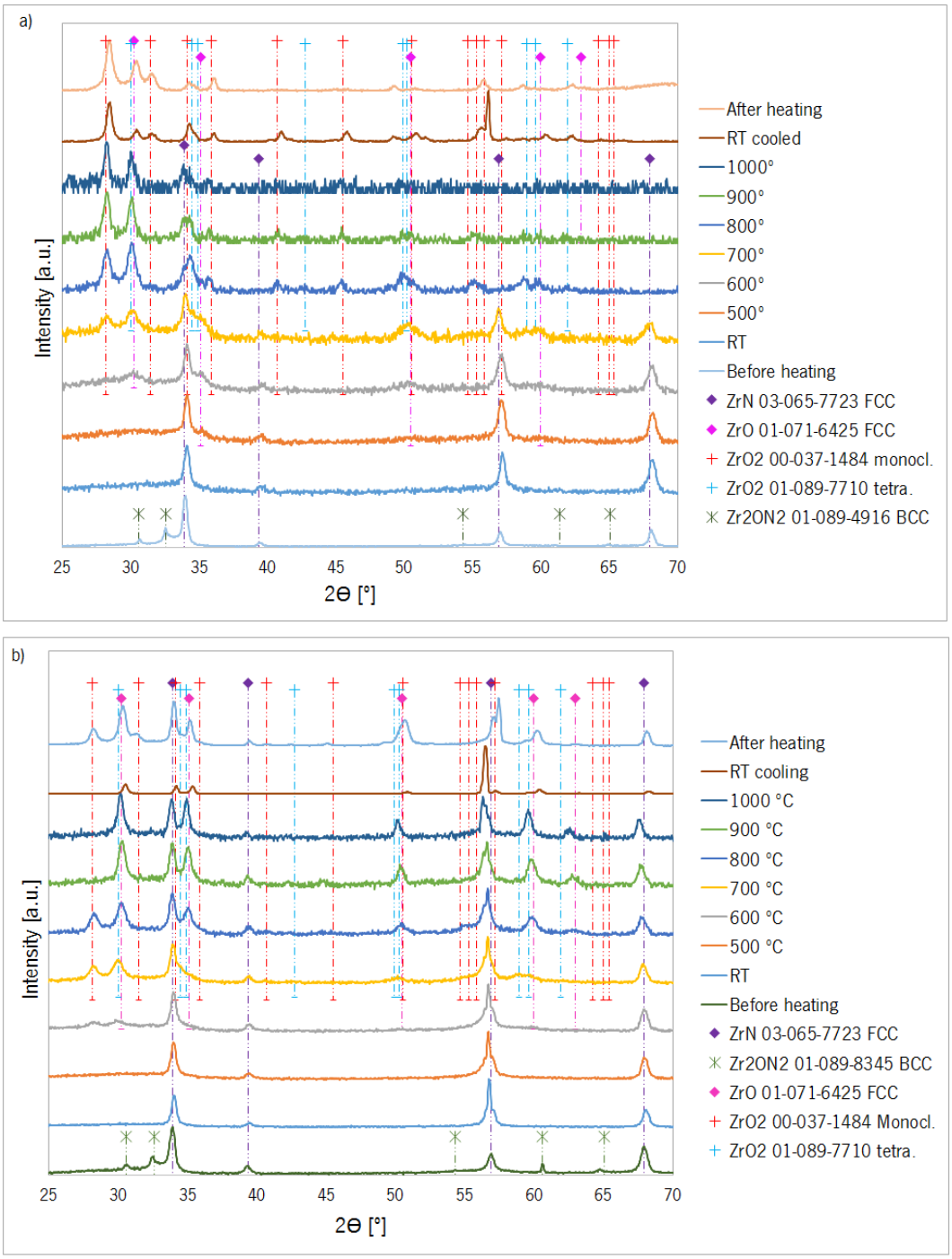

Figure 5.9 Diffractograms with the heating of the samples a) Grounded sample – RG 8.5% b) Biased sample – B 30 8.5%

5.4. Colour

In Table 5.2 the value of the colour coordinates of the samples prepared to explore the parameter space are displayed.

Table 5.2 Colour coordinates of the samples prepared to explore the parameter space

Parameter under study		sample	Colour coordinates [a.u.]		
Parameter	Value		L*	a*	b*
Bias [V]	0	RG 8.5%	56.5	9.1	21.4
	-30	B -30 8.5%	54.7	10.0	17.0
	-40	B -40 8.5%	49.6	8.4	5.0
Deposition time [min]	30	T 30 9%	59.4	7.3	25.3
	60	RG 9%	54.5	9.1	19.0
	120	T 120 9%	49.8	9.5	6.0
Target current [A]	1.5	TC 1.5 7.5%		Transparent	
	2	RG 7.5	69.9	1.1	8.2
	1.5	TC 1.5 8.5%		Transparent	
	2	RG 8.5%	56.5	9.1	21.4
	2.5	TC 2.5 8.5%	71.2	1.1	8.3
Ar flow [sccm]	4	WG 2% 8.5%	68.2	2.3	13.3
	4.25	RG 8.5%	56.5	9.1	21.4
	10	WG 8% 8.5%	56.5	2.4	15.3

Figure 5.10 shows the colour coordinates of the intrinsic coloured coatings prepared while exploring the deposition parameter space. Although the variation of the deposition parameters such as the bias, deposition time, target current and the argon flow influence the colour of the samples comparing with the base series (Figure 4.19), it is possible to see that the coatings are, still, restricted to a very small area of the colour wheel.

A detailed view of the variation of the colour coordinates with the different deposition parameters is depicted in Figure 5.11

In Figure 5.11a it is visible the effect of the bias voltage in the colour of the films. The sample deposited with -30 V is located near the sample deposited with 0 V, but In terms of the trend observed in the RG# series, the sample deposited with -30 V is located farther than sample RG 9%. Even though in terms of chemical composition and structure these samples are distinct. Comparing with the film deposited at 0 V, the biased sample presents a slight decrease in the b* coordinate (Table 5.2). This difference may be related to the small differences in the composition (Figure 5.1), and/or differences in the structure (Figure 5.5). Nevertheless the difference observed in colour coordinates considering the dimension of the colour wheel, is a small.

The film deposited with -40 V reveals a considerable displacement in terms of colour compared to the other two samples. This coating presents mainly a decrease in the b* coordinate comparing to the other two, meaning that this sample starts to lose the yellow-golden appearance. In terms of structure this sample is similar to the ones with 0 and -30 V (Figure 5.5). But regarding the chemical composition, this films is located in the limit between the Zones II

and III, having a chemical composition similar to the samples from Zone III (Table 4.1 and Table 5.1) but with colours still in the intrinsic domain.

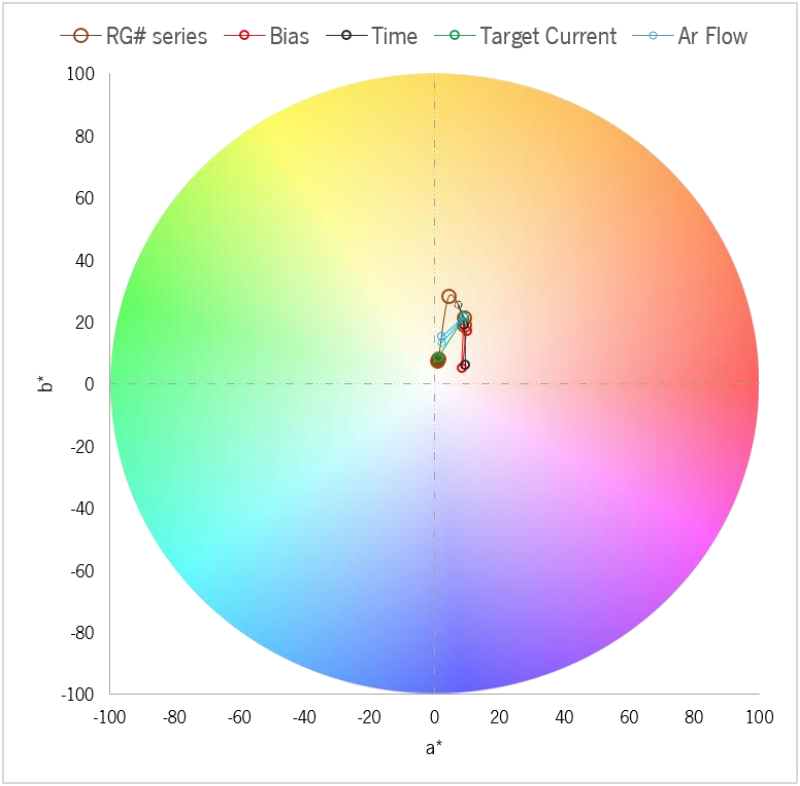

Figure 5.10 Colour wheel with the a* and b*colour coordinates for the samples prepared while exploring the deposition parameter space compared with the base series

Figure 5.11b shows the effect of the deposition time in the colour coordinates comparing to the base series. The sample deposited with the lowest deposition time has similar colour coordinates as the sample deposited with 60 min. This sample presents mainly an increase in the b* coordinate. This differences may be related to the difference in the chemical composition, being the sample deposited with 30 located in the transition between Zone II and III, but in terms of structure the two samples are very similar.

The sample deposited with 120 min is farther away from the other two in terms of colour. This sample has a similar colour to the sample deposited with -40 V although they are very different in terms of chemical composition and structure. Comparing to the samples deposited with 30 min and 60 min, the sample deposited with 120 min has different structure (Figure 5.1 and Figure 5.6), and chemical composition which are both in the limit between Zones I and II.

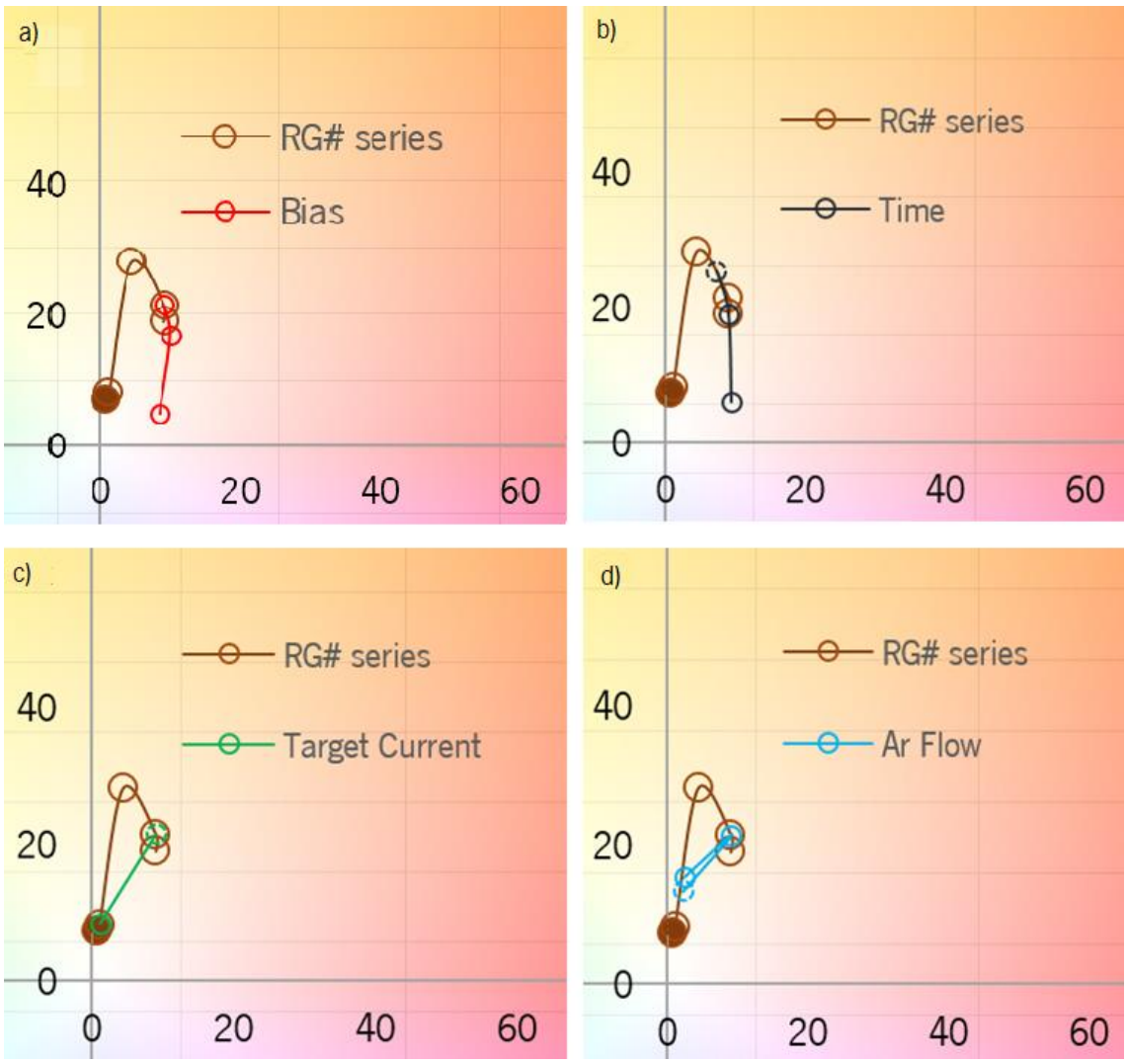

Figure 5.11 Detailed view of the colour wheel with the a* and b*colour coordinates for the samples deposited for exploration of the deposition parameter space, compared with the base series. a) RG 8.5% (0V), B 30 8.5% and B 40 8.5%; b) T 30 9%, RG 9%, T 120 9%; c) RG 8.5% and TC 1.5 8.5%; d) WG 2% 8.5%, RG 8.5%, WG 8% 8.5%. The filled sample and the doted ones corresponds to the lower value of the parameter

. Figure 5.11c illustrates the effect of the target current in the colour of the films comparing to the base series. The samples deposited with 1.5 A is not represented due to their interference characteristics., These samples present similar structure as the RG# samples from Zone III, which also present interference colours, and the chemical composition of these samples are also located in Zone III of the ternary diagram.

The sample deposited with 2.5 A presents a colour similar to the RG# samples from Zone I. It was seen previously that an increase in the target current has a similar effect both in the structure and in the chemical composition as the decrease of the reactive gas flow, so this similarity in the colour of the sample deposited with higher current and the sample with lower flow is congruent with that.

At last, Figure 5.11d shows the effect of the variation of the working gas in comparison with the base series. Increasing and decreasing the working gas flow in comparison with the RG# film presents a similar effect, both samples present colours similar to that of the samples deposited with lower N_2+O_2 flow. In the case of the sample deposited with higher Ar flow, in the case of the structure and chemical composition this sample is in the limit between Zone I and Zone II, so a similar colour to the samples from Zone I is expectable.

In the case of the sample deposited with lower Ar flow, this film is located in the transition between Zone II and III in terms of structure and has a similar composition to the sample from the RG# series. Therefore, the colour variation cannot be explained in this way.

5.4.1. Individual control of the N_2 and O_2 flows during the deposition

In this work the obtained colours were restricted to silver and golden-yellow coatings in the Zr-N-O samples. For this coatings it would be of interest to study the compositional range between the samples RG 8.5% and RG 9.5%, once the samples deposited with 8.5% exhibit golden colours and the samples with flows of 9.5% and above are, already, in the interference Zone. Based on the results reported on the literature, this type of coatings experience red-brownish and dark-blue colours before the interference ones, so all indicates that this is a region of interest. After replicate such colours, and with the increased understanding of the system, produce colours such as light blue (one of the objectives) should be simpler. This independent control of the gas flow would allow to have a higher control over the composition of the films and explore a wider range of compositions which would facilitate obtain different coloured coatings.

To perform this task, the deposition of Zr-N-O coatings with independent control of the O_2 and N_2 flows by using independent mass flow controllers instead of introducing them in the chamber as a mixture was planned. Unfortunately, due to logistic and bureaucratic problems, only a trial series was deposited.

Although different colours the silver and golden were obtained, these colours are mainly interference ones. In fact, reproducing the results at a given composition of the sputtering atmosphere was not possible. Therefore, further tests will be needed with this approach in order to obtain different intrinsic coloured coatings with different colours then the ones already obtained in this work.

5.5. Conclusions:

As was seen in the previous chapter for the samples deposited with different reactive gas flows, it was possible to divide that series of sample in regard to several parameters as the structure, the chemical composition or growth mode of the samples. With the division it was also verified that samples within as certain compositional range presented similar structure, growth mode and film colour. Figure 5.12 illustrates this consistence with the division of the base series in different zones.

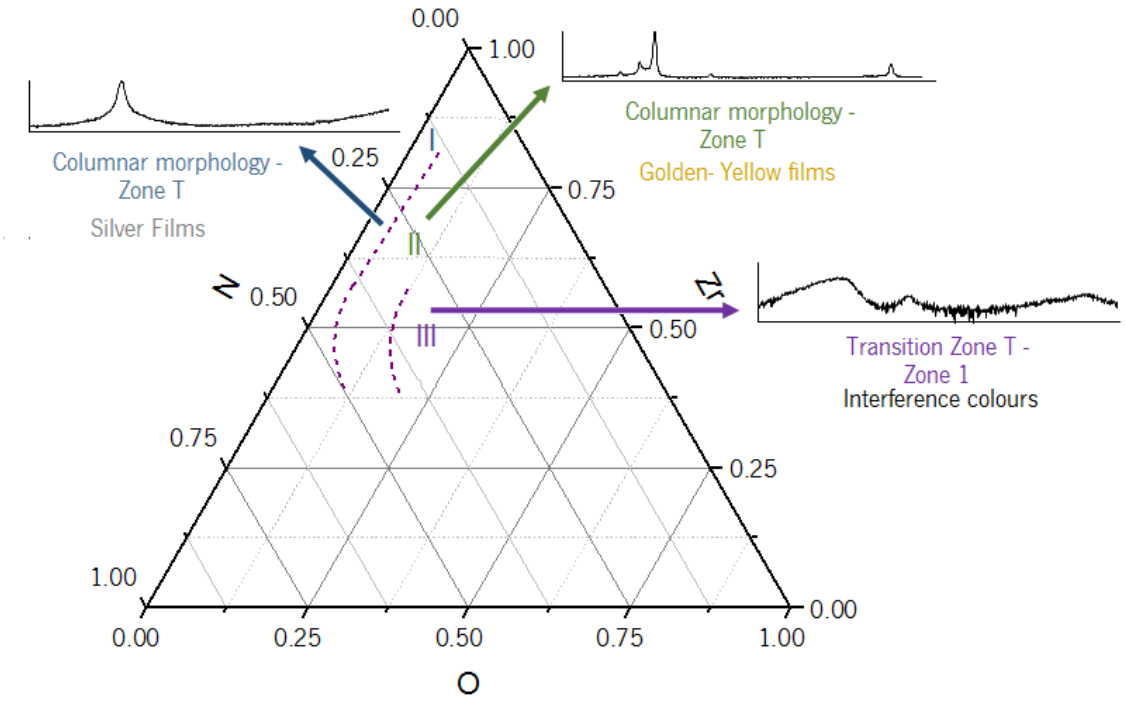

Figure 5.12 scheme of the division of the base series in different zones in terms of chemical composition, structure, growth mode and colour.

In this chapter several batches of samples were deposited with different parameters with the intent of explore the parameter space and comprehend the effect of them in the properties of the samples, namely in comparison with the base series.

In Table 5.3 it can be seen a resume of the effect of each parameter in the sample in comparison with the base series in regard to the Zones previously identified in the samples. The applied bias did not present any major effect in the samples in terms of structure, chemical composition or growth mode. The sample without bias was located in the Zone II in terms of structure and chemical composition and the same was verified for the biased samples.

With the increase of the deposition time the samples present a structure and chemical composition congruent with a transition Zone between Zones I and II but the growth mode was the same. With a decrease in the deposition time the film presented a similar structure as the sample from the base series but in terms of chemical composition the samples are located in a transition between Zone II and III.

With the increase of the target current the samples reveal a transition from Zone II to Zone I either in terms of structure and chemical composition. A decrease in the target current cause a change in the structure and chemical composition form Zone II to Zone III. It was verified that a decrease in the target current presented similar effect as the increase in the reactive gas flow.

Table 5.3 Summary of the effect of each parameters in the properties of the samples

Parameter	Value	Deposition Rate [µm/h]	Chemical composition	Structure	Growth mode
Bias [V]	0	0.686	Zone II	Zone II	Zone T
	-30		Zone II	Zone II	-
	-40	0.707	Zone II	Zone II	Zone T
Deposition time [min]	30	-	Zone II → Zone III	Zone II	-
	60	0.624	Zone II	Zone II	Zone T
	120	0.570	Zone I ← Zone II	Zone I ← Zone II	Zone T
Target current [A]	1.5	0.418	Zone III	Zone III	Tran. Zone T to Zone 1
	2	1.416	Zone II	Zone II	Zone T
	2.5	-	Zone I ← Zone II	Zone I ← Zone II	-
Working gas flow [%]	2%	-	Zone II → Zone III	Zone II → Zone III	-
	5%	0.686	Zone II	Zone II	Zone T
	8%	-	Zone I ← Zone II	Zone I ← Zone II	-

CHAPTER 6

Films doped with titanium (Ti:Zr-N-O)

As it was already referred, some of the coatings were doped with titanium using the approach described in Section 3.2. In this chapter, these films will be analysed using a similar approach to the one used for the Zr-N-O coatings. First, the effect of the addition of Ti will be studied by comparison with undoped films prepared in the same conditions. In addition, the deposition parameter space within the samples with Ti will be investigated. Table 6.1 shows the chemical composition and the deposition rate of the samples doped with titanium. Zr-N-O coatings deposited in the same conditions are also included.

Table 6.1 Chemical composition and deposition rate of the Ti:Zr-N-O films in comparison with similar Zr-N-O coatings (highlighted rows)

Parameter under study		Sample	N_2+O_2 flow		Chemical composition [at. %]				Deposition rate
Parameter	Value		[sccm]	%	Zr	O	N	Ti	[µm/h]
N2+O2 flow [sccm]	5%	Ti TC1.5 5%	2.5	5	-	-	-	-	-
	7.5%	Ti TC1.5 7.5%	3.8	7.5	25	24	32	20	0.665
		TC 1.5 7.5%	3.8	7.5	42	24	34	-	0.418
	8%	Ti TC1.5 8%	4.0	8	-	-	-	-	-
		TC 1.5 8%	4.0	8	40	26	34	-	-
	8.5%	Ti TC1.5 8.5%	4.3	8.5	22	19	38	22	0.468
		TC 1.5 8.5%	4.3	8.5	36	30	34	-	-
	9.5%	Ti TC1.5 9.5%	4.8	9.5	-	-	-	-	-
Target current [A]	1.5 A	Ti TC1.5 8.5%	4.3	8.5	22	19	38	22	0.468
		TC 1.5 8.5%	4.3	8.5	36	30	34	-	-
	2 A	Ti T30 8.5%	4.3	8.5	37	14	38	11	0.965
		RG 8.5%	4.3	8.5	43	13	44	-	0.686
Ti bars and rotation	2 bars	Ti TC1.5 8.5%	4.3	8.5	22	19	38	22	0.468
	1 bar	Ti 1b 8.5%	4.3	8.5	32	17	39	12	0.546
	Static	Ti 1b static	4.3	8.5	31	14	44	12	2.140

The description of the influence of the different deposition parameters will be divided in two groups:

1. Effect of the Ti addition, target current and reactive gas flow;
2. Effect of the number of Ti bars used and the rotation of the substrate holder.

6.1. Chemical composition

Figure 6.1 shows the influence of N_2+O_2 flow and target current on the Ti:Zr-N-O films, and the influence of the Ti addition via the comparison with the corresponding undoped coatings.

It can be seen that the addition of Ti leads to coatings with a higher metal content, although the Zr concentration is lower. The latter observation is expected due to the partial covering of the Zr 'racetrack' by Ti bars. The former is probably connected with the observed increase of deposition rate when Ti bars are included (see Table 6.1 and section 6.2)

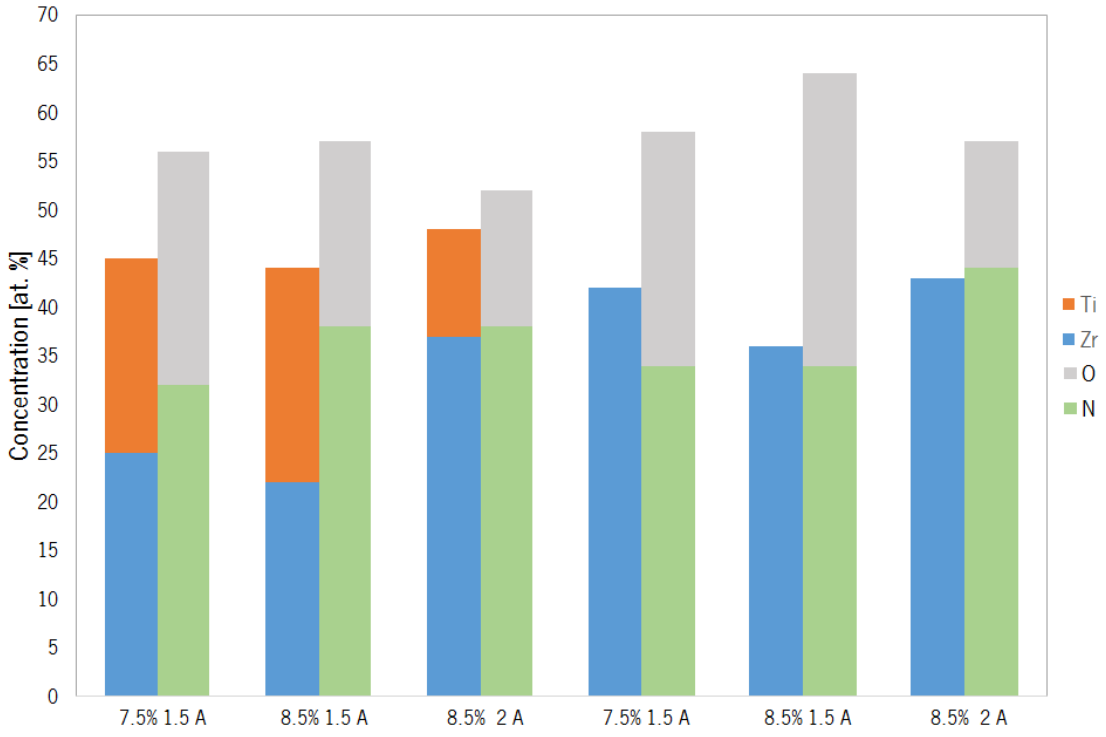

Figure 6.1 Chemical composition of the samples with (Ti TC1.5 7.5%; Ti TC1.5 8.5% and Ti T30 8.5%) and without Ti doping (TC 1.5 7.5%, TC 1.5 8.5% and RG 8.5%) for different deposition parameters.

In both series, a similar general behaviour is observed when the sample-to-sample variations are analysed. In the one hand, the increase of N_2+O_2 flow leads to reduction of metal

content, as expected. Nevertheless, this reduction is lower for the Ti:Zr-N-O films. Thus, although the Zr amount decreases, the Ti concentration stays more or less unmodified. This may indicate that Ti is less sensitive to poisoning than Zr. In fact, the Zr-N-O sample prepared at 8.5% N_2+O_2 and 1.5 A shows a high concentration of O (30%), in contrast to the 20% observed in the corresponding doped sample. To a certain extent, it looks like that the presence of Ti 'protected' the target against the passivation and oxidation observed in the Zr-N-O films. In the other hand, the increase of target current leads to higher values of metal content, as expected as well due to the increased sputtering rate. In addition, the Zr/Ti and N/O ratios increases considerably. The latter effect is likely to be due to the higher deposition rate and less poisoning of the target. The former is probably a consequence of the expansion of the area of sputtering to regions farther than 'race track' (where the Ti bars are located) that occurs at higher currents. In other words, the area of sputtering covered by the Ti bars is proportionally much smaller when the target current is increased. In fact, it can be observed that the chemical composition of both samples deposited at 8.5% of N_2+O_2 and 2 A are very similar. In other words, at higher currents the presence of Ti becomes a small perturbation of the Zr-N-O system.

Figure 6.2 shows the influence of the number of bars and rotation mode on the chemical composition of Ti:Zr-N-O films.

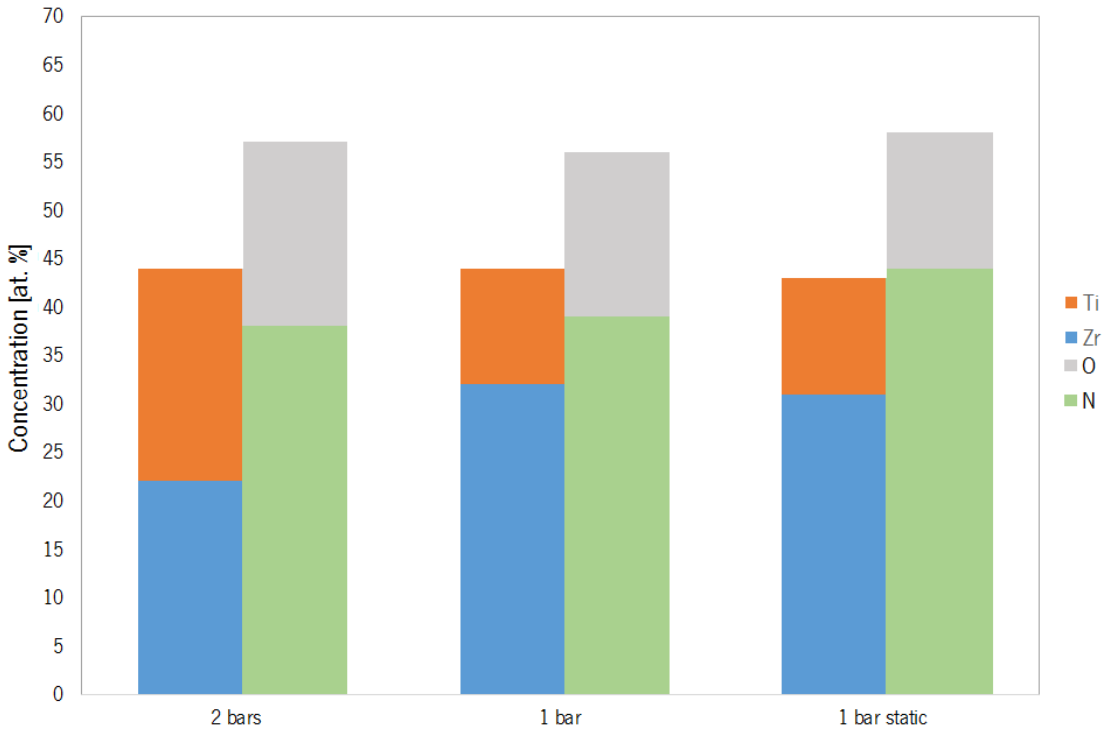

Figure 6.2 Chemical composition of Ti doped samples with different deposition parameters: 2 bars (Ti TC1.5 8.5%); 1 bar (Ti 1b 8.5%) and 1bar static mode (Ti 1bstatic 8.5%)

As it was expected, the removal of 1 Ti bar leads to the reduction of the concentration of titanium in the films (~50% less). Nevertheless, the overall metal concentration remains unchanged, indicating that sputtering of Ti was replaced by Zr. This is because a new area of the Zr target is exposed. The concentration of N and O was approximately the same.

Finally, it can be seen that there is no relevant influence of the rotation mode on the chemical composition of the samples

6.2. Film growth

SEM cross section images of the samples with and without titanium prepared at different conditions of flow of reactive gas and target current are depicted in Figure 6.3.

It can be observed that two pairs of films can be compared to evaluate the influence of the addition of Ti on the growth of the films. In both cases, the addition of Ti leads to an increase of the deposition rate (Table 6.1), from 0.418 and 0.686 μm/h to 0.665 and 0.965 μm/h, respectively[1]. This result is not expected, since zirconium has higher sputtering rate (3.42 μm/h) than titanium (2.07 μm/h)[72]. This could be a consequence of the geometry employed for introducing Ti in the films; as explained in Section 3.2, the titanium bars were placed over the 'race tracks'. It is well known that with the erosion of the target (i.e. increase of the 'race track' depth), there is a reduction of the sputtering rate[64]. The location of the bars over the 'race track' reduced its depth, which would lead to higher values of deposition rate. As was referred previously, the coating deposited without titanium (Figure 6.3b) presents a dense structure with 'interrupted' columns indexed to a transition Zone between the Zone T and 1 of the Thornton's model. The micrograph from the corresponding sample deposited with titanium (Figure 6.3a) is not very clear, but it seems to be similar to the sample deposited without Ti. The films of Figure **6.3**d and e also seem to have a similar microstructure. Both present a columnar morphology characteristic of the Zone T of Thornton's model. Therefore, the inclusion of Ti does not seem to create strong changes on the growth of the films.

In Figure 6.3a and c it is possible to see the cross section SEM images of the Ti doped films deposited with different reactive gas flows. With the increase of the reactive gas flow from

[1] Note that the Ti:ZrNO film deposited using 8.5% of N_2+O_2 and 2 A of target current looks thinner in Figure 6.3 due to the lower deposition time used

7.5% to 8.5% the deposition rate of the samples decreases from 0.665 μm/h to 0.468 μm/h (Table 6.1). This result was expectable, since with the increase of the reactive gas flow the poisoning of the target increases. A similar behaviour was observed for the undoped films, (deposited 2 A of target current instead of 1.5, see Section 4.1). Both samples present a dense microstructure with 'interrupted' columns, although at higher flows of reactive gas the film appears (Figure 6.3c) to become denser and more featureless. Both samples can be indexed to a transition between the Zone T and Zone I of Thornton's model.

A similar evolution was observed in the RG# series at flows of reactive gas above 9% (Figure 4.5d, e, and f). In the RG# series this kind of microstructure appears for higher reactive gas flows. This is because RG# series was deposited with 2 A, while the series with titanium which was deposited with 1.5 A. As explained previously (Section 5.1), the decrease in the deposition current has a similar effect as an increase in the reactive gas flow, and therefore we see the microstructure from Figure 6.3c at lower flows than in the RG# series (Figure 4.5 e) and f.

Figure 6.3c and d show cross section SEM images of the Ti-containing coatings deposited at different target currents. The deposition rate clearly increases at higher target currents, from 0.418 μm/h) to 0.965 μm/h (Table 6.1). This result is in agreement with the observations performed for the undoped films, and can be explained by the higher amount of the ionized argon ions in the plasma, which leads to an increase in the sputtering rate at the target. Nevertheless, it is worth mentioning that the sample prepared with 2 A was deposited during 30 min instead the 60 min typically used. However, it was demonstrated in Section 5.2 that a variation of deposition time does not cause a major variation on the deposition rate, certainly lower than the variation observed in this case. Therefore, the comparison of these two coatings can serve as a valid indicator of the effect of the target current. Regarding the morphology of the films, it is possible to see a difference between both samples. The film deposited at 2 A has a columnar morphology, which is similar to that observed for samples of the RG# series deposited at flows lower than 9% (Figure 4.5a, b and c), which can be indexed to the T Zone of the Thornton's model. In contrast, the sample deposited at 1.5 A starts to lose the columnar microstructure and the columns appear 'interrupted'. Such structure is similar the one developed by the sample of the RG# series deposited with highest flows of reactive gas (Figure 4.5c, d and f), so this sample can be indexed to a transition Zone between Zone T and Zone 1 of the Thornton's Zone model. A similar evolution was verified for Zr-N-O coatings (see Section 5.2)

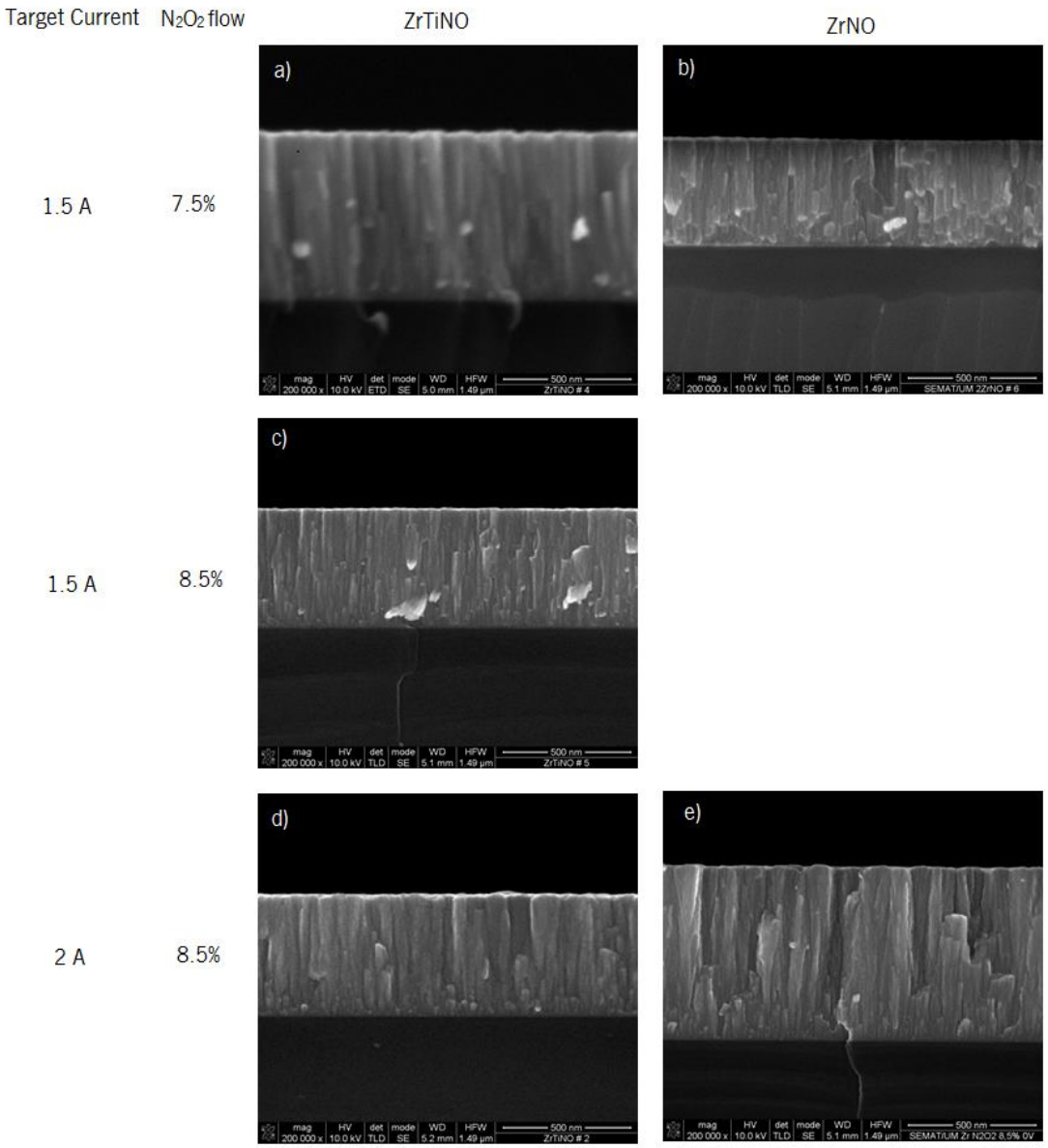

Figure 6.3 Cross section micrograph of the samples with (a) Ti TC1.5 7.5%; c) Ti TC1.5 8.5% and d) Ti T30 8.5%) and without titanium doping (b) TC 1.5 8.5% and e) RG 8.5%)

Figure 6.4 shows the influence of the number of bars located in the 'race track', and the rotation mode on the growth of the Ti:Zr-N-O films. First of all, it can be observed that the removal of 1 Ti bar leads to the increase of the deposition rate from 0.418 to 0.546 μm/h. This result is certainly unexpected, since the removal of both Ti bars (i.e. deposition of Zr-N-O film) leads to films with lower deposition rates, as described before. One might think that the asymmetrical configuration of the sputtering target under plasma may create an abnormally high sputtering rate. Nevertheless, the general behaviour of the deposition rate with the addition of Ti is difficult to explain, and it is probably connected with the unconventional approach used to locate the Ti

on the sputtering target. In fact, the deposition rate for undoped films should be the highest, since the sputtering rate of Zr is higher than that of Ti. Additionally, it is possible to see that with the variation of the amount of Ti (Figure 6.4a and b) the microstructure remains more and less the same. Both coatings present a dense microstructure with interrupted columns and can be indexed to a transition Zone between Zone T and Zone I of the Thornton's model, as stated previously for the sample Ti TC1.5 8.5%.

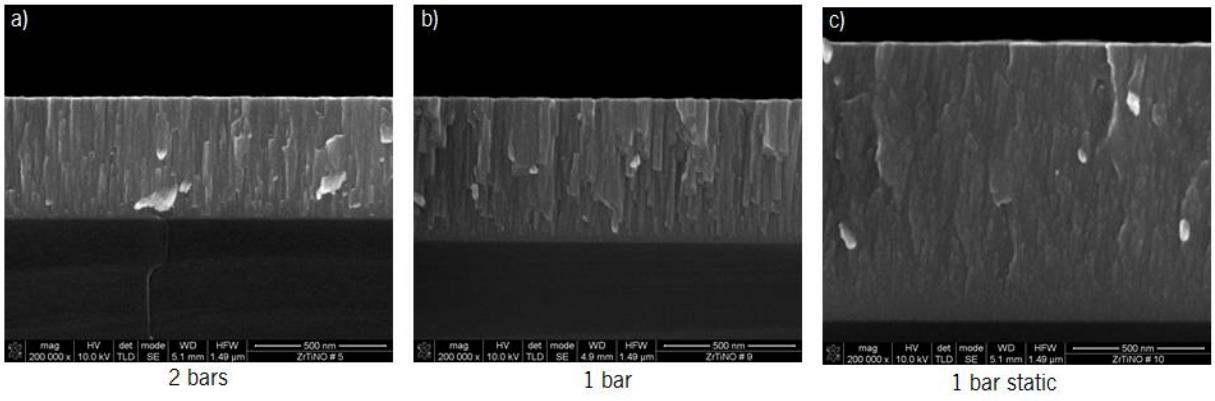

Figure 6.4 Cross section images of the Ti-containing samples deposited with two Ti bars (Ti TC1.5 8.5%), one Ti bar (Ti 1b 8.5%) and one bar in static mode (Ti 1b static 8.5%)

Finally, Figure 6.4b and c show the cross section SEM images of the films deposited with and without substrate rotation. First, it can be seen that the deposition rate of the samples deposited in static mode (2.14 μm/h) is much higher (an increase by a factor 5, see Table 6.1) than the values observed for the corresponding samples deposited with substrate rotation (0.418 μm/h). This is an expected result, since the substrates are directly facing the target in a static mode without spending a part of the time during the rotation in a region of shadow where no deposition takes place. The coating deposited in static mode has a more compact and fibrous structure with no trace of columnar development than the sample with rotation. In terms of the indexation to the Thornton's Zone model, this sample can be indexed to the Zone I.

6.3. Crystallographic structure

In Figure 6.5 it is possible to see the diffractograms of the Zr-N-O and Ti:Zr-N-O samples where is possible to see the effect of different parameters: addition of Ti, reactive gas flow, and target current.

Comparing the samples deposited at 2 A with and without titanium doping (Figure 6.5c)

and d), it is possible to see that the addition of titanium does not change considerably the structure of the Ti:Zr-N-O films in comparison with the base series samples. In both cases the evolution of the composition is similar with the increase of the reactive gas flow. There is a transition from a Zone II structure (or Zone I in the case of Ti:Zr-N-O) to Zone III. For flows of 8.5% the Ti-doped samples has relatively broad peaks consistent with the ZrO and ZrN phases. With the increase of the flow to 9.5% the Ti:Zr-N-O films present broad peaks that englobe mainly the ZrN and ZrO phases as in the case of the sample without titanium. This maintenance of the structure evolution for the samples deposited with Ti and 2 A in comparison to the similar samples of the base series can be related to the chemical composition. As was seen previously (Section 6.1), the addition of Ti represents a small perturbation in the Zr-N-O system when depositing at 2 A.

When comparing the Zr-N-O and Ti:Zr-N-O coatings deposited at 1.5 A (Figure 6.5a) and b, it can be seen that the addition of Ti leads to a big difference in the structure of the films. The Zr-N-O samples are much more amorphous then the ones deposited with Ti. In terms of chemical composition, the main difference between the samples deposited with titanium doping in comparison with the Zr-N-O films, is the presence of Ti, since the total amount of metal and the amount of reactive species are very similar (e.g. see the chemical composition of films deposited with 7.5% N_2O_2 and 1.5 A in Figure 6.1). Therefore, this result indicates that the enhanced crystallinity of the Ti:Zr-N-O films can be related to an easier formation of Ti-N-O phases that the formation of Zr-N-O phases in the base series samples, leading to more amorphous coatings.

Therefore, the reduction of target current from 2 A to 1.5 A causes different behaviours on both systems. Thus, in the case of the Zr-N-O films, the reduction of target current Figure 6.5d to b causes the amorphization of the films, similarly to the abovementioned effect of the increase of N_2+O_2 flow (see Section 4.4). This is because the metal content decreases at lower target current. In contrast, a reduction of power in case of the Ti:Zr-N-O films does not lead to the amorphization of the films (Figure 6.5c to a). This is because the Ti concentration is still high enough to promote the formation of Ti-related crystalline phases.

Depending on the XRD peaks detected, in the case of the Ti:Zr-N-O films deposited at 1.5 A (Figure 6.5a), two regions can be distinguished depending on the N_2+O_2 flow. The first region would be formed by the films deposited with 5% and 7.5% of N_2+O_2, and the second region englobes the coatings deposited with flows of 8%, 8.5% and 9.5%. The first group is characterized by the presence of Zr-O-N peaks (ca. 34°), together with a second contribution of TiN. In this group, the position of the peaks is little displaced to lower angles with respect to the references.

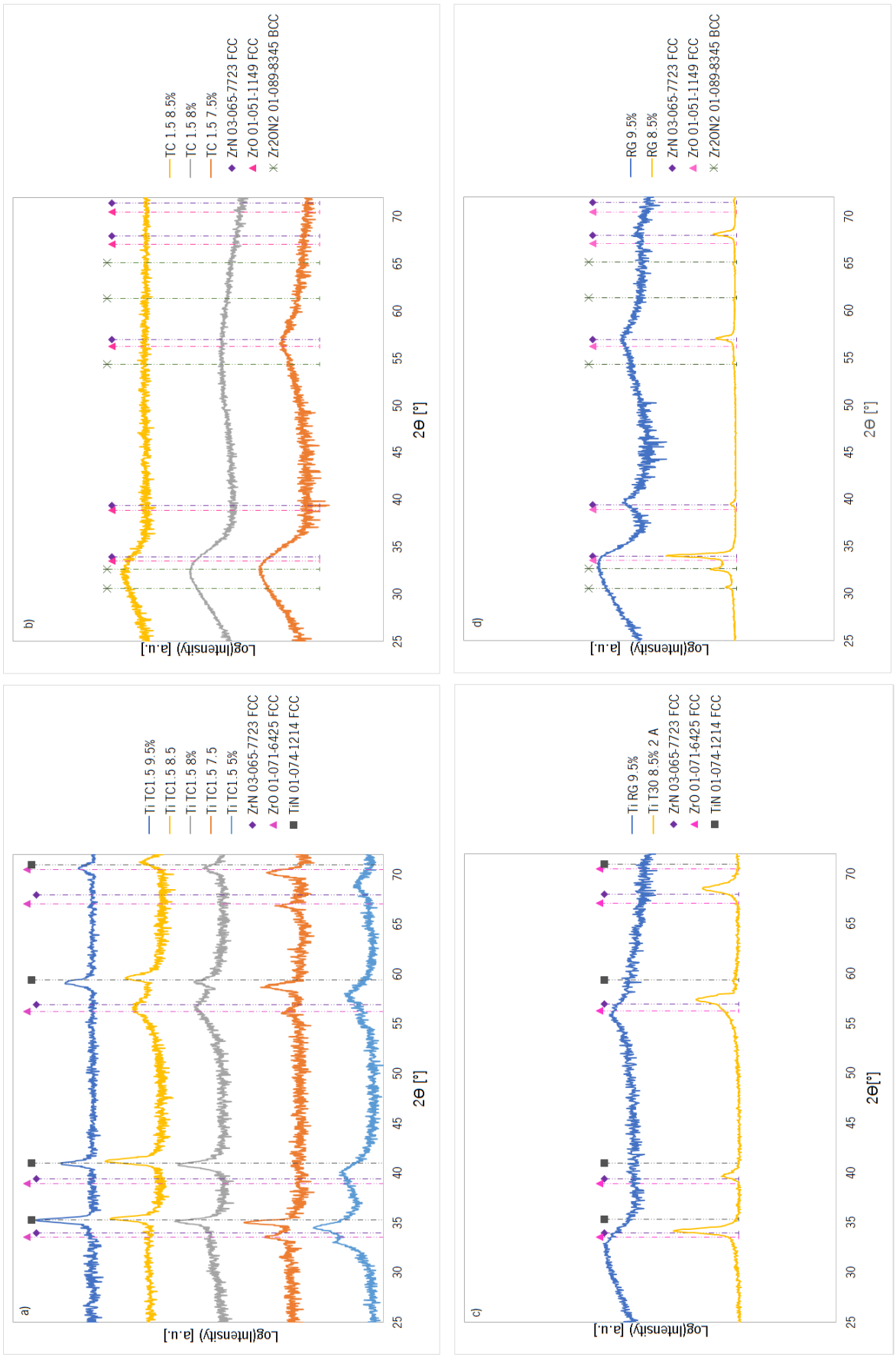

Figure 6.5 Diffractogram of the sample with and without titanium doping deposited with different parameters

In the second group, the diffractograms are basically interpreted as TiN, whose peak positions are better coincident with the TiN reference. Neverthless, for lower N_2+O_2 flows (8 and 8.5%), a broad contribution of Zr-O-N can be still detected (ca. 56º), which disappears at 9.5% N_2+O_2 flow. This behaviour can be explained with the evolution of chemical composition of the coatings with N_2+O_2 flow (cf. Figure 6.1). Thus, the increase of flow of reactive mixture leads to the reduction of Zr, but the overall metal content is more or less the same. In addition, the N/O ratio increases. Therefore, at low gas flow (1st group), the Zr-based phases would be still present, and co-existing with the easier-to-form Ti-based ones. Both phases would be poorly formed by the higher presence of O. At higher N_2+O_2 flows (2nd group), the Zr concentration would be too low to form 'good' Zr-based phases (in fact, they are vanished at 9.5% N_2+O_2). As a consequence, the main peaks are identified as TiN-like phases, which are in fact better crystallized than at low N_2+O_2 flows, since the Ti/Zr and N/O ratios are higher (less competence in growth and lower presence of defects which promotes amorphization).

The increase of target current in the Ti:Zr-O-N system (Figure 6.5a to c) can be explained in terms of the replacement of Ti by Zr atoms. In both cases that we can compare (8.5 and 9.5% N_2+O_2), we move from reasonably well formed TiN phases to Zr phases that are quite different. At 9.5%, we arrive to a film in Zone III, with high concentration of N and O. In contrast, at 8.5%, we arrive to a coating of Zone II, which is characterized with better formed Zr-N-O phases (maybe doped with Ti, since the peaks are little displaced to high angles).

In Figure 6.6 it can be seen the structure of the samples deposited with different amounts of titanium (Ti TC1.5 8.5 – 2 bars, and Ti 1b 8.5% - 1 bar). The sample deposited with 2 has a structure formed by TiN, as was explained before. In the case of the film deposited with one bar, it is possible to see that the peaks in the diffractogram are between the references of the TiN and ZrN phases. This probably indicates that this sample consists in a solid solution of ZrN and TiN. In terms of chemical composition, with the decrease of the number of bars from 2 to 1 there is a decrease in the Ti content of about 50%, which can explain this peak displacement. Additionally the sample deposited with 1 bar also presents one broad peak consistent with ZrN and ZrO phases, similarly to the sample deposited with 2 bars.

Regarding the coating deposited in static, in Figure 6.6 it is possible to see its diffractograms in comparison with the film deposited in dynamic mode (Ti 1b sta 8.5% and Ti 1b 8.5%). In terms of structure both samples are very similar, and the film deposited in static mode also present a structure congruent with a ZrN and TiN solid solution

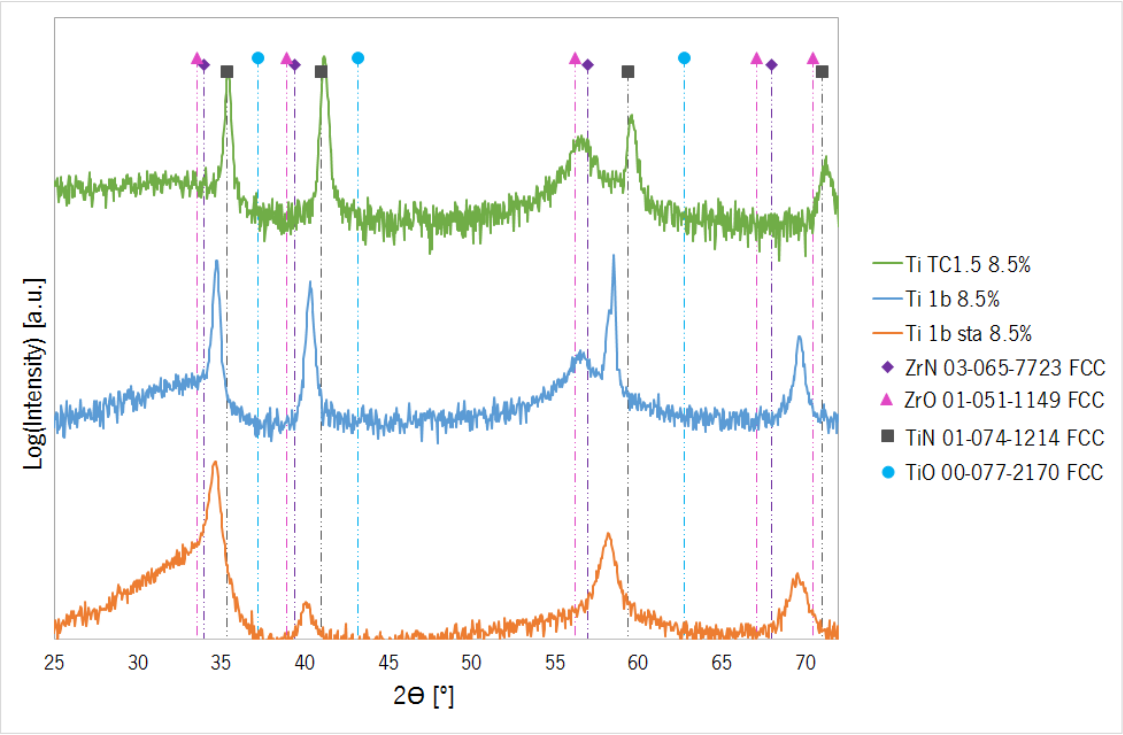

Figure 6.6 Diffractogram of the titanium doped samples deposited with different amounts of titanium and in static mode

6.3.1. Evolution of the crystallographic structure with the temperature

In Figure 6.7 it is possible to see the diffractograms of the Ti samples Ti TC1.5 5% and Ti TC1.5 7.5% during the heat treatment. As was seen before, these films belong to the first group of samples regarding the films deposited under different reactive gas flows. This two samples present a structural evolution with the heating very similar, once their initially structure was also similar.

From room temperature until 600 °C both samples have a similar structure to the one described before. The structure consists mainly in a combination of TiN and Zr-O-N peaks.

With a further increase of the temperature it is possible to see that then main difference in the structure of the samples is the appearance of the peaks at angles lower than 30° and at ca. 50°. These peaks could be attributed to $Zr_5Ti_{17}O_{24}$ (i.e. TiO_2 where some atoms were replaced by Zr) and Zr_3N_4 phases. The other peaks became narrower with the increase of the temperature and some of the broad peaks give raise to several peaks. This indicates that the changes on the structure of these samples with the increase of the temperature consisted mainly in the crystallization of the phases already present in the films, although new phases also appeared. This is opposed to the samples from the base series, where new phases were developed with the

increase of the temperature at expenses of the phases initially existing.

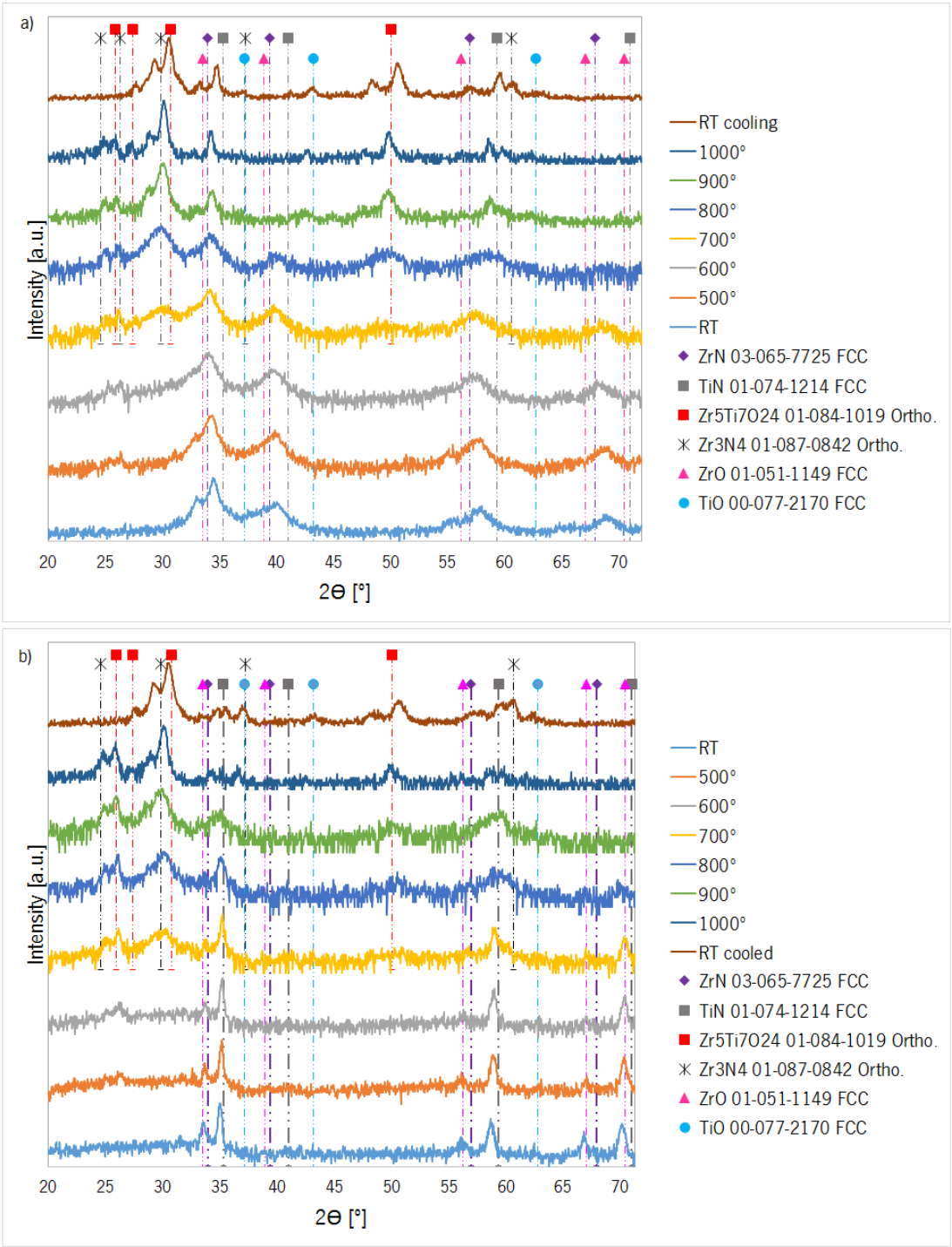

Figure 6.7 Diffractograms with the heating of the titanium samples with different reactive gas flows: a) Ti TC1.5 5% and b) Ti TC1.5 7.5%

6.4. Colour

Table 6.2 indicates the value of the colour coordinates for the Ti:Zr-N-O films in comparison with the coordinates of similar Zr-N-O samples.

Table 6.2 Colour coordinates of the Ti:Zr-N-O films in comparison with similar Zr-N-O coatings. The highlighted rows correspond to the samples without titanium doping.

Parameter under study		sample	Colour coordinates [a.u]		
Parameter	Value		L*	a*	b*
N2+O2 flow [%]	5	Ti TC1.5 5%	71.80	1.08	9.78
	7.5	Ti TC1.5 7.5%	55.77	5.74	15.45
		TC 1.5 7.5%	76.01	1.20	27.49
	8	Ti TC1.5 8%	50.44	3.30	-2.04
		TC 1.5 8%	84.08	-0.65	36.74
	8.5	Ti TC1.5 8.5%	50.67	2.80	-3.04
		TC 1.5 8.5%	84.50	-1.42	36.35
	9.5	Ti TC1.5 9.5%	51.15	3.92	-1.12
Target current [A]	1.5	Ti TC1.5 8.5%	50.67	2.80	-3.04
		TC 1.5 8.5%	84.50	-1.42	36.35
		TC 1.5 9.5%	51.1	3.9	-1.1
	2	Ti T30 8.5%	63.59	3.40	22.32
		RG 8.5%	56.45	9.08	21.44
		Ti RG 9.5%	Transparent		
		RG 9.5%	Transparent		
Ti bars and rotation	2 bars	Ti TC1.5 8.5%	50.67	2.80	-3.04
	1 bar	Ti 1b 8.5%	51.11	4.69	1.00
	Static	Ti 1b static	52.47	5.43	-0.99

Figure 6.8 illustrates the colour wheel with the titanium doped samples with the different deposition parameters in comparison with the RG# series. It is possible to see that the samples deposited with titanium cover a larger area of the colour wheel than the base Zr-N-O series. The majority of the Ti-doped samples have low values of the chromatic coordinates a* and b*, and together with the values of L*, this coatings are in the Zone of the greys. The other Ti-doped samples are in the range of the silver and golden-yellow coatings.

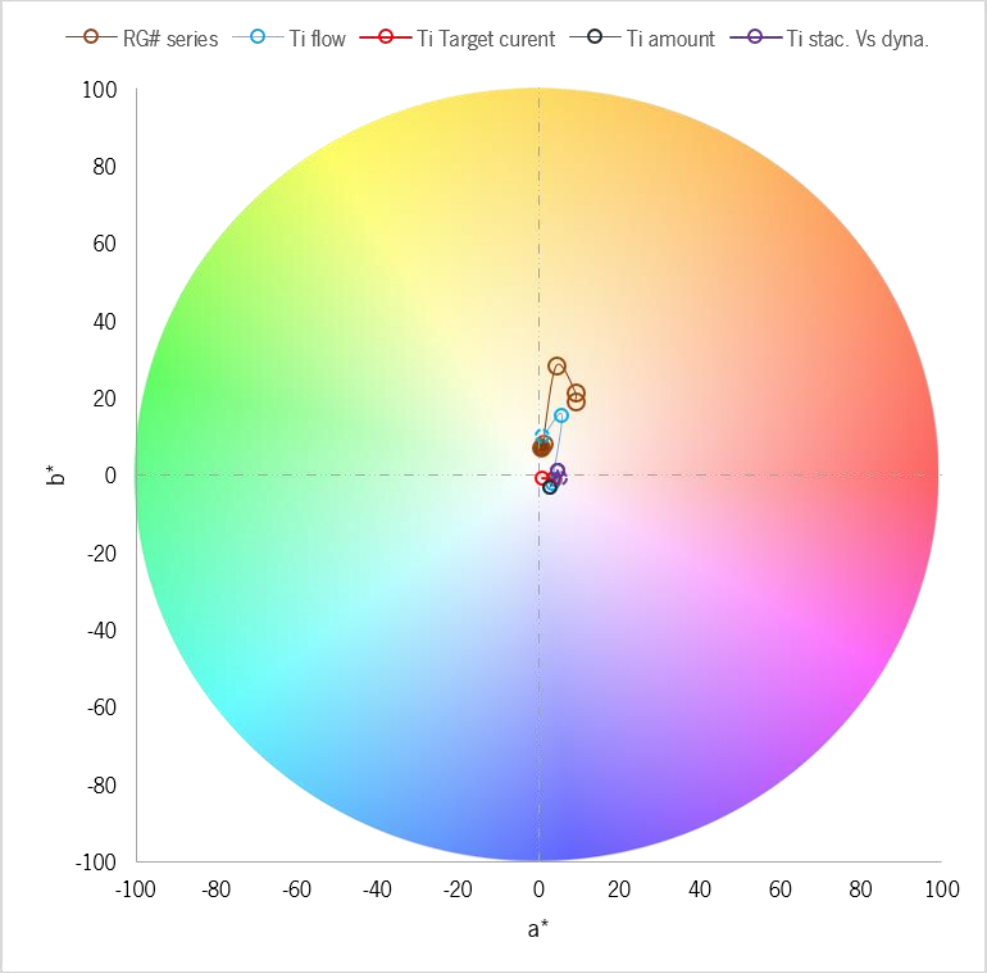

Figure 6.8 Colour whell with the a* and b*colour coordinates from the Ti samples deposited with different deposition parameters in comparison with the base series

In Figure 6.9 it is possible to see in more detail the colour coordinates of the Ti doped samples with different deposition parameters. The samples doped with titanium tend to 'escape' the Zone of the colour occupied by the samples without titanium doping.

Figure 6.9a shows the colour evolution of the Ti doped samples with the reactive gas flow in comparison with similar Zr-N-O films. The coatings deposited without titanium have interference-like colours with higher values of b* and values of a* around zero. The Ti:Zr-N-O coatings deposited with different reactive gas flows have lower values of b* and higher values of a* then the previous films. The sample with lower flow has a metallic colour and with the increase of the flow the coatings have golden colours and for higher flows they present dark grey colours. This difference in the evolution of the colour are probably related to the differences verified in the chemical composition and structure of the samples with and without titanium. The samples deposited with lower gas flows (5% and 7.5% - group 1 in the XRD's) obviously behave different than the others from group 2. The two samples belonging to group 1, which have two

coexisting Ti-based and Zr-based phase are clearly different from the others. The films from group 2 are all probably solid solution of Ti-N and Zr-O-N to a certain extent with very similar diffractogram among them.

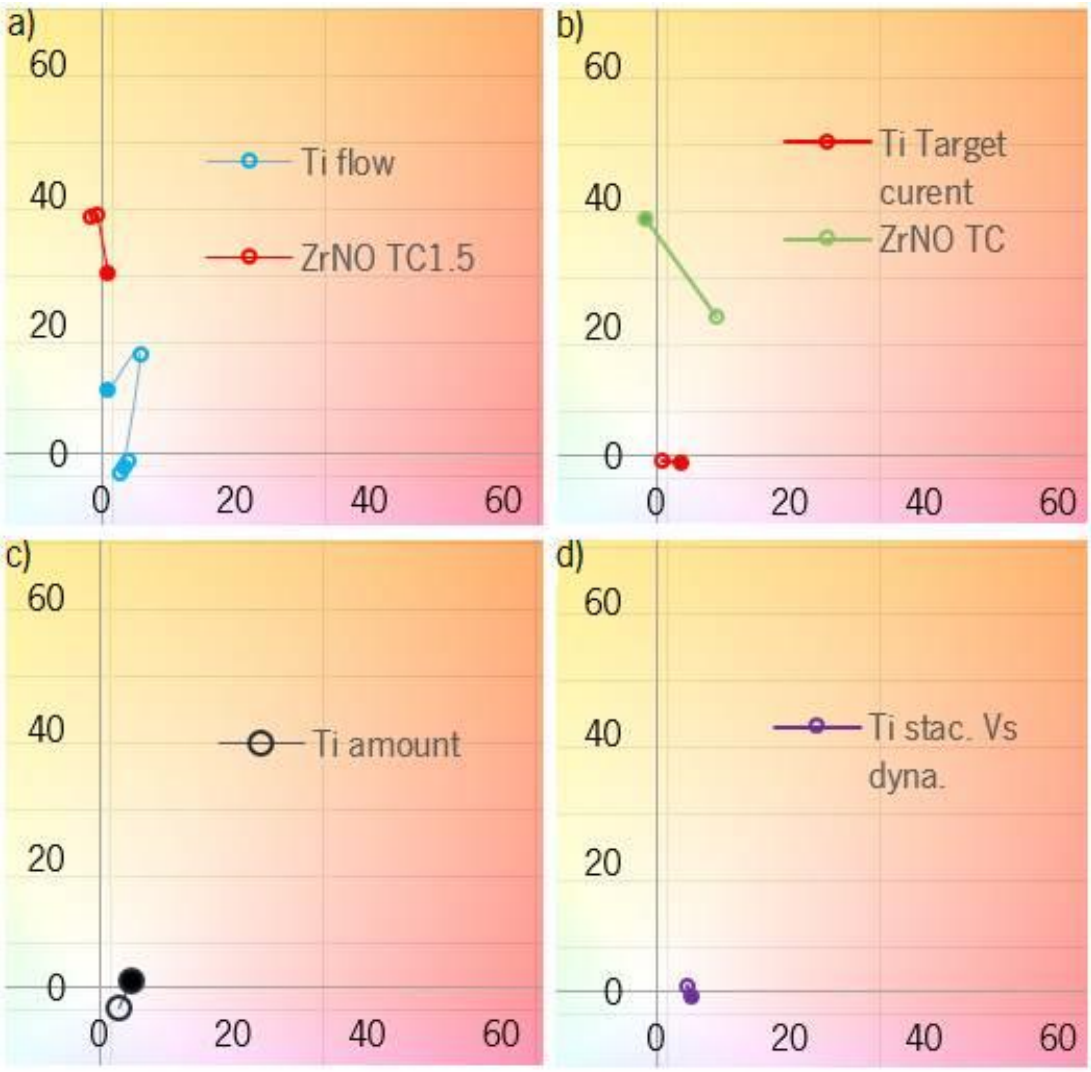

Figure 6.9 Zoom of Colour wheel with the a* and b*colour coordinates from the Ti samples deposited with different parameters compared with the base series. a) Reactive gas flow b) Target current c)Ti amount; d) Static (filed dot) vs dynamic mode. The filed symbols correspond to the lower value of the parameter.

The Ti:Zr-N-O films deposited with different reactive gas flows are the ones that experience larger variations in terms of colour in the Ti-doped samples.

For the other parameters studied in this type of sample, namely the target current, the titanium amount and the static mode, the colours of the films were very similar among them, presenting lower values of chromatic coordinates, and with a dark grey appearance.

In the case of the samples deposited with different amount of titanium and the samples in static vs dynamic mode, this similarity in the colour was expected once this coatings are very

similar in terms of structure (Figure 6.6) and chemical composition (Table 6.1).

The other samples that presented dark grey colour have very different structures and chemical compositions.

6.5. Conclusions

In this chapter the films were doped with titanium in order to see the difference in the properties in comparison with the base series. The main conclusions achieved in this chapter are:

- The introduction of Ti in the coatings has a notorious influence, particularly at low target currents. This is due to the fact that at lower current the Ti/Zr ratio is higher. The Ti:Zr-N-O coatings deposited with lower current present two groups in terms of structure: the first formed by two coexisting Ti-based and Zr-based phases, and the other formed by a solid solution of TiN and Zr-N-O. In contrast, the samples without titanium present similar structure among them at lower currents which is considerably amorphous. In terms of colour, the Ti:Zr-N-O look silver, golden- yellow and dark grey while the Zr-N-O coatings are in the interference zone.
- The formation of dark-grey coatings represent an expansion of the intrinsic colour range obtained in comparison with the samples without titanium which only present intrinsic colours with silver and golden tones.

CHAPTER 7

Conclusion and Future works

7.1. Conclusions

In this work the main objective was to deposit zirconium oxynitride thin films some of which doped with titanium by reactive magnetron sputtering, in order to obtain new coloured coatings. The films were then characterized by means of SEM, RBS, XRD and spectrophotometry.

The samples were deposited in several batches and varying different deposition parameters such as the reactive gas flow (base series), the bias voltage, the target current, the deposition time and the working gas flow. Some of the samples were doped with titanium and for this samples some of the deposition parameters (target current, reactive gas flow, titanium amount and static mode) were varied as well.

The main conclusion archived during the realization of this work was that the samples deposited with different reactive gas flows can be divided into three zone in terms of deposition rate, target voltage, chemical composition, structure, growth mode and colour, which indicates a tight correlation between the chemical composition of the films the structure and colour. In terms of colour tones obtained the samples presented silver, golden-yellow and interference colours.

When exploring the parameters space it was possible to see that the bias voltage does not affect considerably the properties of the films regarding the base series. It was also noticeable that a decrease in the target current and in the working gas flow has a similar effect in the properties of the films as the increase of the reactive gas flow.

In the case of the samples doped with titanium it was possible to see that the samples 'escaped' the zone of the colour wheel occupied by the previous films but almost all the samples present similar dark grey colour.

7.2. Future works

In order to achieve new colour tones (namely light blue) the first step of the future works is to deposited zirconium oxynitrides with individual control of the reactive gases (O_2 and N_2) instead of introducing them as a fixed mixture. This will allow a finer control over the chemical

composition of the films.

Afterwards, once these coatings would be designated as a candidate for decorative applications, it would be important to perform additional characterization such as:

- Hardness tests;
- Adhesion tests;
- Corrosion resistance, namely in sweat solutions once the objects in question will be in contact with the human skin;
- Biocompatibility, once more due to the contact between the object and the skin of the user. It is important to guarantee that the object cause no arm.

Appendix I

From a practical point of view, the idea behind this mathematical development was simple: obtain the standard deviation of the colour coordinates among the different substrates. If the standard deviation would be low, it would mean that the colour of all the substrates is similar and therefore the colour would be intrinsic. If not, there would be some contribution of the substrates, which are different, and therefore a variation of colour from substrate to substrate will be observed, leading to higher standard deviations. The calculation of the standard deviation from a set of numbers is a simple formula. However, the situation is more complex in this case, since each number of the set is accompanied from its standard deviation, since we make several measurements of colour in each substrate.

Therefore, the fundamental question was: how to calculate the overall standard deviation of a set of values with standard deviations? Three possible cases can be imagined, which are illustrated in Figure I.1. In the first case (Figure I.1b1), the error bars are small in comparison with the separation between points. Therefore, the main contribution to the overall SD should come from the separation between them (i.e. the 'conventional' calculation of SD). On the contrary, in the last case (Figure I.1b3) the error bars are much larger than the separation between the points, and therefore the main contribution to the overall SD should come from the values of the SD. The intermediate situation is the Figure I.1b2, where both components (separation of the points and SD's) contribute to the overall SD.

The following mathematical development was performed in order to calculate this overall SD for any of these cases, with the help of Prof. Raquel Menezes, from the Department of Mathematics and Applications of the University of Minho.

The standard deviation (s_N^2)) of a set of data is the square root of its variance. The definition of variance (of a set of N data can be written as;

$$S_N^2 = \frac{1}{N}\sum_{i=1}^{N}(X_i - \bar{X})^2 = \frac{1}{N}\sum_{i=1}^{N}X_i^2 - \bar{X}^2 \qquad (1)$$

Where $\bar{X}$ is the average, which can be defined as:

$$\bar{X} = \frac{1}{N}\sum_{i=1}^{N} X_i \tag{2}$$

Therefore, eq. 1 can be re-written as:

$$S_N^2 = \frac{1}{N}\sum_{i=1}^{N}(X_i - \bar{X})^2 = \frac{1}{N}\sum_{i=1}^{N} X_i^2 - \left(\frac{1}{N}\sum_{i=1}^{N} X_i\right)^2 \tag{1b}$$

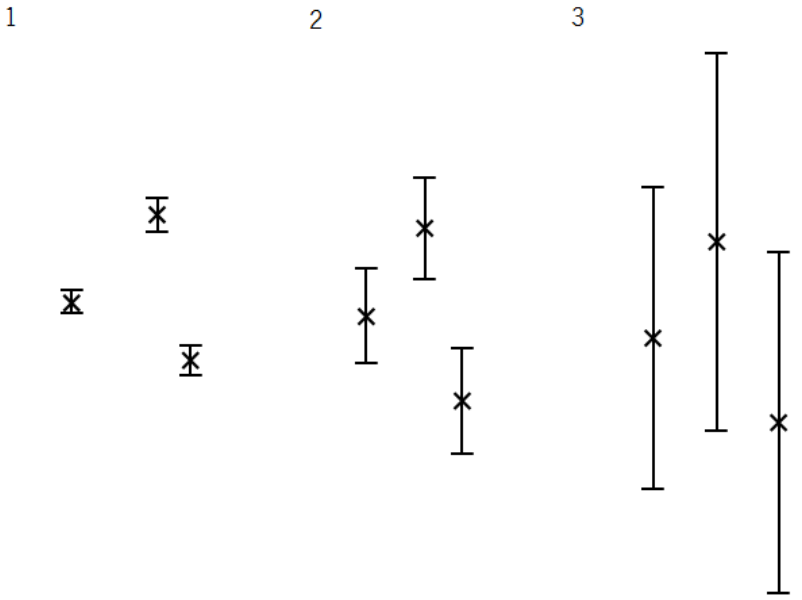

Figure I.1 Representation of the different contributions for the overall SD of the colour.

Our situation is that, instead having the N original values, we have m pairs (average, standard deviation) calculated from the N original values, which are unknown. Moreover, we have to consider the same weight for each pair of data. The standard deviation of the m pairs can be written:

$$s_1^2 = \frac{1}{n_1}\sum_{j=1}^{n_1} x_{j1}^2 - \bar{x}_1^2 \Rightarrow \sum_{j=1}^{n_1} x_{j1}^2 = n_1(s_1^2 + \bar{x}_1^2) \tag{3a}$$

$$s_2^2 = \frac{1}{n_2}\sum_{j=1}^{n_2} x_{j2}^2 - \bar{x}_2^2 \Rightarrow \sum_{j=1}^{n_2} x_{j2}^2 = n_2(s_2^2 + \bar{x}_2^2) \tag{3b}$$

(...)

$$s_m^2 = \frac{1}{n_m}\sum_{j=1}^{n_m} x_{jm}^2 - \bar{x}_m^2 \Rightarrow \sum_{j=1}^{n_m} x_{jm}^2 = n_m(s_m^2 + \bar{x}_m^2) \quad (3m)$$

The two terms on the right in eq. 1 can be written in terms of the pairs of data as:

$$\bar{X} = \frac{1}{m}\sum_{k=1}^{m} \bar{x}_k \quad (4)$$

$$\sum_{i=1}^{N} X_i^2 = \sum_{k=1}^{m}\sum_{j=1}^{n_k} x_{jk}^2 \quad (5)$$

Using eqs 4 and 5, eq. 1 can be re-written as:

$$S_N^2 = \frac{1}{N}\sum_{i=1}^{N} X_i^2 - \bar{X}^2 = \frac{1}{N}\sum_{k=1}^{m}\sum_{j=1}^{n_k} x_{jk}^2 - \left(\frac{1}{m}\sum_{k=1}^{m} \bar{x}_k\right)^2 \quad (6)$$

Replacing the 1st term in eq. 6 using eq. 3, we arrive to:

$$S_N^2 = \frac{1}{N}\sum_{k=1}^{m} n_k\left(s_k^2 + \bar{x}_k^2\right) - \left(\frac{1}{m}\sum_{k=1}^{m} \bar{x}_k\right)^2 \quad (7)$$

Equation 7 correlates the overall variance with the *m* pairs (average, standard deviation), i.e. the *m* pairs ($\bar{x}_k$, s_k). The difficulty is the presence of n_k and *N*. However, since we have to give the same weight to all the *k* pairs, we have to make:

$$n_1 = n_2 = \cdots = n_k = \cdots = n_m \quad (8)$$

And therefore

$$N = \sum_{k=1}^{m} n_k = n_k m \quad (9)$$

And using eq. 9, equation 7 reaches to:

$$S_N^2 = \frac{1}{m}\sum_{k=1}^{m}\left(s_k^2 + \bar{x}_k^2\right) - \left(\frac{1}{m}\sum_{k=1}^{m}\bar{x}_k\right)^2 = \frac{1}{m}\sum_{k=1}^{m}\left(s_k^2 + \bar{x}_k^2\right) - \bar{X}^2 \quad (10a)$$

In other words, the general standard deviation can be expressed in terms of the pairs (average, standard deviation) as:

$$S_N = \sqrt{\frac{1}{m}\sum_{k=1}^{m}\left(s_k^2 + \bar{x}_k^2\right) - \left(\frac{1}{m}\sum_{k=1}^{m}\bar{x}_k\right)^2} = \sqrt{\frac{1}{m}\sum_{k=1}^{m}\left(s_k^2 + \bar{x}_k^2\right) - \bar{X}^2} \quad (10b)$$

Further considerations

This expression should be valid for any relative weight to the contribution of the m averages (s_k) and the standard deviations (s_k) to the overall standard deviation (S_N) (i.e. for the three situations depicted in Figure N). However, we can verify if the equation works in the extremes:

a) Situation where the averages show no standard deviation (i.e. the individual standard deviations are much smaller than the separation between the different values of the averages, Figure I.1 b1). In such case, we would calculate the overall Variance using the general formula (see eq. 1):

$$S_N^2(averages) = \frac{1}{m}\sum_{k=1}^{m}\bar{x}_k^2 - \bar{X}^2 \quad (11a)$$

which is what obtained from eq. 10a after neglecting the standard deviations.

b) Situation where the standard deviations are much larger than the differences among averages (Figure I.1 b3). In this case, the overall Variance can be calculated from the individual standard deviations as:

$$S_N^2(deviations) = \frac{1}{m}\sum_{k=1}^{m}s_k^2 \quad (11b)$$

Which is what obtained from eq. 10a after neglecting the contribution of the averages.

In other words, the expression of the overall Variance (eq. 10a) can be written as the linear addition of two terms:

$$S_N^2 = S_N^2(averages) + S_N^2(deviations) \quad (10c)$$

REFERENCES

[1] F. Vaz, P. Cerqueira, L. Rebouta, S. Nascimento, E. Alves, P. Goudeau, et al., Structural, optical and mechanical properties of coloured TiNxOy thin films, Thin Solid Films. 447-448 (2004) 449–454. doi:10.1016/S0040-6090(03)01123-4.

[2] A. Piegari, F. François, Optical thin films and coatings, Woodhead Publishing Limited, 2013.

[3] E. Ariza, L. Rocha, F. Vaz, L. Cunha, S. Ferreira, P. Carvalho, et al., Corrosion resistance of ZrNxOy thin films obtained by rf reactive magnetron sputtering, Thin Solid Films. 469-470 (2004) 274–281. doi:10.1016/j.tsf.2004.08.091.

[4] E. Ariza, L. a Rocha, S.C. Ferreira, F. Vaz, L. Cunha, P. Carvalho, et al., Corrosion behaviour of single layered ZrNx O y thin films in artificial sweat solutions, in: Proc. Eur. Corros. Conf., 2004.

[5] F. Vaz, P. Carvalho, L. Cunha, L. Rebouta, C. Moura, E. Alves, et al., Property change in ZrNxOy thin films: Effect of the oxygen fraction and bias voltage, Thin Solid Films. 469-470 (2004) 11–17. doi:10.1016/j.tsf.2004.06.191.

[6] P. Carvalho, F. Vaz, L. Cunha, L. Rebouta, C.J. Tavares, C. Moura, et al., Structural and Optical Characterization of Decorative ZrOxNy Thin Films, in: Soc. Vac. Coaters - Annu. Tech. Conf. Proc., 2005: pp. 580–583.

[7] P. Carvalho, J.M. Chappé, L. Cunha, S. Lanceros-Méndez, P. Alpuim, F. Vaz, et al., Influence of the chemical and electronic structure on the electrical behavior of zirconium oxynitride films, J. Appl. Phys. 103 (2008) 104907. doi:10.1063/1.2927494.

[8] P. Carvalho, F. Vaz, L. Rebouta, L. Cunha, C.J. Tavares, C. Moura, et al., Structural , electrical , optical , and mechanical characterizations of decorative ZrOxNy thin films, J. Appl. Phys. 98 (2005) 1–8. doi:10.1063/1.1990261.

[9] R. Kuehni, Color - An Introducton to Practice and Principles, 3rd ed., Wiley, New Jersey, 2013.

[10] G.A. Klein, Industrial Color Physics, 1st ed., Springer, London, 2010.

[11] AZoM.com Staff Writers, How to Measure Solid Colors Using 45/0 and Sphere Geometry,

(2014). http://www.azom.com/article.aspx?ArticleID=10627 (accessed June 12, 2015).

[12] S.F. Johnston, A History of Light and Colour Measurement: Science in the Shadows, 1 st, IOP, London, 2001. doi:10.1088/0957-0233/13/2/704.

[13] M.G. Bamfield, P, Hutchings, Chromic Phenomena - Technological Applications of Colour Chemistry, 2nd ed., RSC Publishing, Cambridge, 2010. doi:10.1039/9781849731034.

[14] R. Mcdonald, Colour Physics for Industry, second edition, Color Res. Appl. 22 (1997) 418–419. doi:10.1002/(SICI)1520-6378(199712)22:6<418::AID-COL9>3.0.CO;2-Y.

[15] K. Nassau, ed., Color for Science, Art and Technology, 1st ed., Elsevier, Amsterdam, 1998.

[16] artinaid, What is light or electromagnetism?, (2015). http://www.artinaid.com/2013/04/what-is-light-or-electromagnetism/ (accessed June 8, 2015).

[17] J.M.M. Chappé, F. Vaz, L. Cunha, C. Moura, M.C.C. Marco de Lucas, L. Imhoff, et al., Development of dark Ti(C,O,N) coatings prepared by reactive sputtering, Surf. Coatings Technol. 203 (2008) 804–807. doi:10.1016/j.surfcoat.2008.05.039.

[18] D. Munteanu, C. Gabor, D.G.G. Constantin, B. Varga, R. Adochite, O.C.C. Andrei, et al., Friction and wear behaviours of Ti(C,O,N) dark decorative coatings, Tribol. Int. 44 (2011) 820–828. doi:10.1016/j.triboint.2011.02.004.

[19] D.F.F. Arias, Y.C.C. Arango, a. Devia, Study of TiN and ZrN thin films grown by cathodic arc technique, Appl. Surf. Sci. 253 (2006) 1683–1690. doi:10.1016/j.apsusc.2006.03.017.

[20] P. Carvalho, F. Vaz, L. Rebouta, S. Carvalho, L. Cunha, P. Goudeau, et al., Structural stability of decorative ZrNxOy thin films, Surf. Coatings Technol. 200 (2005) 748–752. doi:10.1016/j.surfcoat.2005.02.100.

[21] P. Carvalho, Development of new decorative coatings based on zirconium oxynitrides, Universidade do Minho, 2008.

[22] S. Niyomsoan, W. Grant, D.. Olson, B. Mishra, Variation of color in titanium and zirconium nitride decorative thin films, Thin Solid Films. 415 (2002) 187–194. doi:10.1016/S0040-6090(02)00530-8.

[23] Encyclopaedia britannica, reststrahlen | physics | Britannica.com, (2014).

http://www.britannica.com/science/reststrahlen (accessed June 15, 2015).

[24] M.S. Dresselhaus, SOLID STATE PHYSICS PART II Optical Properties of Solids, 2001. http://web.mit.edu/course/6/6.732/www/6.732-pt2.pdf.

[25] A. Delin, O. Eriksson, R. Ahuja, B. Johansson, M. Brooks, T. Gasche, et al., Optical properties of the group-IVB refractory metal compounds, Phys. Rev. B. 54 (1996) 1673–1681. doi:10.1103/PhysRevB.54.1673.

[26] K. Nassau, The causes of color, AZimuth. 1 (1998) 123–168. doi:10.1016/S1387-6783(98)80007-X.

[27] A. Navrotsky, Thermochemical studies of nitrides and oxynitrides by oxidative oxide melt calorimetry, J. Alloys Compd. 321 (2001) 300–306. doi:10.1016/S0925-8388(01)00965-3.

[28] J.V. Ramana, S. Kumar, C. David, a. K. Ray, V.S. Raju, Characterisation of zirconium nitride coatings prepared by DC magnetron sputtering, Mater. Lett. 43 (2000) 73–76. doi:10.1016/S0167-577X(99)00233-5.

[29] M. Matsuoka, K. Ogata, N. Kuratani, N.E. Company, M. Matsuoka, N. Kuratani, et al., Properties of Zr-N thin films prepared by the ion and vapour deposition method, J. Mater. Sci. Lett. 15 (1996) 1340–1342. doi:10.1007/BF00240801.

[30] L. Cunha, F. Vaz, C. Moura, L. Rebouta, P. Carvalho, E. Alves, et al., Structural evolution in ZrNxOy thin films as a function of temperature, Surf. Coatings Technol. 200 (2006) 2917–2922. doi:10.1016/j.surfcoat.2004.09.030.

[31] P. Carvalho, A. Fernandes, L. Rebouta, F. Vaz, L. Cunha, U. Kreissig, et al., Compositional and structural changes in ZrOxNy films depending on growth condition, Nucl. Instruments Methods Phys. Res. Sect. B Beam Interact. with Mater. Atoms. 249 (2006) 458–461. doi:10.1016/j.nimb.2006.03.031.

[32] L. Pichon, T. Girardeau, a. Straboni, F. Lignou, P. Guérin, J. Perrière, Zirconium nitrides deposited by dual ion beam sputtering: physical properties and growth modelling, Appl. Surf. Sci. 150 (1999) 115–124. doi:10.1016/S0169-4332(99)00233-0.

[33] H. Wendel, H. Suhr, Thin zirconium nitride films prepared by plasma-enhanced CVD, Appl. Phys. A Solids Surfaces. 54 (1992) 389–392. doi:10.1007/BF00324208.

[34] D. Constantin, A. Munteanu, Decorative aspects of ZrNx thin films prepared by reactive magnetron sputtering, 3 (2010).

[35] P. Klumdoung, a. Buranawong, S. Chaiyakun, P. Limsuwan, Variation of color in Zirconium nitride thin films prepared at high Ar flow rates with reactive dc magnetron sputtering, Procedia Eng. 32 (2012) 916–921. doi:10.1016/j.proeng.2012.02.032.

[36] A. Singh, P. Kuppusami, S. Khan, C. Sudha, R. Thirumurugesan, R. Ramaseshan, et al., Influence of nitrogen flow rate on microstructural and nanomechanical properties of Zr-N thin films prepared by pulsed DC magnetron sputtering, Appl. Surf. Sci. 280 (2013) 117–123. doi:10.1016/j.apsusc.2013.04.107.

[37] B. Subramanian, V. Swaminathan, M. Jayachandran, Microstructural , Tribological and Electrochemical Corrosion Studies on Reactive DC Magnetron Sputtered Zirconium Nitride Films with Zr Interlayer on Steel, 18 (2012). doi:10.1007/s12540-012-6007-2.

[38] Y. Sui, J. Liu, B. Liu, L. Wang, B. Yao, Influence of flow ratio of N2 to (N2+Ar) mixture on the structure and properties of zirconium nitride films prepared by radio frequency magnetron sputtering, J. Mater. Res. 24 (2009) 3206–3212. doi:10.1557/jmr.2009.0383.

[39] H.. Benia, M. Guemmaz, G. Schmerber, a Mosser, J.-C. Parlebas, Investigations on non-stoichiometric zirconium nitrides, Appl. Surf. Sci. 200 (2002) 231–238. doi:10.1016/S0169-4332(02)00925-X.

[40] A.C. Fernandes, L. Cunha, C. Moura, F. Vaz, D. Munteanu, B. Borcea, TiN-based decorative coatings : colour change by addition of C and O, J. Optoelectron. Adv. Mater. 10 (2008) 900–903.

[41] L.P. Borilo, a M. Shul, O. V Turetskova, Thin-Film Coatings Based on Zirconium and Cobalt Oxides, 59 (2002) 142–144.

[42] S. Venkataraj, O. Kappertz, C. Liesch, R. Detemple, R. Jayavel, M. Wuttig, Thermal stability of sputtered zirconium oxide films, Vacuum. 75 (2004) 7–16. doi:10.1016/j.vacuum.2003.12.127.

[43] P. Gao, L.. J. Meng, M.. dos Santos, V. Teixeira, M. Andritschky, M.P. Santos, et al., Characterisation of ZrO2 films prepared by rf reactive sputtering at different O2 concentrations in the sputtering gases, Vacuum. 56 (2000) 143–148. doi:10.1016/S0042-207X(99)00199-2.

[44] J. Gibkes, F. Vaz, a C. Fernandes, P. Carvalho, F. Macedo, R.T. Faria, et al., Analysis of multifunctional oxycarbide and oxynitride thin films by modulated IR radiometry, J. Phys. D. Appl. Phys. 43 (2010) 395301. doi:10.1088/0022-3727/43/39/395301.

[45] C. Moura, P. Carvalho, F. Vaz, L. Cunha, E. Alves, Raman spectra and structural analysis in ZrOxNy thin films, Thin Solid Films. 515 (2006) 1132–1137. doi:10.1016/j.tsf.2006.07.039.

[46] S. Mohamed, A. Abd El-Rahman, M. Ahmed, Investigation of zirconium oxynitride thin films deposited by reactive pulsed magnetron sputtering, J. Phys. D. Appl. Phys. 40 (2007) 7057–7062. doi:10.1088/0022-3727/40/22/029.

[47] F. Macedo, P. Carvalho, L. Cunha, F. Vaz, J. Gibkes, B.K. Bein, et al., The Role of Modulated IR Radiometry Measurements in the Characterization of Zr□O□N Thin Films, Plasma Process. Polym. 6 (2009) S760–S766. doi:10.1002/ppap.200931802.

[48] A. Rizzo, M. Signore, L. Mirenghi, T. Di Luccio, Synthesis and characterization of titanium and zirconium oxynitride coatings, Thin Solid Films. 517 (2009) 5956–5964. doi:10.1016/j.tsf.2009.03.131.

[49] M. Radecka, E. Pamula, A. Trenczek-Zajac, K. Zakrzewska, A. Brudnik, E. Kusior, et al., Chemical composition, crystallographic structure and impedance spectroscopy of titanium oxynitride TiNxOy thin films, Solid State Ionics. 192 (2011) 693–698. doi:10.1016/j.ssi.2010.07.021.

[50] M. a. Signore, a. Rizzo, L. Mirenghi, M. a. Tagliente, a. Cappello, Characterization of zirconium oxynitride films obtained by radio frequency magnetron reactive sputtering, Thin Solid Films. 515 (2007) 6798–6804. doi:10.1016/j.tsf.2007.02.033.

[51] G.I. Cubillos, J.J. Olaya, M. Bethencourt, G. Antorrena, K. El Amrani, Synthesis and characterization of zirconium oxynitride ZrOxNy coatings deposited via unbalanced DC magnetron sputtering, Mater. Chem. Phys. 141 (2013) 42–51. doi:10.1016/j.matchemphys.2013.04.012.

[52] K.C. Shimpi, K. Ravindranath, a. K. Jani, D.C. Kothari, C.S. Harindranath, Decorative coatings produced using combination of reactive arc evaporation and magnetron sputtering, Surf. Coatings Technol. 90 (1997) 115–122. doi:10.1016/S0257-8972(96)03102-7.

[53] S.C.C. Ferreira, E. Ariza, L. a. a. Rocha, J.R.R. Gomes, P. Carvalho, F. Vaz, et al., Tribocorrosion behaviour of ZrOxNy thin films for decorative applications, Surf. Coatings Technol. 200 (2006) 6634–6639. doi:10.1016/j.surfcoat.2005.11.083.

[54] M. Wautelet, J.P. Dauchot, F. Debal, S. Edart, M. Hecq, Influence of the composition of gas mixture on the stoichiometry of sputter-deposited compound films: The case of zirconium nitrides, J. Mater. Res. 11 (2011) 825–829. doi:10.1557/JMR.1996.0100.

[55] J. Musil, P. Baroch, J. Vlček, K.H.H. Nam, J.G.G. Han, Reactive magnetron sputtering of thin films: present status and trends, Thin Solid Films. 475 (2005) 208–218. doi:10.1016/j.tsf.2004.07.041.

[56] S. Venkataraj, O. Kappertz, H. Weis, R. Drese, R. Jayavel, M. Wuttig, Structural and optical properties of thin zirconium oxide films prepared by reactive direct current magnetron sputtering, J. Appl. Phys. 92 (2002) 3599. doi:10.1063/1.1503858.

[57] S. Venkataraj, D. Severin, S.H. Mohamed, J. Ngaruiya, O. Kappertz, M. Wuttig, Towards understanding the superior properties of transition metal oxynitrides prepared by reactive DC magnetron sputtering, Thin Solid Films. 502 (2006) 228–234. doi:10.1016/j.tsf.2005.07.280.

[58] E. Budke, H. Maidhof, H. Schu, Decorative hard coatings with improved corrosion resistance, Surf. Coatings Technol. 112 (1999) 108–113.

[59] K. Seshan, Handbook of Thin Film Deposition, Third Edit, Elsevier, Oxford, 2012. doi:10.1016/B978-1-4377-7873-1.00006-1.

[60] K.S.S. Harsha, Principles of Physical Vapor Deposition of Thin Films, First Edit, Elsevier, 2005.

[61] DirectVacuum, Magnetron Sputtering Technology, (2015) 3. http://www.directvacuum.com/sputter.asp (accessed July 24, 2015).

[62] G. Dominik, An Investigation of Target Poisoning during Reactive Magnetron Sputtering, Technishen Universität Dresden, 1972.

[63] Gencoa company, Gencoa: Target Erosion – Simulation, (2015) 2. http://www.gencoa.com/target_erosion/ (accessed July 23, 2015).

[64] D.M. Mattox, Handbook of Physical Vapor DepositionDeposition (PVD) Processing, Second Edi, Elsevier, Oxford, 2009. doi:10.1016/B978-0-8155-2037-5.00025-3.

[65] Y. Waseda, E. Matsubara, K. Shinoda, X-Ray Diffraction Crystallography, 2011. doi:10.1007/978-3-642-16635-8.

[66] D. Simeone, G. Baldinozzi, D. Gosset, S. Le Caer, J.F. Bérar, Grazing incidence X-ray diffraction for the study of polycrystalline layers, Thin Solid Films. 530 (2013) 9–13. doi:10.1016/j.tsf.2012.07.068.

[67] M. Ohring, Materials science of thin films Deposition & structure, 2nd Editio, Academic press, Florida, 2002.

[68] J.I. Goldstein, D.E. Newbury, C.E. Lyman, D.C. Joy, Microscopy and Scanning Electron Microscopy and A Text for Biologists , Materials Scientists, and Geologists, 2nd editio, Plenum press, New York, 1992.

[69] S. Ebnesajjad, Surface Treatment of Materials for Adhesive Bonding, 2014. doi:10.1016/B978-0-323-26435-8.00004-6.

[70] J. a Thornton, High Rate Thick Film Growth, Annu. Rev. Mater. Sci. 7 (1977) 239–260.

[71] K. Minolta, spectrophotometer CM-2600d, 2015. http://www.konicaminolta.com/instruments/download/catalog/color/pdf/cm2600d_catalog_eng.pdf (accessed July 7, 2015).

[72] GmbH, SPECS GmbH, (2014) 7. http://www.specs.de/cms/upload/PDFs/IQE11-35/sputter-info.pdf (accessed October 25, 2015).